

Electronic Thesis and Dissertation Repository

---

2-9-2022 9:30 AM

## Synthesis and Characterization of Phosphorus Containing Polymers for the Purpose of Polymer Derived Ceramics

Kelly C. Duggan, *The University of Western Ontario*

Supervisor: Dr. Paul J. Ragogna, *The University of Western Ontario*

A thesis submitted in partial fulfillment of the requirements for the Master of Science degree in  
Chemistry

© Kelly C. Duggan 2022

Follow this and additional works at: <https://ir.lib.uwo.ca/etd>

---

### Recommended Citation

Duggan, Kelly C., "Synthesis and Characterization of Phosphorus Containing Polymers for the Purpose of Polymer Derived Ceramics" (2022). *Electronic Thesis and Dissertation Repository*. 8387.  
<https://ir.lib.uwo.ca/etd/8387>

This Dissertation/Thesis is brought to you for free and open access by Scholarship@Western. It has been accepted for inclusion in Electronic Thesis and Dissertation Repository by an authorized administrator of Scholarship@Western. For more information, please contact [wlsadmin@uwo.ca](mailto:wlsadmin@uwo.ca).

## Abstract

This dissertation focuses on the synthesis and characterization of phosphorus containing polymers for the purpose of polymer derived ceramics. These networks are composed of three different monomeric compounds, and it was found that changes to the stoichiometry of these resulted in different properties such as thermal stability and swellability. Through the analysis of these properties, optimal stoichiometries were decided upon that provided the best ceramic yield and were still able to swell in solvents. These polymeric candidates were then subjected to further reactions as the phosphorus sites present in the networks were tertiary phosphines (Lewis bases). Reacting these phosphines with a Lewis acid resulted in successful coordination. The resulting ceramics were characterized using SEM-EDX and XPS spectroscopies.

## Summary for Lay Audience

Environmental degradation is increasing due to air pollution which creates high levels of carbon dioxide in the atmosphere. Climate change is also prevalent and causes adverse environmental effects. The increasing dependence that society has on fossil fuels only harms the environment more. The burning of fossil fuels contributes to the overproduction of greenhouse gases which only serves to pollute the environment. Due to this, it is imperative that a solution be put into place to lower the harmful impacts that these fossil fuels have on the environment. Research is currently being done to lower the carbon footprint of gas-powered vehicles. This can be made possible by improving battery performance and producing electrocatalysts suitable for their desired application. Metal air batteries and fuel cells are being investigated as a replacement of the current lithium-ion battery, which is approaching its performance limit. For these replacements to be implemented, the development of more suitable electrocatalysts needs to be accomplished. Research thus far has suggested metal phosphides are a suitable candidate for the replacement, however the challenge is brought about through the synthesis of these materials. Throughout this thesis, various polymers are formed to help derive a material that is best suited for an electrocatalyst replacement. The incorporation of phosphorus and cobalt within the polymers followed by pyrolysis produces the desired metal phosphide. For these materials to be suitable, they need to obtain a high ceramic yield throughout pyrolysis which is difficult to achieve. Altering the starting materials in the original formulation produces different effects on the overall thermal stability of the polymer itself. Finding the optimal starting materials and the stoichiometry in which to use them will be imperative to determine if these materials are suitable replacements for the current electrocatalysts.

## Co-Authorship Statement

Chapter one, two, and three were written by Kelly Duggan and edited by Paul J. Ragona, Jeanette Adjei, and Jan Willem Lamberink.

# Dedication

Dedicated to: Mike J. Duggan and Deanna Duggan

## Acknowledgements

This thesis could not have been accomplished without the help of Dr. Paul J. Ragona who consistently provided guidance, support, and an enjoyable work environment. My time at Western not only helped to improve my science knowledge and skills, but also allowed me to focus on professional development while further improving my interpersonal skills. This is a result of the superb mentoring I received from my supervisor.

I would also like to thank the Ragona group for all of your support and ideas throughout my degree and for the fun times had in the lab. I would like to thank Daniela, Mike, Tristan, Julia, and Jeanette for all the fun moments and laughs had throughout my time at Western. This degree would not have been as enjoyable if it were not for the amazing experiences, I shared with you guys in and outside of the lab. I am extremely grateful for the mentorship I received from Dr. Vanessa Beland who brought such a fun energy into the lab every single day. I cannot thank you enough for all the advice and knowledge you've given me.

I would also thank the various staff in the chemistry department who helped to make coming to work every day a positive experience. Specifically, I would like to thank Mat Willans for consistently providing a helping hand when needed and a good laugh on a tough day.

I would like to thank Mark Biesinger and Justin Lomax for obtaining and characterising the XPS data. I would also like to express gratitude to Todd Simpson and Tim Goldhawk for acquiring the SEM-EDX data.

To my parents, I would like to thank you for all of the support and visits over the last two years and reminding me to take a break and enjoy life. To my fiancé Adam, I could not be more thankful for the patience and support you've given me throughout my time at Western University.

# Table of Contents

Abstract.....	ii
Summary for Lay Audience. ....	iii
Co-Authorship Statement.....	iv
Dedication.....	v
Acknowledgements.....	vi
Table of Contents.....	vii
List of Tables.....	x
List of Figures.....	xii
List of Abbreviations.....	xv
1 Introduction.....	1
1.1 Polymers .....	1
1.1.1 Free Radical Polymerisation (FRP) .....	2
1.1.2 Photopolymerisation .....	3
1.1.3 Thiol-ene and Phosphane-ene Reactions .....	6
1.1.4 Polymer Networks .....	7
1.2 Polymer Derived Ceramics .....	11
1.2.1 Pyrolysis.....	12
1.2.2 The Influence of Polymeric Precursors on Ceramics .....	13
1.3 Ceramics in modern society.....	14
1.4 Scope of Thesis.....	15
2 Modifying Polymeric Precursors to Maximize Ceramic Yield .....	19
2.1 Introduction.....	19
2.2 Synthesis .....	21
2.3 Swelling Properties .....	26
2.4 Thermal Properties.....	33
2.5 Oxygen Uptake .....	35

2.6	Pyrolysis.....	38
2.7	Conclusions.....	40
2.8	Experimental.....	40
2.8.1	Preparation of polymers 1.1, 1.2, 1.3, and 1.4.....	41
2.8.2	Characterization of polymers 1.1, 1.2, 1.3, and 1.4.....	42
2.8.3	Preparation of polymers 2.1, 2.2, 2.3, 2.4, 2.5, 2.6, 2.7, fghand 2.8.....	43
2.8.4	Characterisation of polymers 2.1, 2.2, 2.3, 2.4, 2.5, fgh2.6, 2.7, and 2.8.....	44
3	Post Polymerisation Modification.....	47
3.1	Introduction.....	47
3.2	Small molecule control reactions.....	48
3.3	Quaternization of Polymer 3.6 and 3.7.....	50
3.4	Metalation.....	52
3.4.1	Thermal Properties.....	54
3.5	Pyrolysis.....	55
3.6	Conclusion.....	57
3.7	Experimental.....	58
4	Conclusions and Future Work.....	64
4.1	Conclusions.....	64
4.2	Future Work.....	65
	Chapter Five.....	69
5	Appendix.....	69
5.1	Appendix to Chapter Two.....	69
5.1.1	Swelling and Gel Content Experiments.....	69
5.1.2	XPS Data.....	71
5.1.3	SEM Images.....	72



5.2	Appendix to Chapter Three.....	74
5.2.1	Metallated Polymers NMR spectroscopic data.....	74
5.2.2	XPS Data.....	75
5.2.3	SEM Images.....	76

## List of Tables

<b>Table 2.1:</b> Thermal properties of polymers <b>1.1, 1.2, 1.3, 1.4</b> .....	34
<b>Table 2.2:</b> Thermal properties of polymers <b>2.1, 2.2, 2.3, 2.4, 2.5, 2.6, 2.7, 2.8</b> .....	34
<b>Table 2.3:</b> Oxygen uptake for polymers <b>1.1, 1.3, 2.1, and 2.4</b> .....	37
<b>Table 2.4:</b> Composition of the char resulting from pyrolysis of polymers <b>1.1</b> and <b>1.3</b> as depicted theoretically, from XPS and EDX.....	38
<b>Table 2.5:</b> Composition of the char resulting from pyrolysis of polymers <b>2.1</b> and <b>2.4</b> as depicted theoretically, from XPS and EDX.....	39
<b>Table 2.6:</b> Amount of starting materials used for the polymerisation of polymers <b>1.1 – 1.4</b> .....	42
<b>Table 2.7:</b> Amount of starting materials used for the polymerisation of polymers <b>2.1 – 2.8</b> .....	43
<b>Table 3.1:</b> XPS and EDX results from coordinated polymer networks <b>3.62</b> and <b>3.72</b> . ...	54
<b>Table 3.2:</b> Atomic percentages of elements present in the chars ( <b>3.63</b> and <b>3.73</b> ) produced via pyrolysis; analyzed using XPS and EDX.....	56
<b>Table 3.3:</b> Results obtained from XPS revealing the elemental composition and chemical environment of phosphorus and cobalt within the char .....	57
<b>Table 5.1:</b> Swell %, gel content, and molar swellability values obtained for polymers <b>1.1 – 1.4</b> and <b>2.1 – 2.8</b> .....	70
<b>Table 5.2:</b> Atomic percentage results obtained from the XPS data obtained from the chars of polymers <b>1.1, 1.3, 2.1, and 2.4</b> .....	71
<b>Table 5.3:</b> Oxidation states of the elements present in the chars of polymers <b>1.1</b> and <b>1.3</b> , acquired using an XPS instrument.....	72
<b>Table 5.4:</b> Elemental oxidation states of the elements present in the chars of polymers <b>2.1, and 2.4</b> .....	72
<b>Table 5.5:</b> Atomic percentage results obtained from the polymeric precursors <b>3.62</b> and <b>3.72</b> and the char produced from their subsequent thermochemical decomposition ( <b>3.63</b> and <b>3.73</b> ). .....	75
<b>Table 5.6:</b> Oxidation states present in metallated polymeric precursor, <b>3.62</b> and in the resulting char, <b>3.63</b> .....	76

**Table 5.7:** Results obtained for the oxidation states of polymer **3.72** and the char resulting its subsequent heat treatment, **3.73**. ..... 76

## List of Figures

<b>Figure 1.1:</b> Example of addition (chain growth) and condensation (step growth) polymerisation processes. A) Addition (chain growth) <sup>1</sup> ; B) Condensation (step growth) .	1
<b>Figure 1.2:</b> Plots of molecular weight vs % conversion representing the differences between A) chain growth (addition) polymerisation and B) step growth (condensation) polymerisation.....	2
<b>Figure 1.3:</b> Chain polymerisation example utilizing AIBN (azobisisobutyronitrile) as an initiator. a) Initiation, (b) propagation, and (c) termination including coupling (top) and disproportionation (bottom) reactions respectively. ....	3
<b>Figure 1.4:</b> Simplified Jablonski Diagram displaying the potential pathways that can occur throughout photoexcitation. ....	4
<b>Figure 1.5:</b> A) Type I photoinitiator using benzoyl peroxide as an example B) Type II photoinitiator using benzophenone as an example with a tertiary amine as a co-initiating species.....	5
<b>Figure 1.6:</b> General reaction scheme of A) hydrothiolation and B) hydrophosphination..	6
<b>Figure 1.7:</b> Initiating and propagating steps in the phosphane-ene reaction.....	7
<b>Figure 1.8:</b> Comparing the formation of linear polymers versus crosslinked polymers....	8
<b>Figure 2.1:</b> Starting materials used for polymerisation. <b>A)</b> Crosslinkers used in this work. <b>1:</b> 1, 3, 5- triallyl - 1, 3, 5- triazine - 2, 4, 6- trione (TTT), and <b>2:</b> 2, 4, 6, 8 – tetramethyl - 2, 4, 6, 8-tetravinylcyclotetrasiloxane. <b>B)</b> Linear additive used to increase swellability. <b>3:</b> Tetraethyleneglycol diallyl ether (TEGDAE).....	21
<b>Figure 2.2:</b> P-H bond to olefin ratio for polymers ( <b>1.1 - 1.4</b> ) with trifunctional crosslinkers. ....	22
<b>Figure 2.3:</b> P-H bond to olefin ratio for polymers ( <b>2.1 - 2.8</b> ) with tetrafunctional crosslinker. ....	23
<b>Figure 2.4:</b> IR spectra of uncured (purple and green) and cured (black and blue) pucks <b>1.1</b> and <b>2.1</b> . A: $\nu_{\text{P-H}} = 2290 \text{ cm}^{-1}$ ; B: $\nu_{\text{C=O}} = 1680 \text{ cm}^{-1}$ ; C: $\nu_{\text{C=C}} = 991 \text{ cm}^{-1}$ ; D: $\nu_{\text{P-H}} = 2290 \text{ cm}^{-1}$ ; E: $\nu_{\text{Si-CH}_2=\text{CH}_3} = 1596 \text{ cm}^{-1}$ ; F: $\nu_{\text{Si-CH}_3} = 1258 \text{ cm}^{-1}$ . ....	26
<b>Figure 2.5:</b> Swell % by mass for polymers ( <b>1.1 - 1.4</b> ) with tetrafunctional crosslinker. .	28
<b>Figure 2.6:</b> Swell % by mass for polymers ( <b>2.1 - 2.8</b> ) with tetrafunctional crosslinker. .	29
<b>Figure 2.7:</b> Plot of molar swellability values for polymers <b>1.1 – 1.4</b> .....	30

<b>Figure 2.8:</b> Plot of molar swellability values for polymers <b>2.1 – 2.8</b> .....	30
<b>Figure 2.9:</b> $^{31}\text{P}\{^1\text{H}\}$ NMR spectra of polymers <b>1.1 - 1.4</b> in various reaction solvents. ...	31
<b>Figure 2.10:</b> $^{31}\text{P}\{^1\text{H}\}$ NMR spectra of polymers <b>2.1 - 2.8</b> in various reaction solvents. .	32
<b>Figure 2.11:</b> $^{31}\text{P}\{^1\text{H}\}$ NMR spectra of the products resulting from the photo-polymerisation of monoisobutylphosphine with TEGDAE only, crosslinker <b>2</b> only, or both TEGDAE and crosslinker <b>2</b> . .....	33
<b>Figure 2.12:</b> Oxygen uptake thermograms for polymers <b>1.1, 1.3, 2.1, and 2.4</b> .....	37
<b>Figure 3.1:</b> Quaternizing the phosphorus atom present on <b>3.1</b> using the SN2 reaction...	48
<b>Figure 3.2:</b> 5-chloropentyne undergoing the Finklestein reaction to produce the iodoalkyne.....	49
<b>Figure 3.3:</b> Quaternization of <b>3.1</b> using iodopentyne and bromobutyne .....	49
<b>Figure 3.4:</b> $^1\text{H}$ NMR ( $\text{CD}_2\text{Cl}_2$ , 400 MHz) spectrum of metallated 5-chloropentyne.....	50
<b>Figure 3.5:</b> Formation of phosphine polymer network <b>3.7</b> utilizing the phosphane-ene reaction.....	51
<b>Figure 3.6:</b> A) Cyclopentadienylcobalt dicarbonyl ( <b>3.8</b> ); B) Formation of coordinate covalent bond between phosphine (Lewis base) and the cobalt present on <b>3.8</b> ; Lewis acid .....	52
<b>Figure 3.7:</b> SEM images of metallated polymers A) <b>3.62</b> and B) <b>3.72</b> .....	53
<b>Figure 3.8:</b> Thermograms resulting from the thermochemical decomposition of <b>3.6, 3.62, 3.7, and 3.72</b> .....	55
<b>Figure 4.1:</b> Linear additives to use instead of TEGDAE suggested to increase ceramic yield. A) Divinyldimethylsilane, B) 1, 4 – divinyl - 1, 1, 4, 4 – tetramethyl – 1, 4 – disilabutane, C) 1, 5 – divinylohexamethyltrisiloxane .....	65
<b>Figure 4.2:</b> Formation of a polymer network free of oxygen using monoisobutyl phosphine, 1, 3, 5 – trivinyl – 1, 3, 5 – trimethylcyclotrisilazane as the crosslinker, and divinyldimethylsilane as the linear additive. ....	66
<b>Figure 4.3:</b> Formation of a phosphonium polymer using allyl bromide. A proven reaction known to occur in phosphane-ene polymers as demonstrated by Dr. V. A. Beland. <sup>10</sup> .....	67
<b>Figure 5.1:</b> Animation depicting what is taking place throughout the swell % and gel content experiments. ....	69

<b>Figure 5.2:</b> SEM images of the ceramics resulting from the pyrolysis of A) <b>1.1</b> , B) <b>1.3</b> , C) <b>2.1</b> , and D) <b>2.4</b> .....	73
<b>Figure 5.3:</b> $^{31}\text{P}$ $\{^1\text{H}\}$ NMR spectra of the metalation using <b>3.8</b> of polymers <b>3.6</b> and <b>3.7</b> to metallated polymers <b>3.62</b> and <b>3.72</b> . .....	74
<b>Figure 5.4:</b> IR spectra of polymers <b>3.62</b> and <b>3.72</b> following metalation with <b>3.8</b> (also shown). Subsequent metalation resulted in the disappearance of one of the carbonyl signals present in <b>3.8</b> .....	75
<b>Figure 5.5:</b> SEM images of the ceramics resulting from the pyrolysis of A) <b>3.62</b> , B) <b>3.63</b> , C) <b>3.72</b> , and D) <b>3.73</b> .....	77

## List of Abbreviations

AIBN	Azobisisobutyronitrile
ATR	Attenuated total reflectance
BAPO	Phenylbis(2,4,6-trimethylbenzoyl)-phosphine oxide
D <sub>4</sub>	2, 4, 6, 8 – tetramethyl - 2, 4, 6, 8-tetravinylcyclotetrasiloxane
DCM	Dichloromethane
DSC	Differential scanning calorimetry
EDX	Energy dispersive X-ray
Et <sub>2</sub> O	Diethyl ether
EV	Electric vehicle
FRP	Free radical polymerisation
GHG	Greenhouse gases
HER	Hydrogen evolution reaction
IR	Infrared
MeCN	Acetonitrile
M <sub>oxy</sub>	Molar mass of oxygen
M <sub>s</sub>	Molar swellability
MW	Molecular weight
NMR	Nuclear magnetic resonance
N <sub>phos</sub>	Moles of phosphorus
OER	Oxygen evolution reaction
ORR	Oxygen reduction reaction
O <sub>xcalc</sub>	Theoretical value for oxygen uptake
O <sub>xexp</sub>	Experimental value for oxygen uptake
PDCs	Polymer derived ceramics
SEM	Scanning electron microscopy
T <sub>c</sub>	Crystallization temperature
T <sub>d</sub>	Onset of decomposition
TEGDAE	Tetraethylene glycol diallyl ether
T <sub>g</sub>	Glass transition temperature
TGA	Thermogravimetric analysis

THF	Tetrahydrofuran
T <sub>m</sub>	Melting temperature
TTT	1, 3, 5- triallyl - 1, 3, 5- triazine - 2, 4, 6- trione
UV	Ultraviolet
UVA	Ultraviolet A ( $\lambda = 315 - 400 \text{ nm}$ )
UVB	Ultraviolet B ( $\lambda = 280 - 315 \text{ nm}$ )
UVC	Ultraviolet C ( $\lambda = 100 - 280 \text{ nm}$ )
UVV	Ultraviolet V ( $\lambda = 400 - 450 \text{ nm}$ )
W <sub>o</sub>	Sample mass
XPS	X-ray photoelectron spectroscopy



# Chapter 1

## 1 Introduction

### 1.1 Polymers

The terms polymer and macromolecules can be used interchangeably as they describe the bonding between a large repeating sequence of small molecules, that are called monomers. The process describing the formation of a polymer is referred to as polymerisation.<sup>1</sup> “Condensation” and “addition” polymers were used to describe the formation of polymers as introduced by Carothers in 1929.<sup>2</sup> These definitions help in understanding the difference in composition between polymers and the monomers from which they are prepared. A condensation polymer is hallmarked by the elimination of a small molecule (*i.e.* water) whereas an addition polymer is a material consisting of the same atoms in the monomer and in the repeating units of the polymer (**Figure 1.1**).<sup>1</sup>

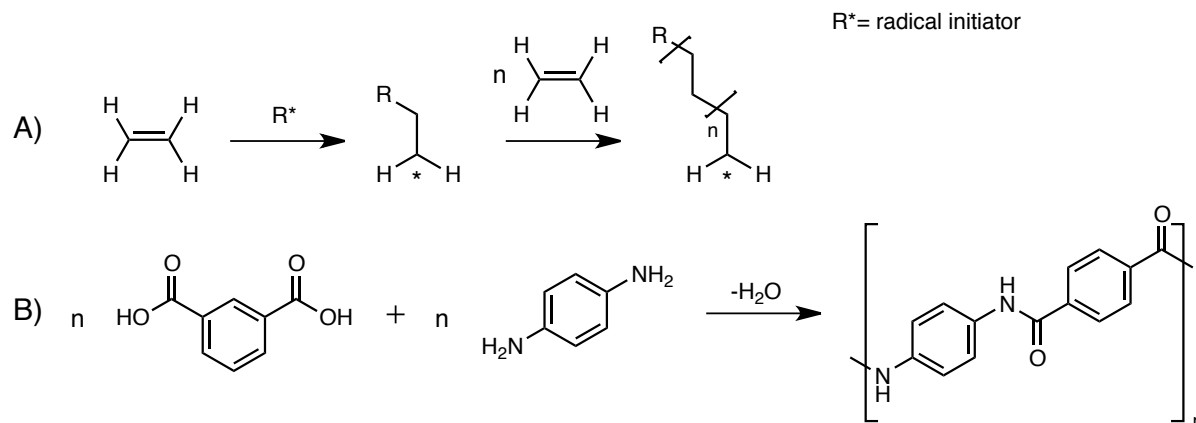


**Figure 1.1:** Example of addition (chain growth) and condensation (step growth) polymerisation processes. A) Addition (chain growth)<sup>1</sup>; B) Condensation (step growth)<sup>3</sup>

New terminology emerged in 1956 to describe the polymerisation processes: chain- and step- growth polymerisation. Step-growth polymerisation describes a stepwise reaction in which bi-functional or multifunctional monomers form dimers, trimers, oligomers until a long molecular weight chain is achieved.<sup>4</sup> As these types of polymerisations proceed, a steady growth in molecular weight can be seen throughout most of the reaction. As the conversion rate becomes high, the molar mass increases rapidly producing a high molecular weight polymer. In contrast, polymers formed via chain-growth polymerisation experience a steady growth in molecular weight throughout conversion. This produces higher

molecular weight polymers at lower conversion rates in comparison to the step growth analogue (**Figure 1.2**). Chain-growth polymerisation describes a synthetic method for the formation of polymers that requires the incorporation of an initiating species. This initiating species can react with a monomer present in solution to induce the polymerisation process. This initiating species can be a free radical, a cation, or an anion resulting in free radical, cationic, or anionic polymerisation, respectively. These three methods are all efficient in synthesizing polymers, however, one method important to research in this area is utilizing free radical polymerisation for the formation of polymers.

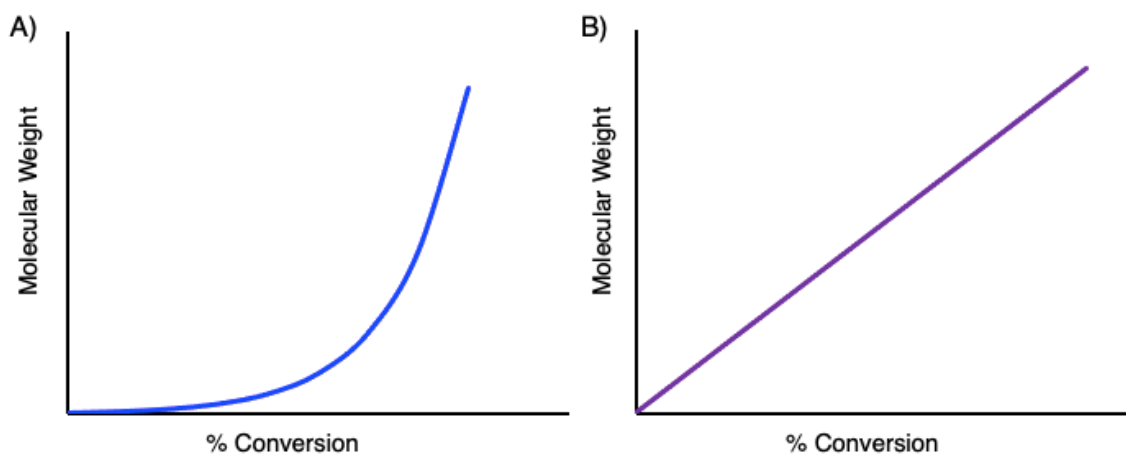


**Figure 1.2:** Plots of molecular weight vs % conversion representing the differences between A) chain growth (addition) polymerisation and B) step growth (condensation) polymerisation

### 1.1.1 Free Radical Polymerisation (FRP)

FRP is a polymerisation technique which results in the formation of polymer species from the addition of monomer units in a chain growth reaction. This technique proceeds through three main steps to form the resulting polymer: initiation, propagation, and termination. Initiation first begins with the formation of a reactive radical species which can typically be formed *via* homolytic dissociation. To finish the initiation step, the reactive radical species reacts with a monomer present in the starting material, resulting in the formation of the chain initiating radical (Error! Reference source not found.a). The propagation step is then underway, which involves the addition of monomer units to formulate the resulting polymer (Error! Reference source not found.b). Once a sufficient amount of monomer is consumed and the polymer is no longer able to propagate, the termination step occurs. In this final stage of FRP, through coupling or disproportionation reactions results in the

termination of the polymerisation taking place. The coupling reaction occurs when two different radicals within the system combine. The disproportionation reaction proceeds by abstracting a hydrogen radical that is beta to another hydrogen center, and results in the formation of two different polymer species- one saturated and one unsaturated (**Error! Reference source not found.c**). The latter of the two is considered the less likely to occur, however, regardless of the termination pathway, the result is the cessation of the polymerisation reaction.<sup>1,5,18</sup>

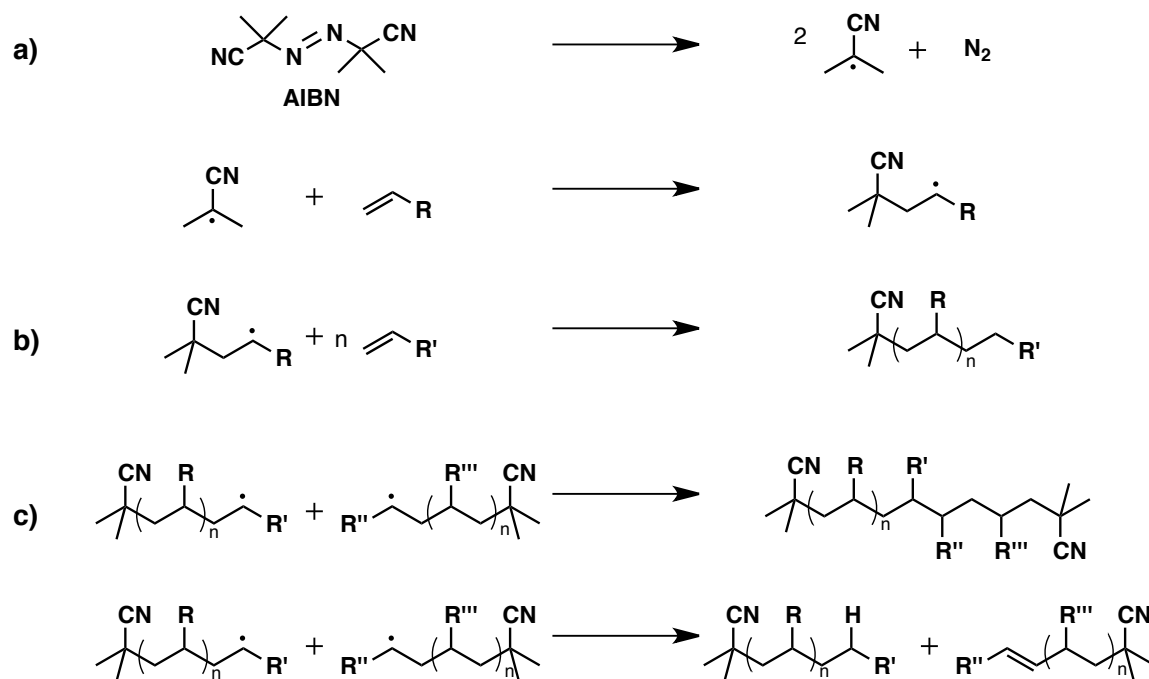


**Figure 1.3:** Chain polymerisation example utilizing AIBN (azobisisobutyronitrile) as an initiator. a) Initiation, (b) propagation, and (c) termination including coupling (top) and disproportionation (bottom) reactions respectively.

## 1.1.2 Photopolymerisation

The formation of free radicals to initiate polymerisation can be accomplished thermally or photolytically.<sup>1</sup> Following irradiation, a photon is absorbed, and the molecule is subsequently forced into an excited state ( $S_n \leftarrow S_0$ ). The molecule then undergoes vibrational relaxation to the  $\nu = 0$  vibrational state, then following internal conversion, a transition to the lowest singlet excited state ( $S_1$ ) is achieved. As the electron relaxes down to the  $\nu = 0$  vibrational state, the singlet ground state ( $S_0$ ) is re-established and a photon is emitted, which is detected as fluorescence.

Alternatively, nonradiative vibrational relaxation to  $S_0$  can also occur. From the lowest singlet excited state ( $S_1$ ) intersystem crossing can occur, which is a transition from  $T_1 \leftarrow S_1$  causing a change in spin multiplicity. Once vibrational relaxation occurs, the excited electron can undergo phosphorescence which produces a transition from  $T_1 \leftarrow S_0$  or it can partake in photolytic reaction. These photochemical pathways can all be explained through the use of a Jablonski diagram (**Figure 1.4**).<sup>6,7,8,11</sup>

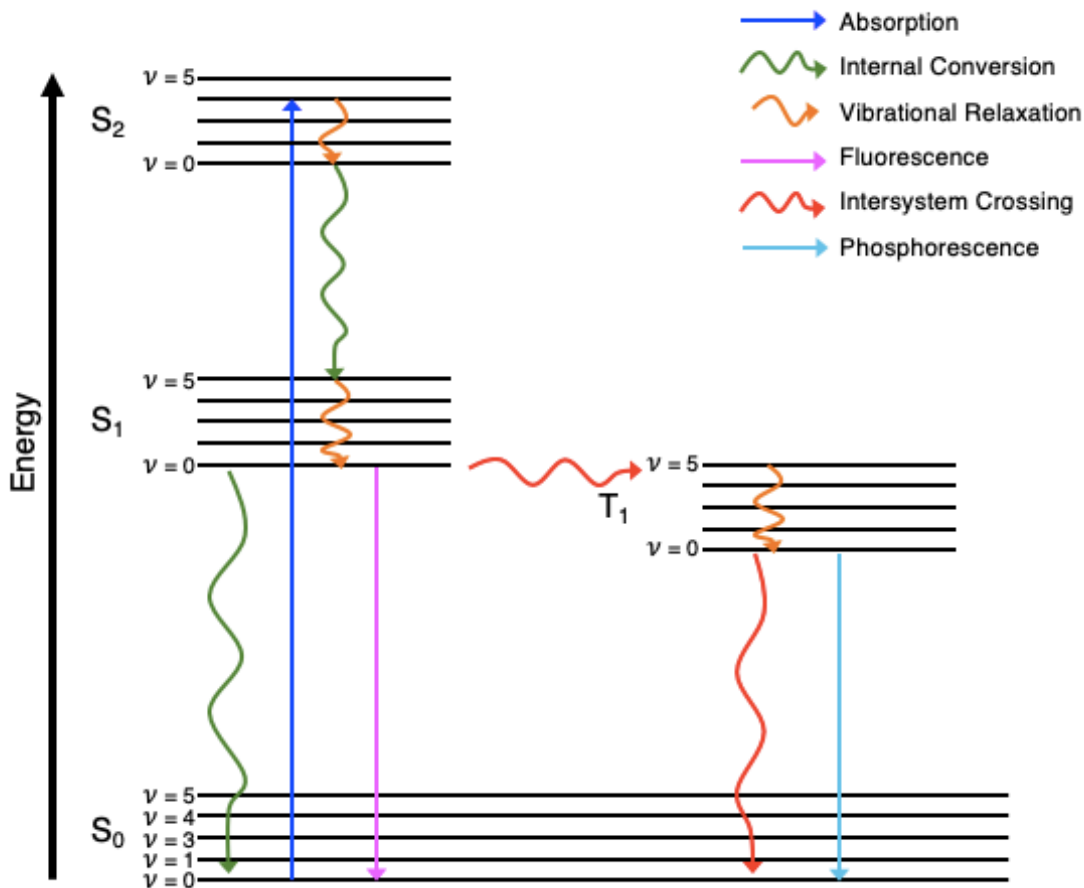


**Figure 1.4:** Simplified Jablonski Diagram displaying the potential pathways that can occur throughout photoexcitation.

Photolysis describes the cleavage of a molecule into two parts which can result in the formation of species containing unpaired electrons, or radicals. Radicals used to initiate polymerisation processes are commonly formed *via* homolytic fission of a covalent bond present in a radical initiator.<sup>7,8</sup> There are two types of photoinitiators, and their classification is dependent the decomposition mechanism. The first type can be referred to as type I or  $\alpha$ -cleavage photoinitiators, which can undergo a decomposition mechanism

immediately following irradiation (Error! Reference source not found.-A). In contrast, type II photoinitiators require co-initiating species to generate the desired radicals (Error! Reference source not found.-B). The interactions taking place between the initiator and co-initiating species are governed by the nature of the co-initiator chosen. For example, when amines are used as co-initiators, it is hypothesized that they interact *via* an electron transfer process resulting in the formation of an ion pair intermediate (exciplex). This intermediate then generates the resulting radicals that can initiate polymerisation. This results in the generation of two radicals: one placed on the photoinitiator and one on the amine. The radical resulting from the photoinitiator is inactive regarding the addition to alkenes, however it tends to couple or terminate initiating radicals. Type II co-initiating species are not limited to amines, as various functional groups such as thiols have proven successful in generating radicals when accompanied with photoinitiators.<sup>9,10</sup>

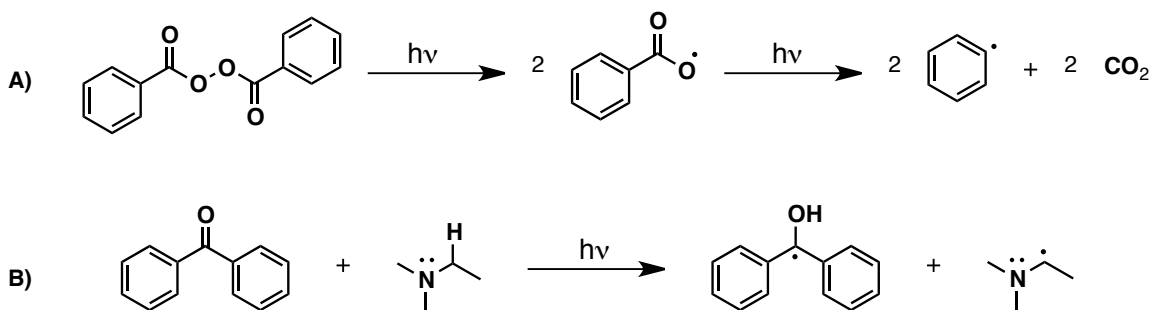


**Figure 1.5:** A) Type I photoinitiator using benzoyl peroxide as an example B) Type II photoinitiator using benzophenone as an example with a tertiary amine as a co-initiating species

There are several known advantages to conducting polymerisations photolytically instead of thermally. The ability to efficiently conduct selective reactions at ambient temperatures as well as providing an abundance of energy in comparison to reactions performed under thermal conditions. For example, the thermal energy present at 25 °C to activate a reaction is 130 times less than the energy present in one mole of photons that exists at 365 nm.<sup>11</sup> When performing these reactions with light, the light source can simply be taken away from the reaction mixture inhibiting further reactions providing excellent temporal control.<sup>11,12</sup> Thermally induced radical reactions do not have the advantage of time control as a result of mass and heat transfer. As a result of the several advantages accompanying photopolymerisations, these are commonly performed in industrial settings.<sup>13</sup>

### 1.1.3 Thiol-ene and Phosphane-ene Reactions

The hydrothiolation and hydrophosphination reactions results in the addition of an S-H or P-H bond, respectively across an alkene or alkyne (**Figure 1.6**).<sup>14,15</sup> These reactions can be used to generate polymers or polymer networks *via* free radical polymerisation and in this context, they are referred to as the thiol-ene and phosphane-ene reactions. These synthetic methods can be used to form high molecular weight polymers rapidly in the presence of a radical initiator resulting in the production of either sulfur- or phosphorus-rich polymer networks.

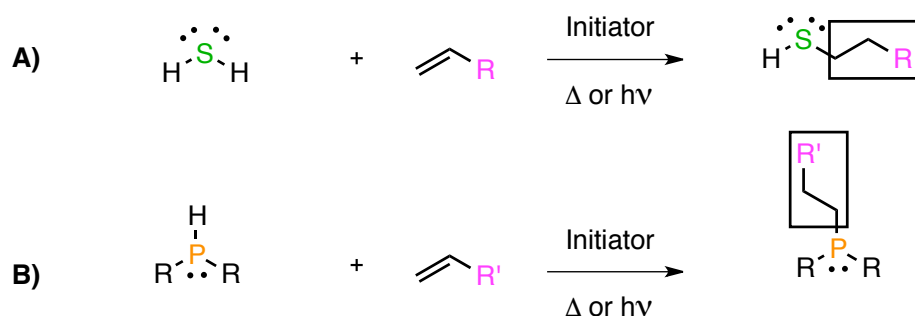


**Figure 1.6:** General reaction scheme of A) hydrothiolation and B) hydrophosphination

The thiol-ene and the phosphane-ene reactions proceed with the use of a radical initiator that promotes hydrogen abstraction from the E-H bond. This leads to the formation of thiyl and phosphinyl radicals that can then add across an alkene or alkyne. Propagation can then occur and ultimately produce a linear polymer or a branched polymer network depending on the functionality of the unsaturated compound (**Figure 1.7**). There were many benefits associated with the discovery of the thiol-ene reaction to form polymer networks as it is a radical-mediated, step-growth process exhibiting a high conversion rate. The use of the thiol-ene reaction to make polymers was developed well before the phosphane-ene reaction, which is reasoned to be a result of the accessibility of the starting materials. The phosphane-ene reaction involves the use of either  $\text{PH}_3$  or primary phosphines, which is likely a deterring factor from conducting reactions in a laboratory as unlike thiols, they are pyrophoric and toxic.<sup>15</sup> However, the formation of phosphorus containing polymers is desirable as they provide a variety of unique properties such as flame retardancy, allowing them to be sought after in various applications.<sup>16</sup>

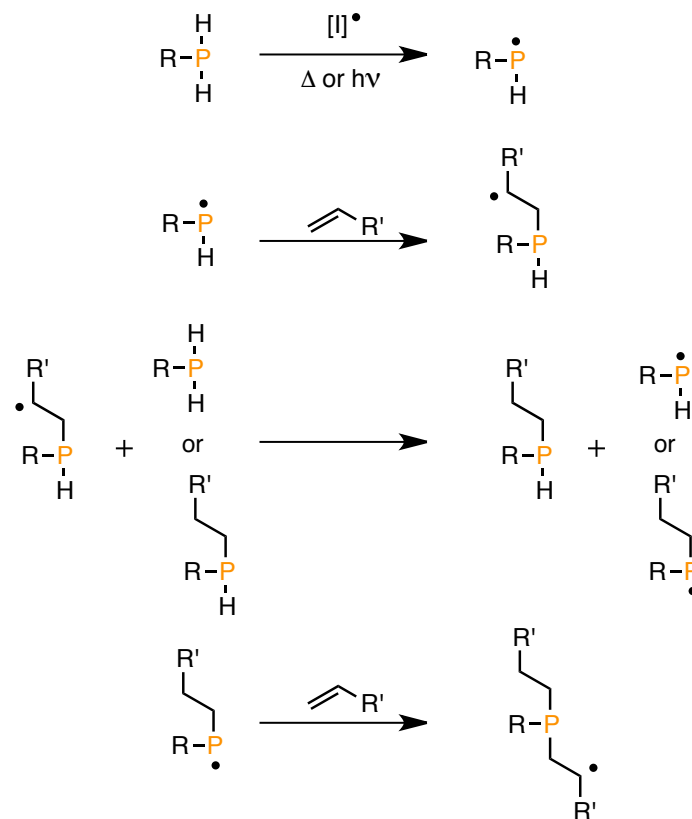


**Figure 1.7:** Initiating and propagating steps in the phosphane-ene reaction.

### 1.1.4 Polymer Networks

The various properties of a polymer are heavily dependent on the monomers chosen for polymerisation. The presence of solely bifunctional monomers throughout polymerisation results in the formation of one-dimensional linear polymers. In contrast, when a monomer with a functionality greater than two is used in polymerisation, a two-dimensional polymer network is the result (**Figure 1.8**). Polymer networks are comprised of crosslinks, which are defined as a bond that links one polymer chain to another. Crosslinking increases the rigidity of the material and manifests in a variety of different properties when compared to a linear analogue.<sup>17,18</sup> The presence of crosslinks in the polymer tend to inhibit the mobility of the material, which can have a profound effect on its solubility.

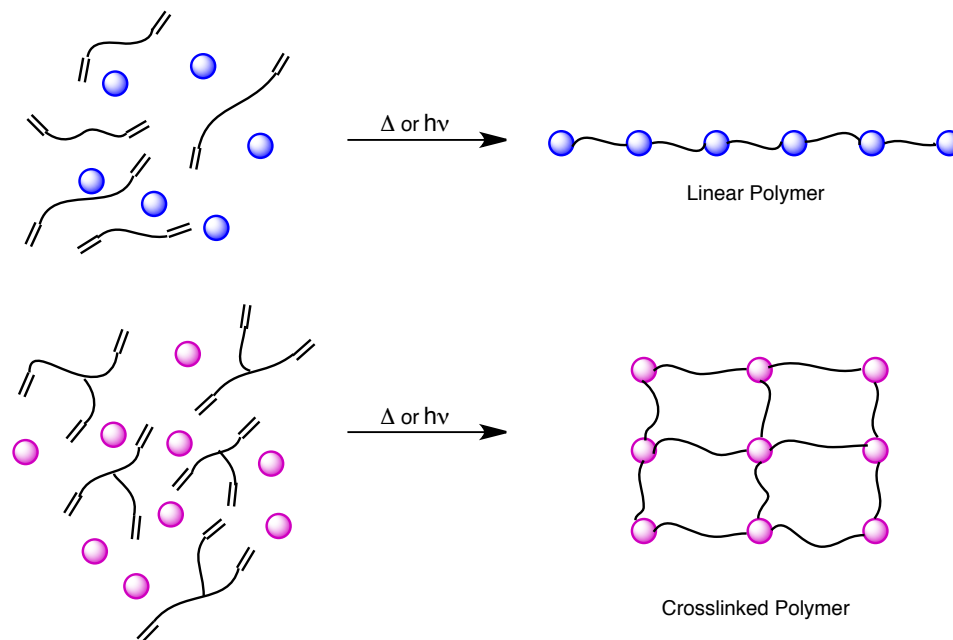


**Figure 1.8:** Comparing the formation of linear polymers versus crosslinked polymers.

### 1.1.4.1 Solubility of Polymer Networks

Depending on the extent of crosslinking within a polymer, the solubility behaviour of the material can be drastically affected. Linear polymers can typically dissolve in selective solvents given sufficient time. However, the dissolution behaviour of a crosslinked polymer is reliant on the extent of crosslinking present in the material. This is due to the solvation of chain segments being unable to overcome the efficacy of the covalent bonds found within the polymer. Some materials are unable to solubilize in solvents as a result of crosslinking. Depending on the polymer network, solvent can penetrate the network, which results in a subsequent increase in volume. This is a reversible process as the removal of solvent results in the polymer returning to its original form.<sup>17,18</sup> This phenomenon is referred to as swelling.

The ability of a polymer to swell in appropriate solvents occurs when the equilibrium concentration is reached. This concentration is contingent on a balance between the entropies of both the polymer-solvent mixing and the increase in free volume of the polymer.<sup>17,18,19,20</sup> This can be quantified using the Flory-Rehner equation, which assumes isotropic swelling.<sup>19</sup> The Flory-Rehner equation has several limitations, specifically, that it cannot be applied to crystalline or semi-crystalline materials due to the solvent inaccessible crystalline regions.<sup>18,21,22,23</sup> At the point of equilibrium, swelling is the



result of the interactions between the network and the liquid molecules. Subsequently, the flexible chains within the polymer become solvated.<sup>20,18,24</sup>

The ability of a polymer to swell accompanied by subsequent solvation results in the ability to perform solution-state nuclear magnetic resonance (NMR) spectroscopy on crosslinked polymer networks. It can be found that in heavily crosslinked polymers there is a difficulty in obtaining high resolution NMR spectra due to the immobility of the chains. This restricted mobility results in shorter relaxation times producing broader lines.<sup>25</sup> To mitigate this obstacle, it has been discovered that solvent swellable polymers can reduce the peak areas allowing for high resolution spectra. The degree of swelling and solvation is directly proportional to signal widths in NMR spectra.<sup>26,27</sup> This is advantageous as it allows for characterisation of materials post polymerisation using solution-state NMR spectroscopy.<sup>28,63</sup>

#### **1.1.4.2 Thermal Properties of Polymers**

The way a polymer behaves when exposed to heat is contingent once again on the composition and structure of the material.<sup>18,29</sup> Polymeric materials can be classified into three different categories describing the transition temperatures - melting temperature, crystallization temperature, and glass transition temperature. Once exposed to heat, a polymer can undergo a transition from a brittle, glassy state to a less rigid and softer consistency. The temperature at which this occurs is referred to as the glass transition temperature ( $T_g$ ). After heating, as the polymer begins to cool, the translational, vibrational, and rotational energies begin to decrease. Once they reach close to zero, the polymer can crystallize if symmetry requirements are met. The temperature at which this occurs is the crystallization temperature ( $T_c$ ).<sup>1</sup> The melting temperature ( $T_m$ ) can simply be defined as the temperature at which, upon heating, a phase change occurs resulting in the melting of the crystalline domains.<sup>18</sup> The values obtained for  $T_g$ ,  $T_m$ , and  $T_c$ , can be measured using differential scanning calorimetry (DSC) which monitors heat flow as a function of temperature.<sup>30</sup>

Not all polymers experience a  $T_g$ , as this is a value that is dictated by the morphology of the polymer. The crystalline domains present in the polymer typically exhibit a  $T_m$  and  $T_c$ , whereas a  $T_g$  occurs in the amorphous region of a polymer as these regions can alter their consistency once exposed to heat. In semi-crystalline polymers, the amorphous regions

would be affected once the  $T_g$  is reached, however, the crystalline regions would remain unaffected and maintain their brittle, glassy state.<sup>18,31</sup>

The value obtained for  $T_g$  is reliant on the mobility and flexibility of the polymer. Once temperatures exceed the  $T_g$ , free rotation occurring about single bonds is more accessible, allowing for the transition to the rubbery mobile state.<sup>18</sup> The energy necessary to free up the chains in the polymer are directly related to the mobility of the material. The more immobile the chains are, the more energy (higher temperature) is required to be put into the system to achieve this rubbery state. The  $T_g$  is also affected by the intramolecular forces experienced within the polymer, molecular weight, and the presence of crosslinking. Strong intermolecular forces require higher temperatures to transition from the glassy state to the rubbery state. This is because of the higher energy required to overcome the barrier resulting from these forces. Having a high molecular weight polymer decreases the mobility of the material resulting in an increased value obtained for  $T_g$ . The presence of crosslinks in a polymer restricts the rotational freedom, thereby increasing the  $T_g$ .

Polymer networks are classified into four different categories, which are related to the thermal or mechanical properties of the material. Thermoplastics are defined as polymers that melt or deform when exposed to heat, and subsequent cooling causes the material to solidify. In contrast, thermosets are referred to as materials that maintain their shape when exposed to heat, however, at sufficiently high temperatures these materials experience decomposition. Typically, thermoplastics are comprised of linear polymers and thermosets are comprised of crosslinked polymers. Polymers can also be classified as either elastomers or gels. Elastomers are materials that can undergo reversible stretching without fracturing. Gels are materials possessing a very soft texture which undergo deformation when experiencing an external force.<sup>18</sup>

Thermoplastics and thermosets are classified based on their interaction with heat. Thermosets typically have a high crosslink density which would result in a higher value obtained for  $T_g$  as more energy is required to cause the transition from the glassy to a rubbery state. In contrast, thermoplastics typically have a lower crosslink density meaning much less energy is required to undergo the transition required to obtain a  $T_g$ . As a result, thermoplastics are typically used well below their  $T_g$ .<sup>17</sup> Depending on the use of the material, thermosets or thermoplastics can be preferred.

## 1.2 Polymer Derived Ceramics

'Ceramic' refers to an inorganic solid material consisting of both metallic and non-metallic elements.<sup>32</sup> They can be formed in two different ways: conventional and advanced methods. Advanced ceramics or polymer derived ceramics (PDCs) are formed from preceramic polymers (*i.e.* polymers converted to ceramics through thermochemical decomposition) and have been gaining interest in the last 40 years due to the advantage they possess over the conventional ceramics. The main asset resulting from the production of advanced ceramics is the ability to shape the polymeric precursor prior to the formation of the ceramic.<sup>33</sup> PDCs are used in many applications, and they are at the forefront of new and emerging material science research.<sup>32,34,35,37,54</sup> Ceramics have found use in various coatings as the high temperature resistant property is desirable for a wide variety of applications and they are finding use in many other applications as a result of the electrical, magnetic, optical, chemical, and mechanical properties they can possess.<sup>35,36</sup>

Advanced PDCs are prepared from modified naturally occurring materials or from materials that are chemically synthesized.<sup>37</sup> These ceramics are formed upon the pyrolysis of a preceramic polymer which is a thermochemical decomposition process that involves heating a sample at medium to high temperatures (300-1300 °C) in the absence of oxygen.<sup>38</sup> As the temperature of the oven increases through the pyrolysis procedure, bond breakage throughout the polymer occurs leading to the formation of small organic compounds. These organic molecules then exit the system as volatile species and are responsible for the mass loss during the experiment.<sup>39</sup>

Advanced ceramics provide an advantage over the traditional ceramic as they can be tuned through the incorporation of different elements within the polymeric precursor producing various ceramics. Transition metal phosphides, for example, can be formed as the inclusion of various metals into the phosphorus containing preceramic material is readily possible.<sup>55,58,59</sup> The metals are then retained within the ceramic, while simultaneously infusing them throughout a carbon support. Where the properties of traditional ceramics are limited due to a lack of starting materials, advanced ceramics offer far more diverse properties because of the predesigned polymeric precursor. The polymer backbones have side chains that, together with the backbone, influence various properties of the polymers that influence the resulting ceramic. Preceramic polymers can be formulated with various

elements with a known stoichiometry of elements to impart numerous properties on the resulting ceramic.

### 1.2.1 Pyrolysis

Pyrolysis describes a decomposition process performed thermally in the absence of oxygen. It involves the breakdown of organic compounds into smaller molecules. As the material is heated, volatile compounds begin to undergo vaporization resulting in a decrease in the mass yield as the gas exits the pyrolysis chamber. Three different products can be formed throughout the thermochemical decomposition process in different states: a gas (exiting the chamber), oil (viscous liquid found in the sample boat), and char (solid material found in sample boat). The resulting composition of the char is dependent on the initial material that was pyrolyzed.<sup>38</sup>

Depending on the intended use of the ceramic, the processing parameters chosen throughout pyrolysis can be favoured to form a material that best suits its purpose. Several reports have been published explaining the various parameters that can be altered to form a ceramic that possess the targeted properties. Factors including porosity, crystallinity, conductivity, and chemical composition can be dictated based on what occurs throughout the heating process.

Preceramic polymers containing silicon have attracted tremendous amount of interest due to the desirable properties observed throughout the conversion to ceramics such as low processing temperature and controllable ceramic compositions.<sup>40</sup> There have been many reports on silicon containing ceramics as they have the potential to be used in many applications and because of that, a plethora of information can be found indicating the correct processing parameters for specific uses.

When deciding on the maximum temperature to choose for pyrolysis, the resulting material needs to be considered. When pyrolyzing silicon-containing polymeric precursors, typically temperatures below 1000 °C result in the production of amorphous ceramics and the introduction of crystallinity is known to occur above this temperature.<sup>41</sup> The temperature of the pyrolysis oven can also affect the resulting chemical composition and functional groups present in the ceramic. Targeting unsaturated bonds is commonly desired in semi-conducting ceramics and can typically be achieved by increasing the temperature.

Silicon carbide containing ceramics have proven to undergo a  $sp^3$  -  $sp^2$  transition when the temperature of the oven is increased from 1000 – 1400 °C.<sup>42,43</sup>

## 1.2.2 The Influence of Polymeric Precursors on Ceramics

Preceramic polymers consist of metal-organic compounds that make up the polymeric backbone. The structure and formation of the preceramic polymers directly influences the ceramic yield obtained after the pyrolysis procedure. A high ceramic yield ( $\alpha_c$ ) is desired for the polymer-to-ceramic conversion process and attests to the efficiency of the thermal treatment. The efficiency of this process is evaluated using Equation 1 where  $m_c$  is the resulting mass of ceramic and  $m_p$  is the initial mass of the preceramic polymer. Mass loss in the range of 10-30% is the ideal value associated with suitable preceramic polymers.<sup>44</sup>

$$\alpha_c = \frac{m_c}{m_p} \quad (\text{Equation 1})$$

There are several considerations to be made when formulating a polymeric precursor as a way to maximize ceramic yield.<sup>20</sup> The elemental composition of the preceramic polymer drastically affects this and pyrolyzing a mostly inorganic polymer network reduces the number of volatile organic fragments that are produced throughout the polymer-to-ceramic conversion process.<sup>45</sup> The thermal stability of the polymers is another crucial consideration when attempting to maximize ceramic yield. Thermal stability can be dictated by the bond dissociation energies (BDE) present within the polymer network, amount of crosslinking, or the side chains present.<sup>37,46</sup> Throughout the polymer-to-ceramic conversion process, low molecular weight materials can easily volatilize and depolymerize, leading to a decrease in ceramic yield. The ideal preceramic polymer would possess a high molecular weight, thereby decreasing volatilization throughout the heating process. Installing crosslinking or ring structures in the backbone can also decrease the degradation of the polymer throughout the experiment.

Crosslinking also provides the opportunity of forming a thermoset polymer. This offers the advantage of forming polymer networks that can retain their shape throughout the polymer-to-ceramic conversion process resulting in a shaped ceramic, which is desired for specific applications.<sup>47,48,49</sup> Maximizing the ceramic yield as well as incorporating various desired attributes for the ceramics (e.g., shaping) could result in the formation of materials for a variety of useful applications.

### 1.3 Ceramics in modern society

As green initiatives are more prevalent in today's society, it has become clear that our dependence on fossil fuels must end. Although these initiatives have become increasingly important amongst society, the greenhouse gas (GHG) emissions have risen by 1.5 % per year.<sup>50</sup> In an attempt to decrease the GHG emissions, substitutions for materials that contribute to air pollution are being investigated. Researchers are currently investigating renewable energy sources to try and mitigate the uses of non-renewable materials such as fuel in the automotive industry. Electric vehicles (EV) have become the forefront of this research as they can limit the dependence on non-renewable energy sources as well as mitigate GHG emissions that are a result of gas-powered vehicles.<sup>51</sup>

Research conducted on metal-air batteries have shown them to be a viable alternative to gas-powered vehicles. Electricity is generated from these batteries through a redox reaction that takes place between a metal and oxygen in the air.<sup>52</sup> They consist of a metal anode and an air breathing cathode that are separated by a suitable electrolyte composed of metal ions.<sup>51,52,53</sup> The electrolyte can be either aqueous or non-aqueous depending on the material chosen for the anode. The oxygen evolution reaction (OER) takes place as the metal anode is oxidized upon discharge. In this process, electrons are released into the electrical circuit. The electrons are accepted into the cathode as oxygen is diffused into the electrode. The metal ions and reduced oxygen species can combine to form metal oxides. The process is reversed upon recharge where the oxygen reduction reaction (ORR) takes place.<sup>51,52</sup>

Metal-air batteries have been around longer than the lithium-ion battery, as the first zinc-air battery was formulated in 1878. These batteries have not yet been applied to large scale industries because of the problems associated with the metal anodes and electrolytes. The ORR involves the breaking of a  $\pi$ -bond between the oxygen atoms which is associated with a high bond dissociation energy. This bond is difficult to break electrochemically and requires the use of electrocatalysts. The inefficiency of the current catalysts used in these systems inhibits the deployment of these batteries into various industries.<sup>51,53</sup>

As an alternative to EV's, hydrogen powered vehicles have also been considered as a substitute for gas powered vehicles. For hydrogen-powered vehicles to be a viable alternative, the industrial production of hydrogen needs to be optimized. There are currently three main production methods for hydrogen: steam methane reforming, coal

gasification and water electrolysis. Out of these methods, water electrolysis can potentially cleanly produce hydrogen whereas as the other two methods are dependent on fossil fuels.<sup>54</sup> Water electrolysis encompasses both the hydrogen evolution reaction (HER) and the oxygen evolution reaction (OER) to generate hydrogen gas and oxygen gas upon the dissociation of water. Oxygen gas is released into the atmosphere, whereas hydrogen gas is stored for later use as a fuel.<sup>54</sup>

Both potential alternatives to gas powered vehicles face an obstacle as platinum group metals are used as catalysts throughout the electrochemical reactions which entail a high cost as they are in the class of critical raw materials meaning they have a low earth abundance and limited availability.<sup>55</sup> This is resulting in the need for materials that can be used in place of platinum group metals. Some of the current examples being investigated in literature are transition metal chalcogenides, metal carbides, metal nitrides, metal phosphides, and metal oxides.<sup>56</sup> Amongst these metal phosphides have attracted interest amongst a variety of research groups.<sup>55,56,57,58,59</sup>

There are a variety of requirements to be met when formulating an electrocatalyst for the ORR and HER. When considering the HER, for example, the phosphorus atom acts as a proton-acceptor site, and the transition metals function as hydride-acceptor sites.<sup>59</sup> A challenge surrounding the introduction of metal phosphides as electrocatalysts is the complex synthetic procedures.<sup>58</sup> Another important consideration to be had in regards to these materials is their conductivity. Previous work in this area has determined that the percentage of phosphorus can alter the conductivity of these materials.<sup>55,60</sup> One of the challenges then, lies in finding a material that can provide the electrocatalytic properties as well as imparting the conductivity required for the HER. The ORR is similar in the sense that metal phosphides, specifically cobalt phosphide has proven to be a suitable substitute for the current Pt/C catalyst being used. Not only did the new metal phosphide catalyst display comparable catalytic properties, but it also displayed a better stability in some instances.<sup>55,59,61</sup> As a result, the desire for a facile synthetic method for these metal phosphides is sought after in this field.

## 1.4 Scope of Thesis

The above discussion encompasses the work depicted in this dissertation focusing on the optimization of phosphorus-containing photopolymer networks. Previous work targeting

the formation of PDC's accomplished by Dr. V. A. Beland focused extensively on characterization of the preceramic polymers and their resulting ceramics. The work presented in this thesis investigates methods to maximize ceramic yields of the polymeric precursors which better suits the application of polymer derived ceramics.<sup>28,62,63</sup>

Chapter two focuses on maximizing ceramic yield through the incorporation of new crosslinkers and through formulation variations. Each of the polymer networks formed consists of an organophosphorus compound, a crosslinker, and the linear additive, tetraethyleneglycoldiallyl ether, (TEGDAE). The amount of TEGDAE incorporated into the polymeric materials impacted the swelling ability of the networks as well as the ceramic yield. Finding a balance between the two was the first goal for this work. An optimal formulation was discovered for each network finding a perfect balance that not only allowed the polymer to swell for ease of further reactions taking place in the polymer, but also maintained a high ceramic yield with respect to the rest of the formulations. It was also discovered that the introduction of a new silicon containing crosslinker resulted in a much higher ceramic yield in comparison to the work performed by Dr. V. A. Beland. This is likely a result of new compound being mostly inorganic allowing the elements to be retained throughout the heating process. Chapter three explores the implications of metal coordination and subsequent pyrolysis of the optimal polymer formulations determined in chapter two.

---

<sup>1</sup> Odian, G.; *Principles of Polymerization*, 4<sup>th</sup> Ed.; Staten Island, NY, 2004

<sup>2</sup> Carothers, W.; H.; *J. Am. Chem. Soc.*; **1929**, *51*, 2548-2559

<sup>3</sup> Mills, N.; Jenkins, M.; Kukureka, S.; *Plastics Microstructure and Engineering Applications*; 4<sup>th</sup> Ed.; United Kingdom. 2020

<sup>4</sup> Zhang, D.; *Advances in filament yarn spinning of textiles and polymers*, 1<sup>st</sup> Ed.; United Kingdom, 2014

<sup>5</sup> Chen, M.; Zhong, M.; Johnson, J.; A.; *Chem. Rev.* **2016**, *116*, 10167-10211

<sup>6</sup> Feng, G.; Zhang, G.; Ding, D.; *Chem. Soc. Rev.*; **2020**, *49*, 8179-8234

<sup>7</sup> Tao, S.; Zhu, S.; Feng, T.; Zheng, C.; Yang B.; *Angew. Chem. Int. Ed.*; **2020**, *59*, 9826-9840

<sup>8</sup> Wardle, B.; *Principles and Applications of Photochemistry*; Padstow, Cornwall, Great Britain, 2009

<sup>9</sup> Dadashi-Salib, S.; Doran, S.; Yagci, Y.; *Chem. Rev.*; **2016**, *116*, 10212-10275

<sup>10</sup> Allushi, A.; Kutahya C.; Aydogan, C.; Kreutzer, J.; Yilmaz, G.; Yacgi, *Polym. Chem.*; **2017**, *8*, 1972-1977

<sup>11</sup> Chatani, S.; Kloxin, C. J.; Bowman, C. N.; *Polym. Chem.* **2014**, *5*, 2187-2201



- 
- <sup>12</sup> Corrigan, N.; Yeow, J.; Judzewitsch, P.; Xu, J.; Boyer, C.; *Angew. Chem. Int. Ed.*; **2019**, *58*, 5170-5189
- <sup>13</sup> Foussaier, J. P.; Lalevee, J.; *Photoinitiators for Polymer Synthesis*; Weinheim, Germany, 2012
- <sup>14</sup> Vaughan, W. E.; Rust, F. F.; *J. Org. Chem.*; **1942**, *7*, 472-476
- <sup>15</sup> Guterman, R.; Kenaree, A. R.; Gilroy, J. B.; Gillies, E. R.; Ragogna, P. J.; *Chem. Mater.*; **2015**, *4*, 1412-1419
- <sup>16</sup> Maiti, S.; Banejee, S.; Palit, S. K.; *Prog. Polym. Sci.*; **1993**, *18*, 227-261
- <sup>17</sup> Gu, Y.; Zhao, J.; Johnson, J. A.; *Angew. Chem. Int. Ed.*; **2020**, *59*, 5022-5049
- <sup>18</sup> Nicholson, J. W.; *The Chemistry of Polymers*, 3<sup>rd</sup> Edition; Chatham, Kent, UK, 2006.
- <sup>19</sup> Flory, P. J.; Rehner Jr.; J.; *J Chem. Phys.*; **1943**, *11*, 521-526
- <sup>20</sup> Jonquieres, A.; Roizard, D.; Lochon, P.; *J. Applied Polym. Sci.*; **1994**, *54*, 1673-1684
- <sup>21</sup> Rogers, C. E.; Stannett, V.; Szwarc, M.; *J. Chem. Phys.*; **1959**, *63*, 1406-1413
- <sup>22</sup> Brockmeier, N. F.; McCoy, R. W.; Meyer, J. A.; *Macromolecules*, **1973**, *6*, 176-180
- <sup>23</sup> Blackadder, D. A.; Keniry, J. S.; *J Applied. Polym. Sci*; **1972**, *16*, 1261-1280
- <sup>24</sup> Eslami, H.; Muller-Plathe, F.; *Solvation Effects on Molecules and Biomolecules*, 6<sup>th</sup> Ed.; 2008
- <sup>25</sup> Neppel, A.; Eaton, D. R.; Hunkeler, D.; Hamielec, A. E.; *Polymer*, **1988**, *29*, 1338-1342
- <sup>26</sup> Yokota, K.; Abe, A.; Hosaka, S.; Sakai, I.; Saito, H.; *Macromolecules*, **1978**, *11*, 95-100
- <sup>27</sup> Horowitz, D.; Horowitz, R.; Pinnell, R. P.; *Anal. Chem.*; **1980**, *52*, 1532-1534
- <sup>28</sup> Beland, V.A.; Ragogna, P. J.; *Chem Eur. J.*; **2020**, *26*, 12751-12757
- <sup>29</sup> Seymour, R. B.; Carraher Jr., C. E.; *Structure- Property Relationships in Polymers*, Boston, MA, 1984
- <sup>30</sup> Zheng, Q.; Zhang, Y.; Montazerian, M.; Gulbiten, O.; Mauro, J. C.; Zannotto, E. D.; Yue, Y.; *Chem. Rev.*; **2019**, *119*, 7848-7939
- <sup>31</sup> Balani, K.; Verma, V.; Agarwal, A.; Narayan, R.; *Biosurfaces: A Materials Science and Engineering Perspective*, 1<sup>st</sup> Ed.; Hoboken, New Jersey, 2015
- <sup>32</sup> Tanzi, M. C.; Fare, S.; Candiani, G.; *Foundations of Biomaterials Engineering*, London, United Kingdom, 2019
- <sup>33</sup> Bernardo, E.; Fiocco, L.; Parcianello, G.; Storti, E.; Colombo, P.; *Materials*, **2014**, *7*, 1927-1956
- <sup>34</sup> Han, S.; Feng, Y.; Zhang, F.; Yang, C.; Yao, Z.; Zhao, W.; Qiu, F.; Yang, L.; Yao, Y.; Zhuang, X.; Feng, X.; *Adv. Funct. Mater.*; **2015**, *25*, 3899-3906
- <sup>35</sup> Barroso, G.; Li, Q.; Bordia, R. K.; Motz, G.; *J. Mater. Chem. A.*; **2019**, *7*, 1936-1963
- <sup>36</sup> Colombo, P.; Mera, G.; Riedel, R.; Soraru, G. D.; *J. Am. Ceram. Soc.*; **2010**, *93*, 1805-1837
- <sup>37</sup> Segal, D.; *Chemical Synthesis of Advanced Ceramic Materials*, 1<sup>st</sup> Ed. Cambridge, England, 1989
- <sup>38</sup> Manara, P.; Zabaniotou, A.; *Renew. Sust. Energ. Rev.*, **2012**, *16*, 2566-2582
- <sup>39</sup> Eckel, Z. C.; Zhou, C.; Martin, J. H.; Jacobsen, A. J.; Carter, W. B.; Schaedler, T. A.; *Science*, **2016**, *351*, 58-62
- <sup>40</sup> Duan, L.; Ma, Q.; *Ceram. Int.*; **2012**, *38*, 2667-2671
- <sup>41</sup> Santhosh, B.; Ionescu, E.; Andreolli, F.; Biesuz, M.; Reitz, A.; Albert, B.; Soraru, G. D.; *J. Eur. Ceram Soc.*; **2021**, *41*, 1151-1162

- 
- <sup>42</sup> Wang, K.; Ma, B.; Li, X.; Wang, Y.; An, L.; *J. Am. Ceram. Soc.*; **2014**, *7*, 2135-2138
- <sup>43</sup> Cordelair, J.; Greil, P.; *J. Euro. Ceram. Soc.*; **2000**, *20*, 1947-1957
- <sup>44</sup> Greil, P.; *Adv. Eng. Mater.*, **2000**, *2*, 339-348
- <sup>45</sup> Blum, Y. D.; Schwartz, K. B.; Laine, R. M.; *J. Mater. Sci.*; **1989**, *24*, 1707-1718
- <sup>46</sup> Giannetti, E.; *J. Fluor. Chem.*; **2005**, *126*, 625-632
- <sup>47</sup> Gu, Y.; Zhao, J.; Johnson, J. A.; *Angew. Chem. Int. Ed.*; **2019**, *59*, 5022-5049
- <sup>48</sup> Odian, G.; *Principles of Polymerization*, 4<sup>th</sup> Ed.; Staten Island, NY, 2004
- <sup>49</sup> Nicholson, J. W.; *The Chemistry of Polymers*, 3<sup>rd</sup> Ed.; Cambridge, United Kingdom, 2006
- <sup>50</sup> Liu, L.; Qu, J.; Maraseni, T. N.; Niu, Y.; Zeng, J.; Zhang, L.; Xu, L.; *Int. J. Environ. Res. Public Health*, **2020**, *17*, 7077
- <sup>51</sup> Li, Y.; Dai, H.; *Chem. Soc. Rev.*; **2014**, *43*, 5257
- <sup>52</sup> Cheng, F.; Chen, J.; *Chem. Soc. Rev.* **2012**, *41*, 2172
- <sup>53</sup> Li, Y.; Lu, J.; *ACS Energy Lett.* **2017**, *2* 1370
- <sup>54</sup> Zou, X.; Zhang, Y.; *Chem Soc. Rev.*; **2015**, *44*, 5148-5180
- <sup>55</sup> Parra-Puerto, A.; Ng, K. L.; Fahy, K.; Goode, A. E.; Ryan, M. P.; Kucernak, A.; *ACS Catal.*; **2019**, *9*, 11515
- <sup>56</sup> Wang, J.; Fan, Y.; Qi, S.; Li, W.; Zhao, M.; *J. Phys. Chem. C.*; **2020**, *124*, 9350
- <sup>57</sup> Jiang, P.; Liu, Q.; Sun, X.; *Nanoscale*, **2014**, *6*, 13440
- <sup>58</sup> Tang, D.; Li, T.; Li, C. M.; *Int. J. Hydrog.* **2019**, *44*, 1720.
- <sup>59</sup> Lv, Y.; Wang, X.; *Catal. Sci. Technol.* **2017**, *7*, 3676
- <sup>60</sup> Carenco, S.; Portehault, D.; Boissiere, C.; Mezailles, N.; Sanchez, C.; *Chem. Rev.*; **2013**, *113*, 7981-8065
- <sup>61</sup> Doan-Nguyen, V. V. T.; Zhang, S.; Trigg, E. B.; Agarwal, R.; Li, J.; Su, D.; Winey, K. I.; Murray, C. B.; *ACS Nano*, **2015**, *9*, 8108-8115
- <sup>62</sup> Beland, V. A.; Ragogna, P. J.; *ACS Appl. Mater. Interfaces*, **2020**, *12*, 27640-27650
- <sup>63</sup> Beland, V.A.; Wang, Z.; Sham, T.K.; Ragogna, P. J.; *Angew. Chem. Int. Ed.* **2018**, *57*, 13252-13256

## Chapter Two

# 2 Modifying Polymeric Precursors to Maximize Ceramic Yield

## 2.1 Introduction

Polymeric materials have attracted interest as they are integrated into everyday life due to their range of properties. These materials can possess properties such as elasticity, rigidity, conductivity, flame retardancy, corrosion resistance, etc.<sup>1,2</sup> Until recently, excluding polyphosphazenes and polysiloxanes, organic polymers were the most widely used polymers. Research efforts have targeted inorganic polymers for their unique chemical and physical properties which could be relevant in applications that organic polymers cannot satisfy. One area that benefits from the use of inorganic polymers is in the formation of polymer derived ceramics (PDCs), which are predominately derived from silicon based polymeric materials.<sup>2,3,4</sup> PDCs have gained considerable amounts of interest in the last 50 years as a result of the superb properties (conductivity, hardness, etc.) they possess and the synthetic ease required for formation.<sup>5</sup> To form PDCs, organometallic or inorganic polymers are subjected to thermochemical decomposition in a controlled atmosphere, such as a tube furnace.<sup>10</sup> The formation of the polymer, prior to pyrolysis is imperative when forming ceramics as the preceramic polymer dictates the resulting product.<sup>6,7</sup>

This work has been extended into the phosphane-ene reaction which utilizes monomeric organophosphorus compounds to form phosphorus containing polymers.<sup>8,9,24</sup> The implementation of various inorganic elements (besides silicon) has been shown to alter the thermostability and various properties of the resulting ceramics.<sup>10</sup> Phosphorus containing ceramics are advantageous in terms of electrocatalysts for the automotive industry. Subsequent pyrolysis of a polymer containing various metals (Co, Ni, Fe, Cu, etc.) results in the formation of ceramics that contain metal phosphides. These ceramics have shown promising results as replacements to the current platinum catalyst being used in various applications, the HER or ORR for example.<sup>11</sup> In these materials, the phosphorus atoms acts as a proton-acceptor site, and the transition metals function as hydride-acceptor sites, required for the catalytic process within fuel cells or metal-air batteries.<sup>12,13</sup> The challenge

then, lies in finding a material that can provide the electrocatalytic properties as well as imparting the necessary conductivity.<sup>14,15</sup>

To overcome the conductivity obstacle, the Ragogna group has previously attempted forming PDCs from phosphorus containing polymers. In doing this, the hydrophosphination reaction was used to produce a polymer network with high molecular weights. Prior to pyrolysis, these polymeric precursors underwent further modification at the tertiary phosphine active sites allowing for the implementation of metals.<sup>8,9,24</sup> These metallopolymers were then pyrolyzed in an attempt to see if this method was suitable for PDCs. It was found that incorporating metals, specifically cobalt, in the polymer prior to pyrolysis resulted in the formation of a metal phosphide with an increased ceramic yield in comparison to the unmetallated analogue.<sup>8</sup>

Although this work revealed that cobalt phosphides could be produced while embedded into a carbon support, the low ceramic yield limited the applicability of these materials as PDCs. Increasing the presence of crosslinks within the polymer as well as incorporating more inorganic elements into the polymeric precursor is hypothesized to have a positive increase in the ceramic yield. Having the ability to modify the polymers post polymerisation is a valuable advantage as it could potentially lead to enhanced mobility into the material. A crosslinker produces links between polymer molecules and the elasticity or rigidity of a polymer is dependent on the number of crosslinks present. Specifically, the higher the crosslink density, the more rigid the polymer.<sup>16</sup> To accommodate further modification of the polymer, a high crosslink density can restrict the motion of the chains resulting in challenges with further reactions. To combat this issue, linear additives can be added to the formulation which in contrast to the crosslinker, will allow for more interstitial space within the polymer. This allows the active sites within the polymers (tertiary phosphines) to be more accessible; however, the ceramic yield will decrease because of the less crosslinked network. To achieve the highest ceramic yield while maintaining the swelling properties required for polymerisation, a balance needs to be made between the starting monomers (crosslinker, linear additive, phosphine).

This chapter focuses heavily on the synthesis and characterisation of solvent-swelling preceramic polymer networks with a phosphorus containing backbone. The phosphane-ene reaction was employed to form these networks utilizing a commercially available primary

phosphine and various crosslinkers/chain extenders. Finding the balance between the linear additive and crosslinkers present in the networks was the main goal in this work. The networks were then pyrolyzed to understand the impact of crosslinking on ceramic yield in these phosphane-ene polymers.

## 2.2 Synthesis

In this work, polymer networks were generated *via* a hydrophosphination reaction between monoisobutylphosphine, various ratios of trifunctional (**1**) and tetrafunctional (**2**) crosslinkers, and a linear additive, tetraethylene glycol diallyl ether (TEGDAE) (**3**) (**Figure 2.1**). Ceramic yield was maximized through the incorporation of a higher percentage of crosslinker, since this decreases the volatility of the polymer throughout the thermal decomposition process. It was hypothesized that although a higher ceramic yield will be achieved, limiting the amount of TEGDAE will result in a decreased percent swellability. This will inhibit the ability to perform post polymerisation modification due to the inaccessibility of the reactive sites throughout the network.

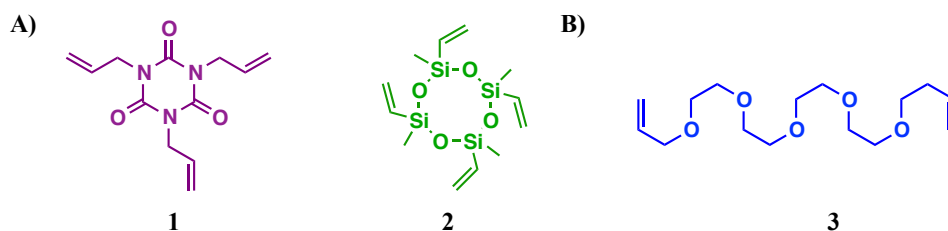


**Figure 2.1:** Starting materials used for polymerisation. **A)** Crosslinkers used in this work. **1:** 1, 3, 5- triallyl - 1, 3, 5- triazine - 2, 4, 6- trione (TTT), and **2:** 2, 4, 6, 8 – tetramethyl - 2, 4, 6, 8-tetravinylcyclotetrasiloxane. **B)** Linear additive used to increase swellability. **3:** Tetraethyleneglycol diallyl ether (TEGDAE)<sup>17</sup>

Solvent swellable phosphane-ene polymer networks were prepared using a previously reported procedure.<sup>28</sup> In the present work, formation of each polymer utilized monoisobutylphosphine with linear additive TEGDAE; **3** as well as trifunctional crosslinker, 1, 3, 5- triallyl - 1, 3, 5- triazine - 2, 4, 6- trione (TTT; **1**) or tetrafunctional crosslinker, 2, 4, 6, 8 – tetramethyl - 2, 4, 6, 8- tetravinylcyclotetrasiloxane (**2**). The networks were formed photolytically in the presence of phenylbis(2,4,6-trimethylbenzoyl)-phosphine oxide (BAPO; 0.5 wt%;  $\lambda_{\text{max}} = 371 \text{ nm}$ ) as the photoinitiator. Polymer networks were formed by the free radical hydrophosphination reaction of monoisobutylphosphine

(4) to the crosslinker and TEGDAE. The goal of this work is to determine the threshold for the amount of TEGDAE needed to create the least amount of impact on the ceramic yield. Varying ratios of the starting formulations were tested to determine the optimal quantity required. The ratios were manipulated to ensure that the number of olefins from both the crosslinker and the linear additive were equal to the number of P-H bonds in the system. This allowed for the generation of only tertiary phosphine environments within the network. The trifunctional crosslinker was added in ratios that steadily decreased by 1/6 (Figure 2.2) whereas the tetrafunctional crosslinker was added in ratios that decreased by 1/8 (Figure 2.3). In both cases TEGDAE was added in ratios that steadily increased by 1/4. For the polymer containing the trifunctional crosslinker (1), four derivatives were made (1.1 - 1.4). The polymer synthesized with tetrafunctional crosslinker (2) had eight different derivatives made (2.1 - 2.8). As the presence of TEGDAE increased after formulations 1.4 and 2.8 the polymers no longer maintained their shape throughout testing eliminating these derivatives from further investigation.

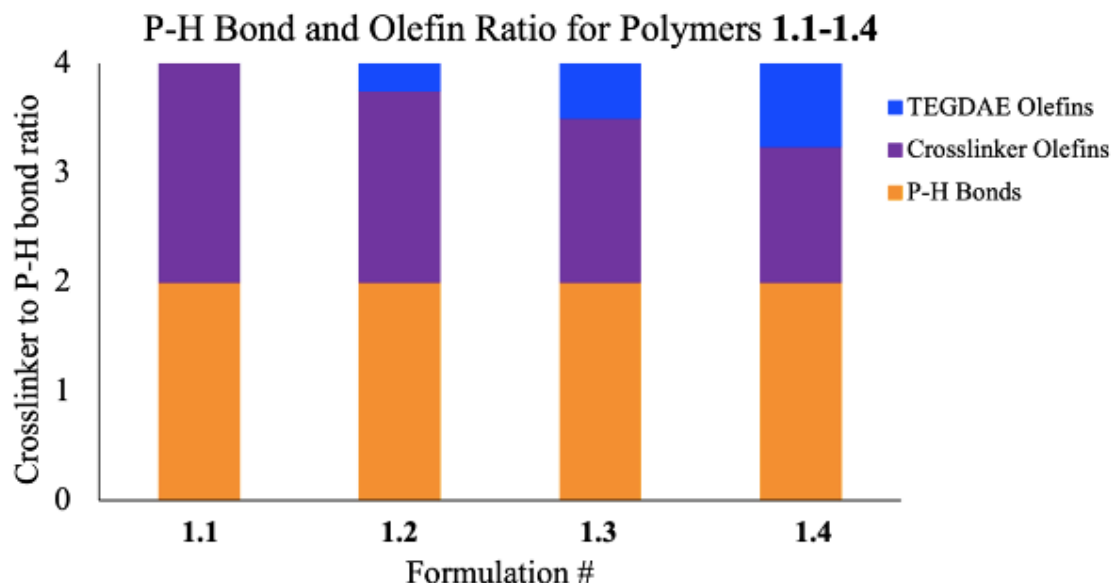
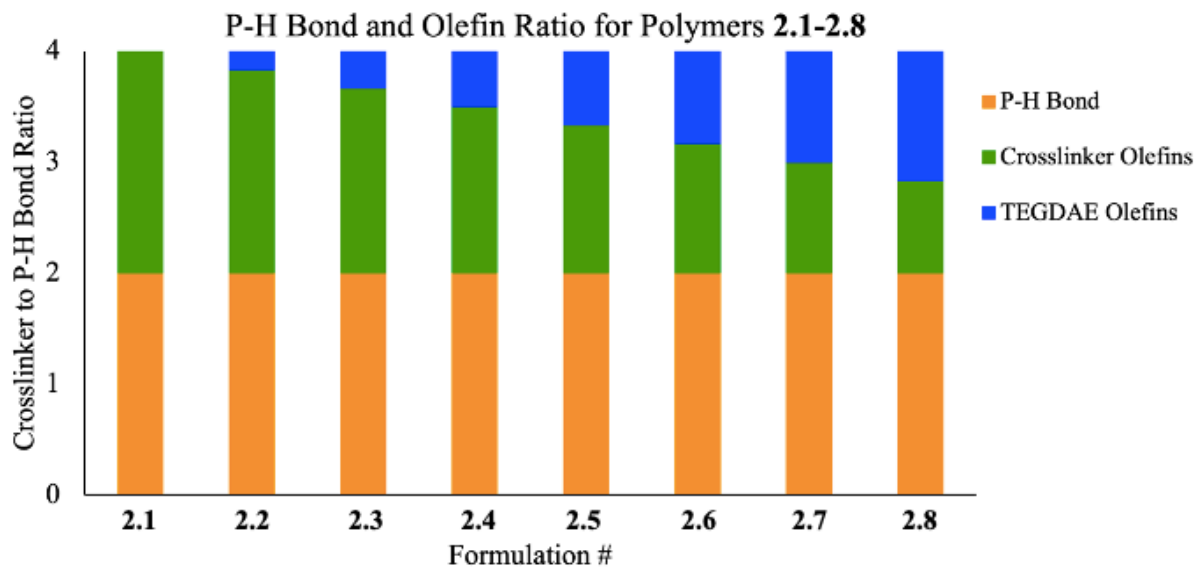
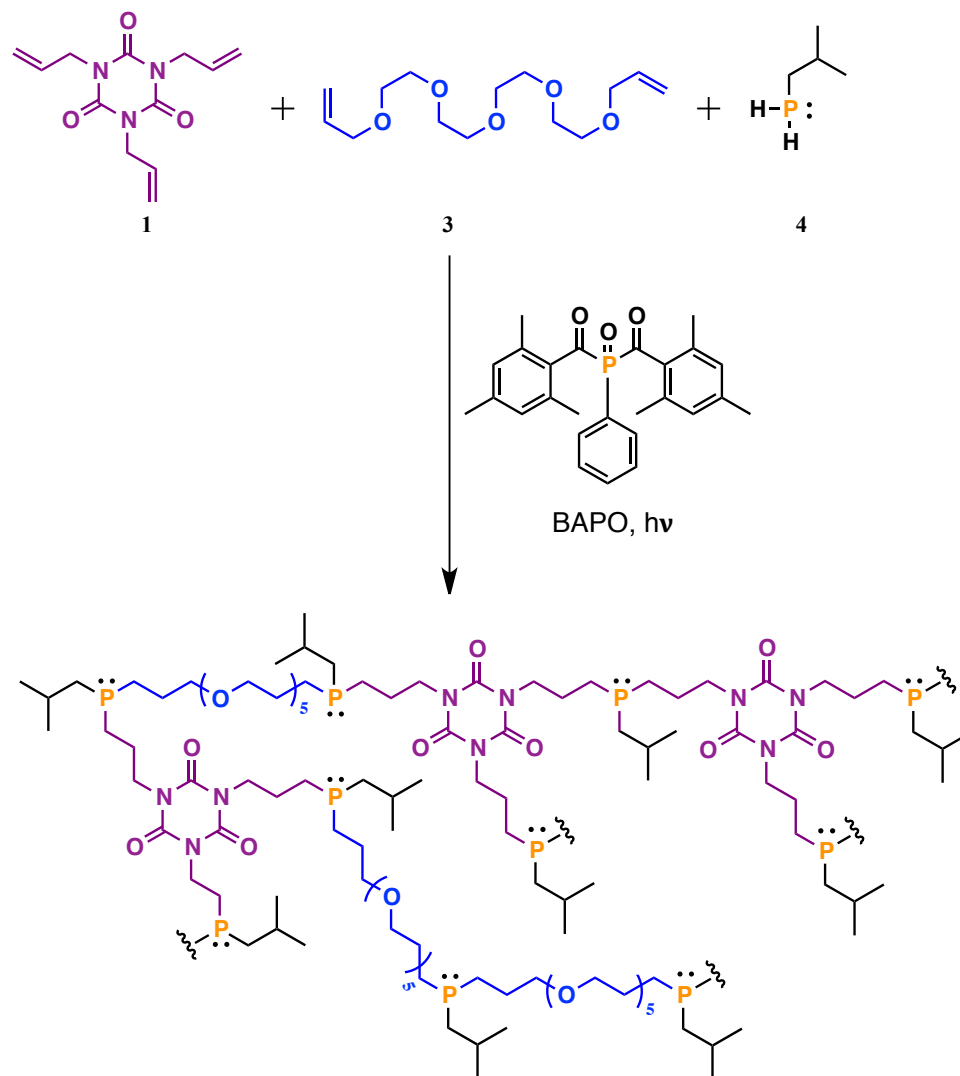


Figure 2.2: P-H bond to olefin ratio for polymers (1.1 - 1.4) with trifunctional crosslinkers.



**Figure 2.3:** P-H bond to olefin ratio for polymers (2.1 - 2.8) with tetrafunctional crosslinker.

Once monoisobutylphosphine, TEGDAE (3), either crosslinker 1 or 2, and BAPO were mixed, a clear yellow mixture resulted and was irradiated under a UV light belt for 15 minutes, which formed a clear and colourless gel (Scheme 1.1). Polymer 1.1 and 2.1 displayed the hardest profile and as the ratio of TEGDAE increased each polymer became more malleable resulting from the increased flexibility within the polymer.



**Scheme 1.1:** Phosphane-ene reaction to form polymer networks with a trifunctional crosslinker.

This reaction was monitored using  $^{31}\text{P}$  NMR spectroscopy, which upon synthesis of the network has the potential to show distinct substitution patterns at phosphorus environments: primary, secondary, and tertiary. The ratios targeted each P-H bond undergoing the hydrophosphination reaction and the resulting tertiary phosphine signals (typically **1.1**:  $\delta_{\text{P}} = -35.0$ ; **2.1**:  $\delta_{\text{P}} = -25.0$ ) and, occasionally, a primary phosphine signal (typically  $\delta_{\text{P}} = -150.5$ ;  $^1J_{\text{PH}} = 193.2$  Hz) was observed. This is a result of the tertiary phosphine sites present within the polymer as well unreacted primary phosphine (**4**) present in the network, which can be removed under reduced pressure. The progress of this reaction was also monitored using  $^{13}\text{C}\{^1\text{H}\}$  NMR spectroscopy, which confirmed the reaction had



reached completion as indicated by the disappearance of the olefin signals (**4**:  $\delta_C = 135.1, 116.4$ ; **1**:  $\delta_C = 131.1, 118.0$ ; **2**:  $\delta_C = 136.2, 133.3$ ).

The reaction progress can also be observed using infrared (IR) spectroscopy, which can aid in assessing the cure percentage (**Equation 1** and **Equation 2**). Acquiring the IR spectra of both the cured and the uncured formulations allows for the reaction to be monitored both quantitatively and qualitatively. The calculation of cure % can be done using the ratios of two different functional groups present in the network. One of the signals (signal 1) involves an alkene functionality as the peak intensity will decrease significantly throughout the hydrophosphination reaction. The second signal (signal 2) chosen should be for a functionality that remains consistent throughout the reaction (**1.1**: C=O;  $1680\text{ cm}^{-1}$ , **2.1**: Si-CH<sub>3</sub>;  $1258\text{ cm}^{-1}$ ). Prior to determining the peak intensity, the spectra were normalized to account for any baseline differences. Using signals 1 and 2, a ratio can be obtained, which can be used to calculate cure % (**Equation 1**).

$$\text{Ratio} = \frac{\text{Signal 1}}{\text{Signal 2}} \quad (\text{Equation 1})$$

Once the ratio is determined **Equation 2** can be used (X= ratio of uncured material; Y= ratio of cured material) to determine a quantitative value for cure %. Polymer **1.1** displayed a cure % of 61 % indicating the presence of unreacted TTT still trapped within the network. Polymer **2.1** displayed a cure percentage of 93 % suggesting that most of the material was cured with initial exposure to UV light.

$$\text{Cure \%} = \frac{X-Y}{X} \times 100 \% \quad (\text{Equation 2})$$

Cure % was also estimated qualitatively as a decrease in the intensity of the P-H stretch ( $\nu_{\text{P-H}} = 2290\text{ cm}^{-1}$ ) can be observed when comparing the uncured spectra to the cured spectra for both polymers **1.1** and **2.1** (**Figure 2.4**). Similar to this, a significant decrease

can be observed in the signal corresponding to the alkene functionality (**1.1**:  $\nu_{\text{C}=\text{O}} = 1680 \text{ cm}^{-1}$ ; **2.1**:  $\nu_{\text{Si}-\text{CH}_3} = 1258 \text{ cm}^{-1}$ ) as it is participating in the hydrophosphination reaction.

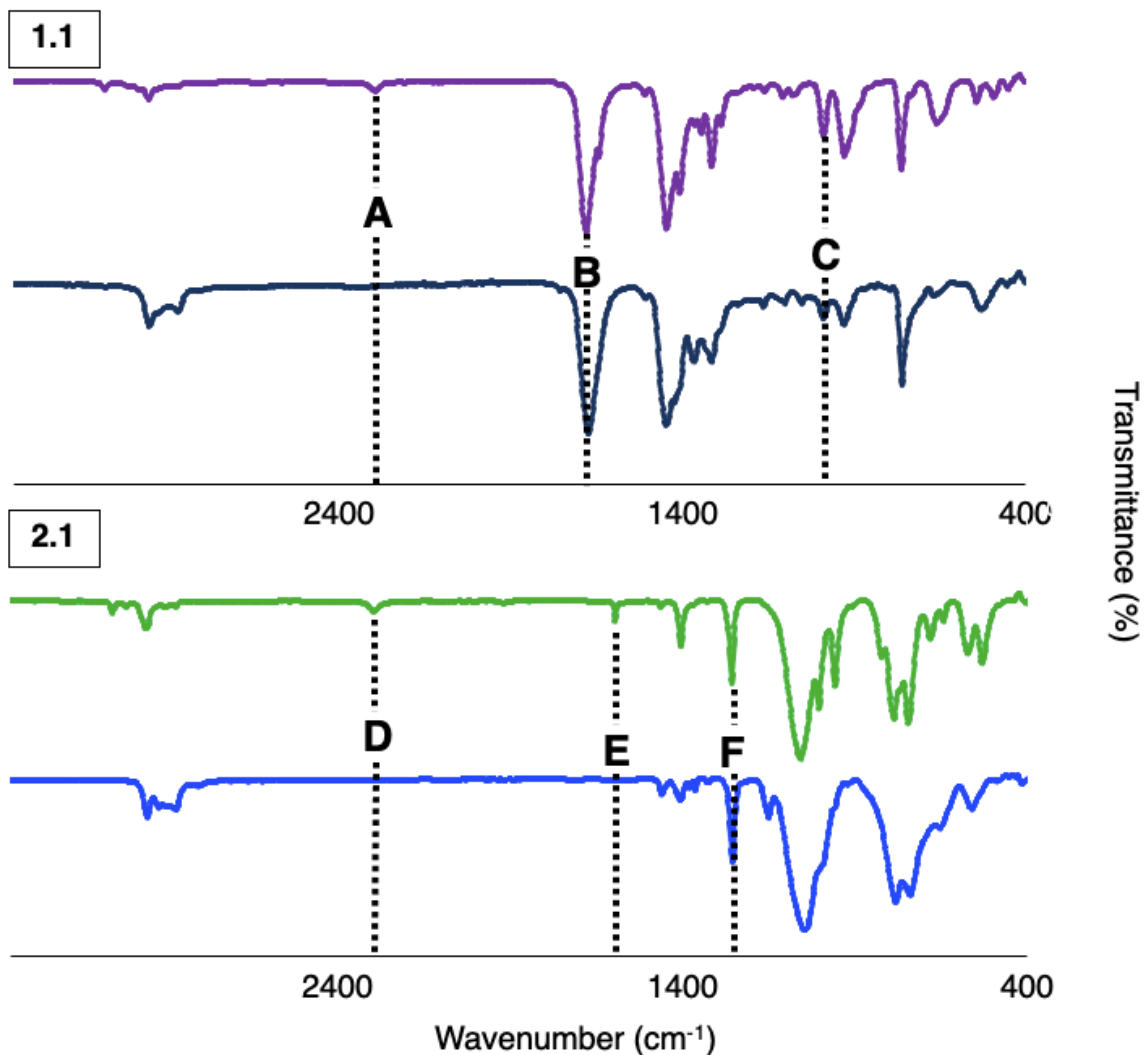


**Figure 2.4:** IR spectra of uncured (purple and green) and cured (black and blue) pucks **1.1** and **2.1**. A:  $\nu_{\text{P-H}} = 2290 \text{ cm}^{-1}$ ; B:  $\nu_{\text{C}=\text{O}} = 1680 \text{ cm}^{-1}$ ; C:  $\nu_{\text{C}=\text{C}} = 991 \text{ cm}^{-1}$ ; D:  $\nu_{\text{P-H}} = 2290 \text{ cm}^{-1}$ ; E:  $\nu_{\text{Si}-\text{CH}_2=\text{CH}_3} = 1596 \text{ cm}^{-1}$ ; F:  $\nu_{\text{Si}-\text{CH}_3} = 1258 \text{ cm}^{-1}$ .

### 2.3 Swelling Properties

Depending on the intended use for the material, the ability for a polymer to swell in a given solvent is a desirable property to allow for the ability to further modify the polymer. This will allow for different reactions to take place at active sites, such as a phosphine, within the material. With the polymers in hand, swellability and gel content tests were performed

to understand how a given solvent interacts with the polymer. The purpose of these tests was to understand the impact that TEGDAE imposed on the overall system. Upon formation of the polymers, swell tests were performed as well as gel content values were collected. In this work, a materials ability to swell can be explained by a mass increase experienced in the polymer as a result of the uptake of a solvent.<sup>18</sup>

$$\text{Swelling \%} = \frac{m_s - m_i}{m_i} \quad (\text{Equation 3})$$

Determining a polymer's ability to swell can be calculated using **Equation 3**, where the swelled weight ( $m_s$ ) was compared to the dried network weight ( $m_i$ ). Once the swelled network is dried, gel content could be calculated using **Equation 4**, where  $m_i$  is the mass of the initial dried network and  $m_d$  is the mass of the final dried network. The values obtained from a gel content experiment determine the ability of a solvent to leach unreacted materials from the network. Each polymer puck sample was swelled in triplicate in each solvent, allowing for the collection of an average and a standard deviation.

$$\text{Gel Content} = \frac{m_i}{m_d} \times 100 \quad (\text{Equation 4})$$

The formulations shown in **Figure 2.2** and **Figure 2.3** were combined with photoinitiator, BAPO, placed in a mold and irradiated to form a polymer network that were shaped as disks with diameters of 1.8 cm. Pucks were then swelled in several common reaction solvents and their mass difference was noted to calculate the swelling properties of the networks. Drying the swelled networks ultimately enabled the acquisition of gel content values.

Networks composed of only monoisobutylphosphine and crosslinker **1** or **2** (polymers **1.1** and **2.1**) were generated to obtain a baseline measurement to allow for the comparison of the other polymer series containing TEGDAE. In these derivatives, phosphine and crosslinker **1** or **2** were combined in a 3:2 and a 3:4 molar ratio respectively, ensuring that each P-H bond underwent the hydrophosphination reaction with the corresponding olefin present on the crosslinkers. After performing the swell tests, it was evident that polymer derivatives that are completely devoid of TEGDAE not only displayed a limited swelling capability, but also resulted in a broad signal in the  $^{31}\text{P}\{^1\text{H}\}$  NMR spectra. This further attests to the low swellability of this derivative, signalling that post polymerisation modification would be more challenging.

These data agreed with the hypothesis that the inclusion of TEGDAE allows for a material to possess a high swelling capability. As shown in **Figure 2.5** and **Figure 2.6**, a direct correlation is observed between the incorporation of TEGDAE and swell %. As the amount of TEGDAE increased from derivative **1.2** and **2.2** to derivatives **1.4** and **2.8**, a noticeable increase was observed in the swelling ability of these materials. The presence of TEGDAE allows for larger interstitial spaces within the polymer, enabling more solvent to enter the material, causing it to swell thus making onwards chemistry of the networks much more accessible.<sup>28</sup>

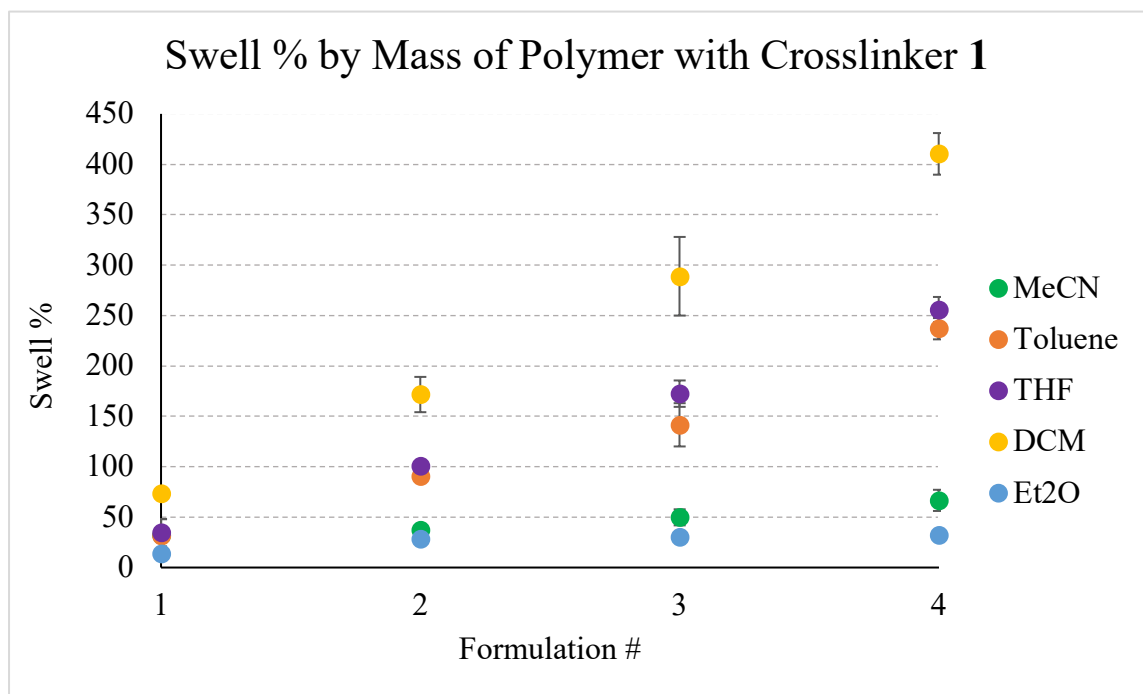


**Figure 2.5:** Swell % by mass for polymers (**1.1 - 1.4**) with tetrafunctional crosslinker.

Polymers containing either the trifunctional or tetrafunctional crosslinkers displayed the same general trend in terms of ranking the solvent by their ability to swell the material. Dichloromethane (DCM), tetrahydrofuran (THF) and toluene were consistently the best ranked solvents for all the polymer derivatives. These solvents were best able to enter the interstitial spaces within the polymer causing a high swell % by mass value. Acetonitrile (MeCN) and diethyl ether (Et<sub>2</sub>O) were the solvents that persistently displayed low values for swell % indicating that these solvents have a lower ability to enter the interstitial spaces present in the polymer network and are likely poor solvents to explore onwards chemistry.

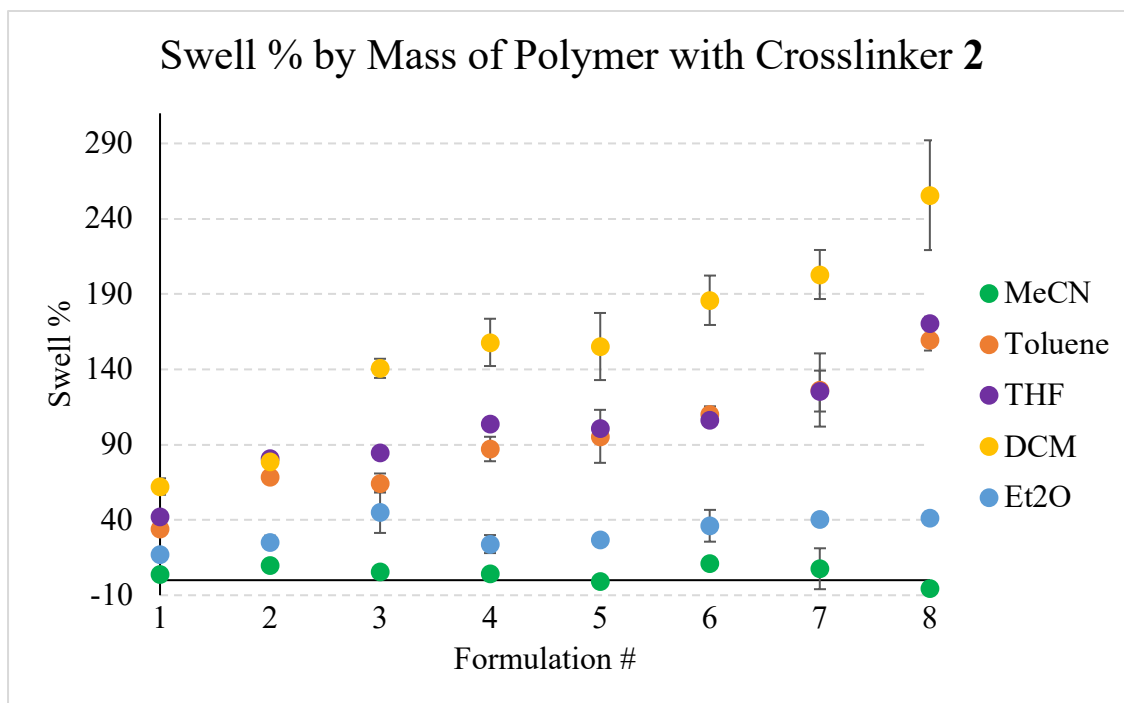


**Figure 2.6:** Swell % by mass for polymers (2.1 - 2.8) with tetrafunctional crosslinker.

The next step in this work was to prove that the ability of a material to swell was in direct correlation with the line width of polymer derivatives on a NMR spectrum. In the work previously done by our group, it was observed that the line width was dependent on a solvent that both swelled the polymer networks and interacted with the polymer chains.<sup>25</sup> In order to prove this determination, the values obtained for swell % by mass were converted to values expressed in terms of molar swellability ( $M_s$ ). This was done using **Equation 3** which divides the solvents molecular weight (MW) by the value obtained for swell % by mass of each of the given polymers. This equation expresses values for  $M_s$  in terms of mmol/g.<sup>19</sup>

$$M_s = \frac{\text{Swelling \% value}}{\text{Solvent MW}} \quad (\text{Equation 3})$$

When expressing the values in terms of  $M_s$ , the same general trend was observed when ranking solvents. DCM, THF, and toluene proved to be the most suitable solvents for performing post polymerisation modification as they were best able to enter the interstitial spaces within the polymer. Polymer 1.1 was an anomaly however, as acetonitrile (MeCN) and DCM were the solvents that were best able to swell the material. This can be attributed to the small size of acetonitrile in comparison to the remaining solvents. As the presence

of TEGDAE increased in the various derivatives an increase can be noted in the swelling ability of the material as shown in **Figure 2.7** and **Figure 2.8**.

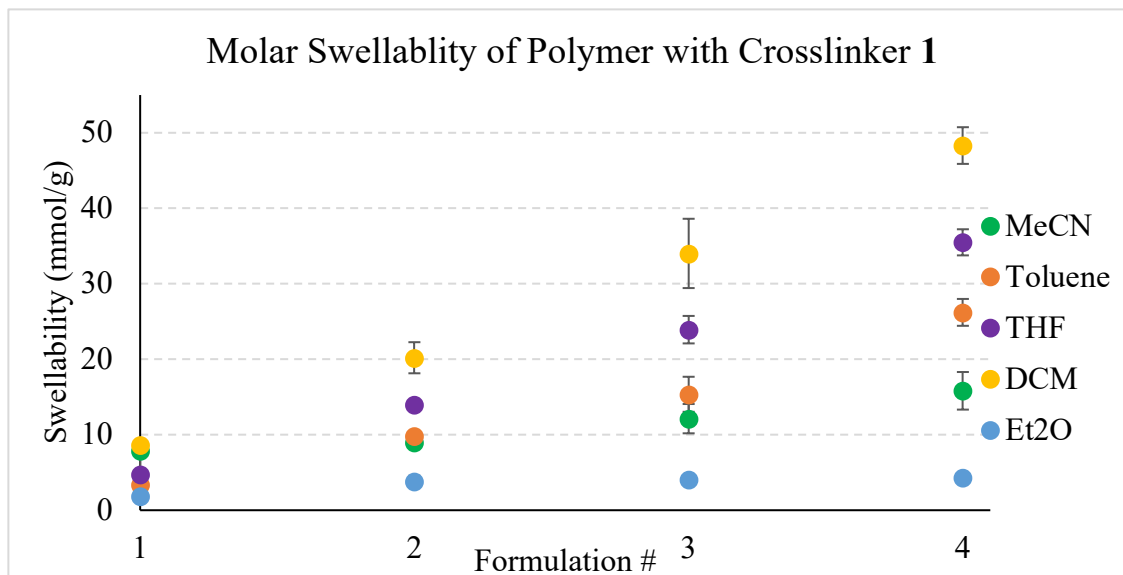


**Figure 2.7:** Plot of molar swellability values for polymers **1.1 – 1.4**.

Polymer derivatives **2.4** and **2.5** do not show significant contrast in terms of molar swellability values (**Figure 2.8**). This indicates that in this instance, altering the amount of TEGDAE does not play a substantial role in the inner workings of the polymer. The size of interstitial spaces present in the material do not increase by a critical amount resulting in a limited swelling ability.

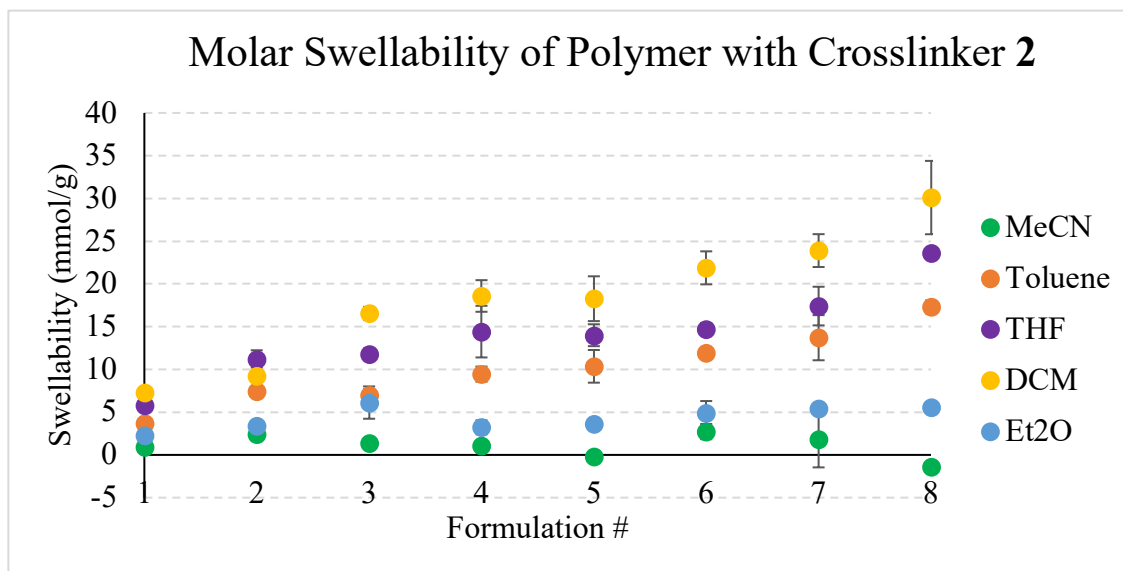


**Figure 2.8:** Plot of molar swellability values for polymers **2.1 – 2.8**.

The conversion of values to  $M_s$  allows for the comparison of the swelling abilities of materials to the NMR signal's line width of acquired spectra. Acquiring NMR spectra for the various derivatives in each of the reaction solvents used for testing and comparing them to the data collected in **Figure 2.7** and **Figure 2.8** led to some interesting conclusions. It was noted that there was a relationship between line width from a signal in an NMR spectrum and  $M_s$ .<sup>25</sup> This relationship is most clearly exhibited in polymer **1.1**. **Figure 2.9** depicts the NMR spectra for each of the polymer derivatives formed using crosslinker, **1**, collected in each of the reaction solvents used for testing. Derivative **1.1** displays the broadest signals which is indicative of a crosslinked polymer network. When the NMR spectra was obtained in MeCN and DCM the line width of the polymer become much more narrow. By comparing these data to those presented in **Figure 2.7**, MeCN and DCM were the two solvents that were best able to swell the polymer in terms of  $M_s$ .

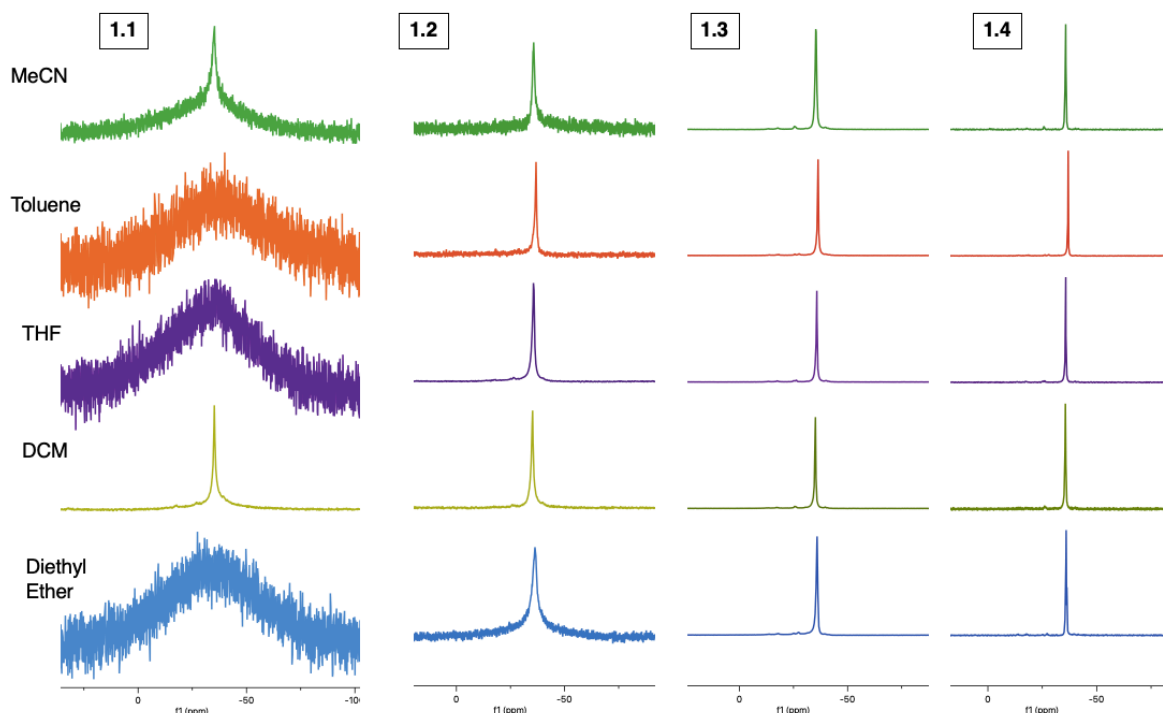


**Figure 2.9:**  $^{31}\text{P}\{^1\text{H}\}$  NMR spectra of polymers **1.1** - **1.4** in various reaction solvents.

The reason for the change in the signal line width is not only because of  $M_s$ , but it can also be attributed to the chains being solvated when introduced to various solvents. Upon uptake of solvent the polymer first undergoes swelling then a subsequent solvation of the chains takes place.<sup>25,19</sup> The solvation of polymer chains in certain instances mainly affects the flexible chains within the polymer. These flexible chains, likely from TEGDAE, contain

high swelling properties, which explains why the swelling values increase as the presence of TEGDAE is higher. This conclusion also supports the data which sees the signals line width of each of the derivatives getting narrower as the presence of TEGDAE is increased.

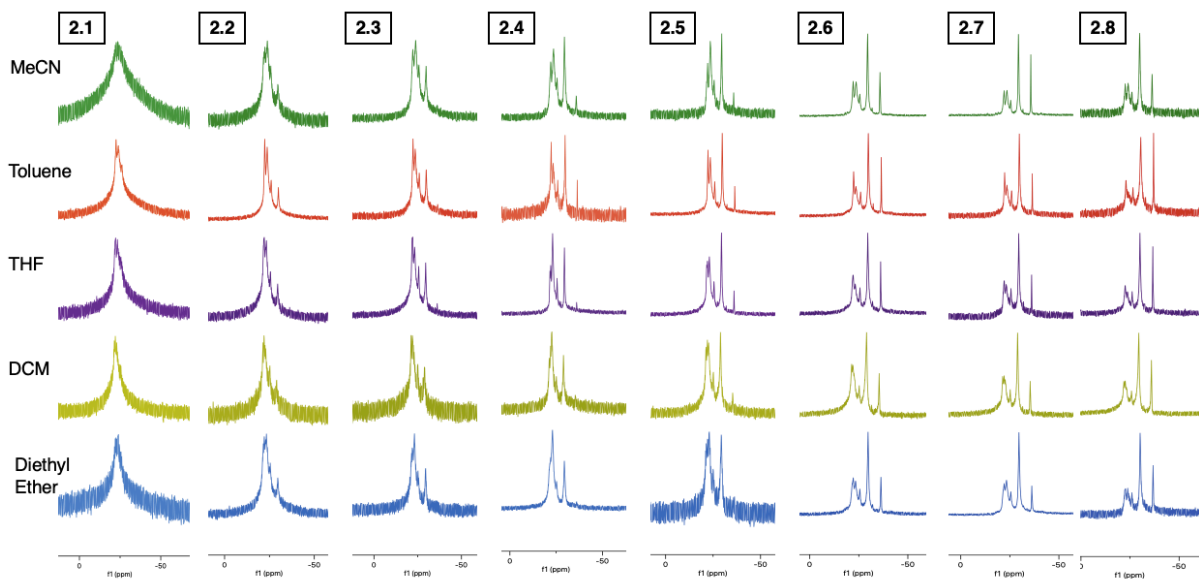


**Figure 2.10:**  $^{31}\text{P}\{^1\text{H}\}$  NMR spectra of polymers **2.1** - **2.8** in various reaction solvents.

The NMR spectra acquired for the polymer derivatives formed using crosslinker **2** displayed three distinct signals in the cluster (**Figure 2.10**). The signal positions were all indicative of tertiary phosphines and can be explained by phosphorus being bound either to two crosslinkers, two TEGDAE, or one crosslinker and one TEGDAE. Model reactions completed with only phosphine and TEGDAE confirmed the signal at the lower  $\delta$  correspond to phosphorus bound to TEGDAE only (**Figure 2.11**). The peak furthest downfield is associated with phosphorus bound to the siloxane crosslinker only. As shown in **Figure 2.10**, as the amount of TEGDAE increases and **2** decreases, a qualitative difference in peak height in the NMR spectrum can be observed for phosphorus bound to TEGDAE only and crosslinker only. This difference corresponds to the changing ratios used in each of the derivatives. For example, derivative **2.8** displays a higher peak height for furthest upfield peak, which signifies phosphorus bound to TEGDAE only. In contrast, the NMR spectrum of derivative **2.3** displays the TEGDAE peak at a much lower peak height which suggests TEGDAE was used in a much lower quantity when the material was synthesized.



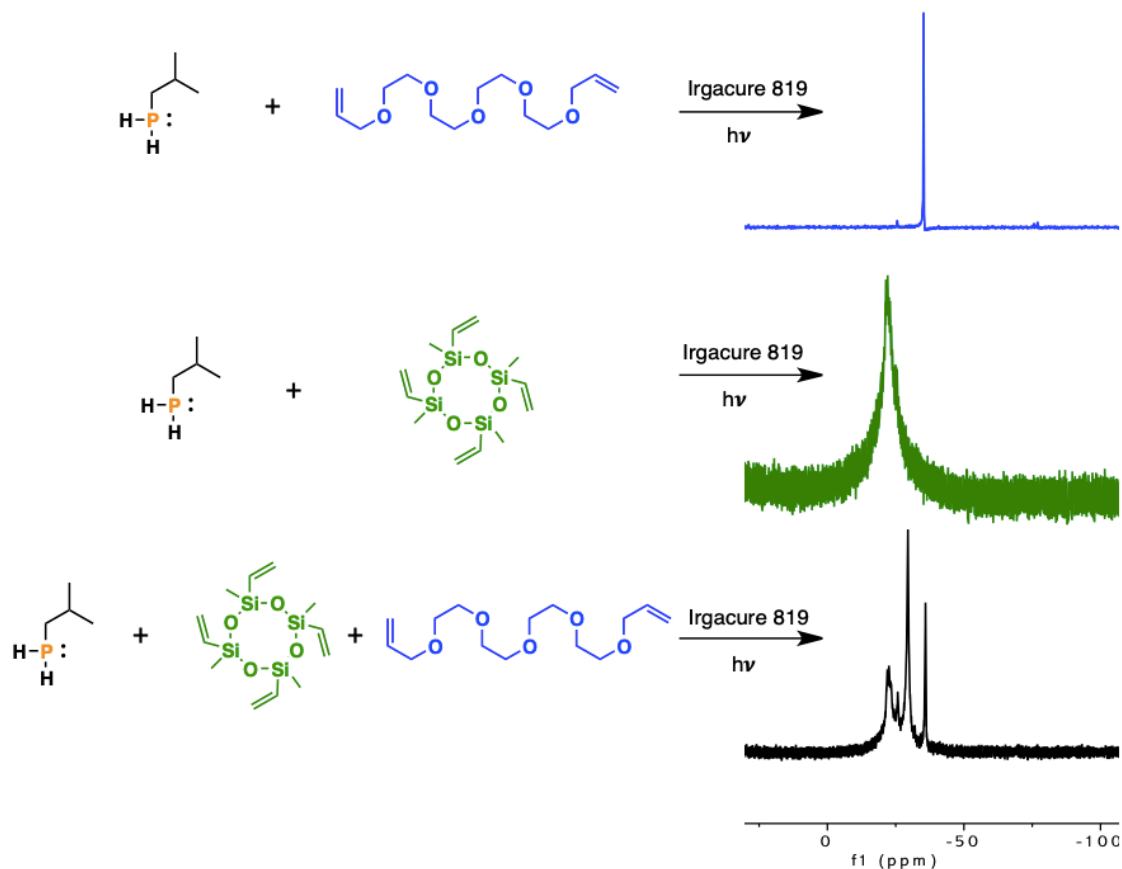


**Figure 2.11:**  $^{31}\text{P}$   $\{^1\text{H}\}$  NMR spectra of the products resulting from the photopolymerisation of monoisobutylphosphine with TEGDAE only, crosslinker **2** only, or both TEGDAE and crosslinker **2**.

## 2.4 Thermal Properties

Once the polymers were leached of unreacted low molecular weight oligomers and dried, the ceramic yields were determined using thermogravimetric analysis (TGA). The TGA curves obtained for each of the derivatives revealed the effects that TEGDAE imposed on the thermal stability of the polymer. The resulting ceramic yields for the polymers prepared with **1** display ceramic yields below 20% (**Table 2.1**) indicating they are not sufficient as preceramic polymers. Perhaps, the predominately organic backbone present in these polymers are forming volatile organic compounds such as  $\text{CO}_2$ ,  $\text{H}_2$ , and  $\text{CH}_4$ , upon heating which contributes to mass loss.<sup>20,21</sup> Although these polymers display low values for ceramic yields, valuable information can still be obtained from the thermal data. Polymer **1.1** possesses the highest overall ceramic yield in comparison to the other polymer derivatives made with the trifunctional crosslinker, TTT. As the concentration of TEGDAE

increases and TTT decreases, a decrease in ceramic yield was noted. This can be attributed to the presence of crosslinking, which helps to inhibit polymer backbone degradation and the volatilization of low molecular weight backbone components as a result of the heating process.<sup>20</sup>

**Table 2.1:** Thermal properties of polymers **1.1, 1.2, 1.3, 1.4**

Polymer	Temperature at 2% Mass Loss (T <sub>d</sub> )	Ceramic Yield at 800°C
<b>1.1</b>	349 °C	18 %
<b>1.2</b>	355 °C	10 %
<b>1.3</b>	344 °C	8 %
<b>1.4</b>	266 °C	6 %

**Table 2.2** displays the ceramic yields obtained for polymers containing crosslinker **2**. The values reported are much higher when compared to materials synthesized with crosslinker **1**. This is attributed to the inorganic elements that are present in the preceramic polymer that are likely to be retained throughout the heating process. Although the ceramic yield did not reach the desired 70%, it provided useful insight as to how to increase the yield. Surprisingly, for the polymer derivatives formed with crosslinker **2**, the ceramic yield does not deviate too heavily until derivative **2.5**, thus indicating crosslinking is more heavily affected with an increased amount of TEGDAE in the system.

**Table 2.2:** Thermal properties of polymers **2.1, 2.2, 2.3, 2.4, 2.5, 2.6, 2.7, 2.8**

Polymer	Temperature at 2% Mass Loss (T <sub>d</sub> )	Ceramic Yield at 800°C
<b>2.1</b>	250 °C	44 %
<b>2.2</b>	363 °C	37 %
<b>2.3</b>	317 °C	43 %
<b>2.4</b>	348 °C	44 %
<b>2.5</b>	337 °C	39 %
<b>2.6</b>	329 °C	33 %
<b>2.7</b>	333 °C	33 %
<b>2.8</b>	270 °C	29 %

Moving forward, data collected from the derivatives formed with **1** indicate that polymer derivative **1.3** was the most sufficient polymer to perform further modification on. The presence of TEGDAE in this derivative specifically showed a marked increase in the swell % and did not limit the ceramic yield too heavily in comparison to the other derivatives where TEGDAE was incorporated. When tetrafunctional crosslinker **2** was incorporated, derivative **2.4** was the best candidate moving forward for further modification as a marked increase in swell % (**Figure 2.8**) was noted. This accompanied by a well-maintained high ceramic yield indicates that this was the optimal derivative for further testing.

## 2.5 Oxygen Uptake

The oxidation behaviour of these air-sensitive polymers was tested to see if TEGDAE impacted the likelihood of these materials to oxidize when removed from an inert atmosphere. Based on the results obtained from the swell tests and the TGA data, the materials chosen for the following experiments were polymer pucks **1.1**, **1.3**, **2.1**, and **2.4**. The oxidation behaviour of these polymers was analyzed using TGA. Prior to analysis, these materials were dried *in vacuo* at 95 °C to remove any existing volatiles still present in the polymer. These polymers were exposed to medical grade air for thirty minutes at 30 °C, followed by heating at a rate of 2 °C/ min to 100°C to increase the oxidation process.<sup>22</sup> This temperature was held for three and a half hours. A slight drop in weight was observed in the thermogram from 30-100 °C which can be explained by existing volatiles present in the polymer exiting the chamber in the gaseous form. At the 100 °C mark the polymer weight began to stagnate indicating an equilibrium had been reached and the resulting thermograms were analyzed at this segment.

The amount of oxygen that penetrated the network was first calculated theoretically ( $Ox_{calc}$ ) using **Equation 4**, where  $n_{phos}$  is the moles of phosphorus in the sample,  $M_{oxy}$  is the molar mass of oxygen, and  $W_o$  is the weight of the sample. This equation assumes a 1:1 ratio between phosphorus and oxygen. The value obtained for  $Ox_{calc}$  in each of the polymers was approximately 6 %, which was anticipated as the amount of phosphorus in each of the materials was similar. This indicates that the amount of oxygen able to penetrate the network is directly related to phosphorus content.<sup>22,23</sup>

$$Ox_{Calc} = \left( \frac{(n_{Phos} \times M_{Oxy}) + W_o}{W_o} - 1 \right) \times 100 \quad (\text{Equation 4})$$

To determine the accuracy of the values obtained for  $O_{x_{calc}}$  each of the four polymers were subjected to an oxidation experiment in a TGA instrument and the resulting thermograms were analyzed (**Figure 2.12**). Polymers **1.1** and **2.1** both appear to be more resistant to oxidation in comparison to the analogous polymers containing TEGDAE. When TEGDAE is present in the network, the extent of oxidation for the polymers increased, likely due to the increased flexibility within the polymer. Larger interstitial spaces were being produced within the network resulting in a less crosslinked network. This makes the material more penetrable, which manifested in the values obtained experimentally for oxygen uptake ( $O_{x_{exp}}$ ). Once the temperature in the TGA instrument reached the 100 °C mark, an initial, steady uptake of oxygen occurred. This is likely a result of the exposed phosphine environments present in the polymer. As the heating process continues while the polymer is consistently being exposed to oxygen, the assumption is that the amount of free phosphine sites in the polymer become less accessible, explaining why the thermogram appears to approach an asymptote at the 3-hour mark. Polymer **2.4** is more successfully oxidized throughout this experiment and is likely a result of the less rigidity in the material due to the use of crosslinker **2** in the polymerisation, which allows for easier oxygen penetration.

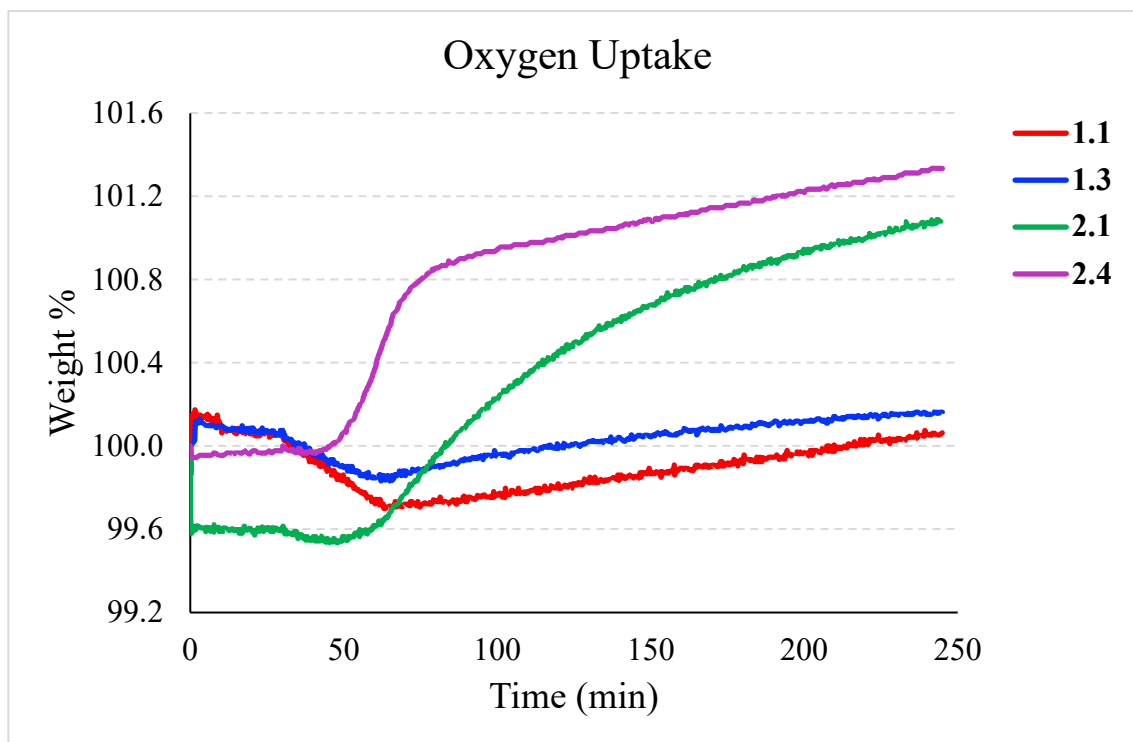


**Figure 2.12:** Oxygen uptake thermograms for polymers **1.1**, **1.3**, **2.1**, and **2.4**

In contrast, the thermograms produced from the polymers devoid of TEGDAE exhibited a plot that appeared to steadily increase with time. This is likely due to the excess time it takes for oxygen to penetrate the harder profile of these thermosets leading to exposure of more P(III) environments which are susceptible to oxidation.

When comparing the values obtained for  $O_{x_{calc}}$  and  $O_{x_{exp}}$  a significant difference can be seen. As shown in **Table 2.3**, the  $O_{x_{calc}}$  values obtained for each of the polymers is much higher than the actual values obtained gravimetrically suggesting that oxygen had difficulty infiltrating the network which is likely a result of the crosslinking taking place in the material.

**Table 2.3:** Oxygen uptake for polymers **1.1**, **1.3**, **2.1**, and **2.4**

<b>1.1</b>		<b>1.3</b>		<b>2.1</b>		<b>2.4</b>	
$O_{x_{calc}}^a$	$O_{x_{exp}}^b$	$O_{x_{calc}}^a$	$O_{x_{exp}}^b$	$O_{x_{calc}}^a$	$O_{x_{exp}}^b$	$O_{x_{calc}}^a$	$O_{x_{exp}}^b$
6.24 %	0.06%	5.51 %	0.16 %	5.99 %	1.08 %	5.44 %	1.34 %

<sup>a</sup> Mass increase obtained theoretically (**Equation 4**) <sup>b</sup> Value obtained at the 250-minute mark

## 2.6 Pyrolysis

To determine the consequence of TEGDAE in the resulting ceramics, polymers **1.1**, **1.3**, **2.1**, and **2.4** were pyrolyzed. This occurred after each material was leached of any unreacted materials and dried for four nights at 85 °C to ensure accurate results. Pyrolysis was performed under reducing conditions (5 % H<sub>2</sub> balanced by N<sub>2</sub>) where each polymer was heated to 800 °C at a rate of 10 °C/min. Once the maximum temperature was reached, it was held there for either one or four hours and the resulting char was analyzed using x-ray photoelectron spectroscopy (XPS), scanning electron microscopy (SEM), and energy dispersive x-ray spectroscopy (EDX).

The resulting chars obtained from the pyrolysis of all four polymers pyrolyzed were analyzed to determine porosity and uniformity. The char resulting from polymers **1.1**, **1.3**, **2.1**, and **2.4** all appeared to be uniform materials as observed from the SEM images. The only char that possessed porosity was the char resulting from polymer **1.1**. These materials were also subjected to XPS and EDX analysis to determine the elemental composition and the chemical environments present within the char produced. Values were first determined theoretically to predict the quantities of each element and the resulting data was compared against these values.

**Table 2.4:** Composition of the char resulting from pyrolysis of polymers **1.1** and **1.3** as depicted theoretically, from XPS and EDX.

	<b>1.1</b>			<b>1.3</b>		
	Theoretical	XPS	EDX	Theoretical	XPS	EDX
P	5.8 %	1.3 %	4.1 %	5.3 %	1.0 %	3.9 %
C	70.6 %	75.7 %	95.0 %	72.0 %	92.2 %	94.4 %
N	11.8 %	2.2 %	-	8.0 %	2.1 %	-
O	11.8 %	15.9 %	1.0 %	14.8 %	3.9 %	1.7 %

**Table 2.4** depicts the elemental composition present in the chars from the polymers containing TTT as the crosslinker (**1.1** and **1.3**). The inclusion of TEGDAE did not provide too large of an impact on the resulting material formed after pyrolysis. Interestingly, oxygen was the only element that displayed a large difference in abundance within the char through the inclusion of TEGDAE. When TEGDAE was included in the network the

amount of oxygen present in the polymer was much lower. This is likely a result of the mobility within the material. Due to the hard interior and exterior of polymer **1.1**, which is completely devoid of TEGDAE, the ability of the H<sub>2</sub> gas entering the furnace to penetrate the network removing any unwanted oxygen is low. Once TEGDAE is introduced into the network, there is an increase in the swelling ability and a softer material is obtained. This may allow for the penetration of H<sub>2</sub> resulting in the formation of water which exits the furnace thus contributing to mass loss.

**Table 2.5:** Composition of the char resulting from pyrolysis of polymers **2.1** and **2.4** as depicted theoretically, from XPS and EDX.

	<b>2.1</b>			<b>2.4</b>		
	Theoretical	XPS	EDX	Theoretical	XPS	EDX
P	6.5 %	0.08 %	0.1 %	6.8 %	0.00 %	0.03 %
C	66.5 %	28.0 %	26.3 %	65.4 %	27.5 %	34.5 %
Si	13.5 %	16.4 %	18.2 %	17.4 %	27.9 %	6.47 %
O	13.5 %	55.8 %	55.4 %	10.4 %	44.0 %	58.9 %

**Table 2.5** displays the results obtained from XPS and EDX analysis of the resulting chars from polymers formed utilizing the siloxane crosslinker (**2.1** and **2.4**). The implications of TEGDAE were seen in the elemental composition regarding silicon. When TEGDAE was present in the original formulation, the resulting char possessed less silicon than when it was not used. The other elements present in the polymers excluding silicon did not appear to be greatly impacted by the presence or absence of TEGDAE.

Results obtained from XPS revealed that the percentage of phosphorus in the materials were much lower than expected. This is likely due to the formation of P<sub>4</sub>O<sub>10</sub> throughout heating which then sublimates at 360 °C.<sup>24,25</sup> This hypothesis was only further corroborated with XPS data which revealed that the majority of phosphorus present in the chars was either from P<sub>2</sub>O<sub>5</sub> or phosphate. The remaining phosphorus in the ceramic was present as tertiary phosphine sites. The XPS data also confirmed that the carbon present in the char was likely carbon black. This was exhibited by the presence of various functional groups typically seen in carbon black such as esters, alcohols, ketones, and alkenes.<sup>26</sup>

## 2.7 Conclusions

This work was centralized around exploring the overall impact of TEGDAE into polymer networks. The linear additive not only increased the swellability of the polymers but also contributed to lower values obtained for ceramic yields. When polymer networks can swell in various solvents this provides the advantage of performing solution like chemistry and acquiring solution-state NMR spectroscopy. As the amount of TEGDAE was increased in the starting formulations of the polymer networks, an increase in swellability was obtained, narrower line widths appear in the resulting  $^{31}\text{P} \{^1\text{H}\}$  NMR spectra, and the more permitting the network is to oxygen. The more swellable the network is, the more amenable it is to post polymerisation modification, which, if desired is important. Subsequent pyrolysis of the purified phosphorus containing polymer networks resulted in the formation of char. Upon analysis of the ceramic it was found that the composition of phosphorus in the material was quite low which is likely a result of the oxophilicity of the element forming  $\text{P}_4\text{O}_{10}$ . Incorporating different elements, such as transition metals, could reduce the formation of  $\text{P}_4\text{O}_{10}$  throughout the thermochemical decomposition process resulting in a higher ceramic yield and the retention of phosphorus. The addition of TEGDAE to the polymer prior to pyrolysis did not appear to affect the resulting composition of the ceramic, excluding the amount of silicon present in the material.

## 2.8 Experimental

Instrumentation: Unless stated, all reactions were done under a nitrogen atmosphere either in a MBraun Labmaster 130 glovebox or on a Schlenk line. Phosphines were obtained from Cytec Solvay (Niagara Falls, ON, Canada) and used as received. Tetraethyleneglycoldiallylether (TEGDAE) was prepared as stated in literature.<sup>22</sup> Glassware was dried in a 150 °C oven before use. Unless otherwise stated, solvents were purchased from Caledon, dried using the MBraun solvent purification system and stored over 4Å sieves (3Å for acetonitrile). Deuterated solvents were dried over  $\text{CaH}_2$  and distilled under a nitrogen atmosphere. 2, 4, 6, 8 – tetramethyl - 2, 4, 6, 8-tetravinylcyclotetrasiloxane was purchased from Alfa Aesar and used without purification. Unless otherwise noted, reagents were purchased from Sigma Aldrich and used without purification. NMR spectra were acquired on an INOVA 400 MHz, INOVA 600 MHz, or Bruker 400 MHz NMR



spectrometer.  $^{31}\text{P}\{^1\text{H}\}$  NMR spectra were acquired using an external standard (85%  $\text{H}_3\text{PO}_4$ ,  $\delta_{\text{p}} = 0$ ) as a reference. Units for couplings constants (J) are Hertz (Hz). ATR-FTIR samples (solid) were collected using a Bruker ALPHA II ATR spectrometer. Thermogravimetric analysis (TGA) was performed to obtain ceramic yields using Mettler Toledo TGA 2 instruments where  $\sim 7$  mg samples were placed in an alumina crucible heated from 30 – 1000 °C with a heating rate of 10 °C/min. Oxygen uptake experiments were also run on a Mettler Toledo TGA 2 instrument where 7 mg samples were placed in an alumina crucible and exposed to medical grade air (100 mL/min) for 30 minutes at 30 °C. The heat was then increased to 100 °C at a heating rate of 2 °C/min and held at this temperature for 3 hours. Differential scanning calorimetry (DSC) was completed using a Mettler Toledo DSC 3 under a nitrogen atmosphere in an aluminium Tzero™ pan with a heating rate of 40 °C per minute. Data was acquired from the third heating cycle. Photopolymerisation was performed on a CON-TROL-CURE conveyor belt and irradiated with UV light (Irradiance – UVA: 134 mW/cm<sup>2</sup>; UVB: 112 mW/cm<sup>2</sup>; UVC: 34 mW/cm<sup>2</sup>; UVV: 149 mW/cm<sup>2</sup>. Energy density – UVA: 7319 mJ/cm<sup>2</sup>; UVB: 6210 mJ/cm<sup>2</sup>; UVC: 1759 mJ/cm<sup>2</sup>; UVV: 7879 mJ/cm<sup>2</sup>). Energy densities were determined using a PP2-H-U Power Puck II which was purchased from EIT Instrument Markets (Sterling, VA, USA). SEM was conducted on a Zeiss 1540XB CrossBeam SEM equipped with an Oxford x-ray detector and Inca analysis software. EDX was performed at an 8 mm working distance while operating at 20 keV. X-ray photoelectron spectroscopy data was acquired using a Kratos AXIS Supra X-ray photoelectron spectrometer using a monochromatic Al K(alpha) source (15 mA, 15 kV). Pyrolysis was performed using a Lindberg Blue M tube furnace equipped with a quartz tube and run under reducing conditions (5% H<sub>2</sub>, balance with N<sub>2</sub>).

### 2.8.1 Preparation of polymers 1.1, 1.2, 1.3, and 1.4

**General procedure:** Monoisobutyl phosphine, TTT, and TEGDAE were combined together with BAPO (0.5 wt. %) to form a clear, yellow liquid. Upon irradiation for 15 minutes a clear and colourless tacky gel was remaining. Unreacted primary phosphine was removed *in vacuo* for eight hours at 85 °C. The network was cut into quarters and leached using dichloromethane. The resulting polymers were dried under *vacuo* for 4 nights at 85°C

to removed any solvent and volatiles present in the material. The final material was characterized.

**Table 2.6:** Amount of starting materials used for the polymerisation of polymers **1.1 – 1.4**

Polymer	Amount of Monoisobutyl phosphine	Amount of TTT	Amount of TEGDAE
<b>1.1</b>	0.294 g, 3.26 mmol	0.551 g, 2.21 mmol	-
<b>1.2</b>	0.296 g, 3.29 mmol	0.468 g, 1.88 mmol	0.120 g, 0.436 mmol
<b>1.3</b>	0.286 g, 3.26 mmol	0.401 g, 1.61 mmol	0.224 g, 0.816 mmol
<b>1.4</b>	0.284 g, 3.15 mmol	0.335 g, 1.34 mmol	0.331 g 1.21 mmol

## 2.8.2 Characterization of polymers **1.1, 1.2, 1.3, and 1.4**

**1.1:**  $^{13}\text{C}\{^1\text{H}\}$  NMR (100.6 MHz):  $\delta_{\text{C}} = 148.9$  (carbonyl,  $(\text{R}_2\text{N})_2\text{C}=\text{O}$ ), 46.9, 44.6, 38.1, 24.4 (alkyl  $\text{CH}_2$ ),  $^{31}\text{P}\{^1\text{H}\}$  NMR (161.8 MHz):  $\delta_{\text{P}} = -35.1$ ; ATR-IR (ranked intensity): 2954 (8), 2870 (9), 1675 (1), 1448 (2), 1366 (4), 1317 (5), 992 (7), 930 (6), 762 (3), 532 (10);  $T_{\text{d}}$  (at 2% mass loss) = 349 °C ; Char yield at 800 °C = 18 %.  $T_{\text{g}} = 250$  °C.

**1.2:**  $^{13}\text{C}\{^1\text{H}\}$  NMR (100.6 MHz):  $\delta_{\text{C}} = 148.8$  (carbonyl,  $(\text{R}_2\text{N})_2\text{C}=\text{O}$ ), 70.4, 62.8, 60.5, 54.9 (ethereal,  $\text{CH}_2$ ), 46.7, 44.4, 44.0, 38.1, 26.2, 24.1, 22.1, 13.56 (alkyl  $\text{CH}_2$ );  $^{31}\text{P}\{^1\text{H}\}$  NMR (161.8 MHz):  $\delta_{\text{P}} = -35.0$ ; ATR-IR (ranked intensity): 2952 (9), 2868 (8), 1676 (1), 1451 (2), 1366 (4), 1320 (5), 1103 (6), 762 (3), 531 (7);  $T_{\text{d}}$  (at 2% mass loss) = 355°C ; Char yield at 800 °C = 10 %. No  $T_{\text{g}}$  was observed.

**1.3:**  $^{13}\text{C}\{^1\text{H}\}$  NMR (100.6 MHz):  $\delta_{\text{C}} = 148.7$  (carbonyl,  $(\text{R}_2\text{N})_2\text{C}=\text{O}$ ), 72.0, 70.5, 70.0, 61.5 (ethereal,  $\text{CH}_2$ ), 44.7, 44.6, 43.9, 38.1, 26.2, 24.1 (alkyl  $\text{CH}_2$ );  $^{31}\text{P}\{^1\text{H}\}$  NMR (161.8 MHz):  $\delta_{\text{P}} = -35.1$ ; ATR-IR (ranked intensity): 2951 (8), 2867 (7), 1679 (1), 1454 (2), 1367(5), 1332 (6), 1103 (4), 763 (3), 532 (9);  $T_{\text{d}}$  (at 2% mass loss) = 340 °C ; Char yield at 800 °C = 7 %. No  $T_{\text{g}}$  was observed.

**1.4:**  $^{13}\text{C}\{^1\text{H}\}$  NMR (100.6 MHz):  $\delta_{\text{C}} = 148.7$  (carbonyl,  $(\text{R}_2\text{N})_2\text{C}=\text{O}$ ), 72.6, 72.0, 70.6, 70.1, 63.0, 61.6 (ethereal,  $\text{CH}_2$ ), 44.8, 44.2, 38.3, 26.4, 26.0, 25.0, 24.2, 22.4, 13.9 (alkyl  $\text{CH}_2$ );  $^{31}\text{P}\{^1\text{H}\}$  NMR (161.8 MHz):  $\delta_{\text{P}} = -35.6$ ; ATR-IR (ranked intensity): 2953 (10), 2867

(9), 1678 (2), 1459 (4), 1101 (3), 1003 (1), 843 (7), 816 (6), 763 (5), 552 (8);  $T_d$  (at 2% mass loss) = 266 °C ; Char yield at 800 °C = 6 %. No  $T_g$  was observed.

### 2.8.3 Preparation of polymers **2.1**, **2.2**, **2.3**, **2.4**, **2.5**, **2.6**, **2.7**, and **2.8**

**General Procedure:** A clear, yellow solution containing 2,4,6,8-tetramethyl-2,4,6,8-tetravinylcyclotetra-siloxane, tetraethyleneglycol diallyl ether, monoisobutylphosphine, and BAPO (0.5 wt. %) was irradiated for 15 minutes to afford a clear and colourless polymer. Unreacted isobutyl phosphine was removed *in vacuo* affording a completely tertiary phosphine polymer network. The network was cut into quarters and leached using dichloromethane. The resulting polymers were dried under *vacuo* for 4 nights at 85°C to remove solvent and any volatiles still remaining in the polymers. The final material was characterized.

**Table 2.7:** Amount of starting materials used for the polymerisation of polymers **2.1** – **2.8**

Polymer	Amount of Monoisobutyl phosphine	Amount of crosslinker <b>2</b>	Amount of TEGDAE
<b>2.1</b>	0.265 g, 2.95 mmol	1.012 g, 1.48 mmol	-
<b>2.2</b>	0.281 g, 3.12 mmol	0.498 g, 1.44 mmol	0.080 g, 0.291 mmol
<b>2.3</b>	0.281 g, 3.12 mmol	0.454 g, 1.32 mmol	0.143 g, 0.521 mmol
<b>2.4</b>	0.285 g, 3.16 mmol	0.418 g, 1.21 mmol	0.229 g, 0.835 mmol
<b>2.5</b>	0.285 g, 3.16 mmol	0.367 g, 1.07 mmol	0.292 g, 1.06 mmol
<b>2.6</b>	0.290 g, 3.22 mmol	0.326 g, 0.946 mmol	0.380 g, 1.39 mmol
<b>2.7</b>	0.284 g, 3.15 mmol	0.274 g, 0.795 mmol	0.439 g, 1.60 mmol
<b>2.8</b>	0.276 g, 3.06 mmol	0.224 g, 0.649 mmol	0.505 g, 1.84 mmol

## 2.8.4 Characterisation of polymers **2.1**, **2.2**, **2.3**, **2.4**, **2.5**, **2.6**, **2.7**, and **2.8**

**2.1:**  $^{13}\text{C}\{^1\text{H}\}$  NMR (100.6 MHz):  $\delta_{\text{C}} = 65.5, 63.2, 60.8, 47.1, 44.8, 26.6, 24.4, 21.3, 11.9$  (alkyl  $\underline{\text{C}}\text{H}_2$ ),  $-0.8$  (Si- $\underline{\text{C}}\text{H}_3$ );  $^{31}\text{P}\{^1\text{H}\}$  NMR (161.8 MHz):  $\delta_{\text{P}} = -22.5$ ; ATR-IR (ranked intensity): 2957 (9), 2900 (8), 1464 (6), 1408 (5), 1259 (2), 1045 (1), 781 (3), 744 (4), 572 (7);  $T_{\text{d}}$  (at 2% mass loss) = 250 °C ; Char yield at 800 °C = 44 %.  $T_{\text{g}} = 110$  °C.

**2.2:**  $^{13}\text{C}\{^1\text{H}\}$  NMR (100.6 MHz):  $\delta_{\text{C}} = 72.0, 70.6, 69.6$  (ethereal,  $\underline{\text{C}}\text{H}_2$ ), 45.0, 44.7, 37.3, 26.5 24.6, 22.3, 19.3, 19.0, 11.9 (alkyl  $\underline{\text{C}}\text{H}_2$ ),  $-0.7$  (Si- $\underline{\text{C}}\text{H}_3$ );  $^{31}\text{P}\{^1\text{H}\}$  NMR (161.8 MHz):  $\delta_{\text{P}} = -22.0$ ; ATR-IR (ranked intensity): 2954 (9), 2871 (8), 1462 (6), 1407 (5), 1365 (10), 1258 (2), 1152 (1), 1044 (1), 783 (3), 742 (4), 566 (7);  $T_{\text{d}}$  (at 2% mass loss) = 363 °C ; Char yield at 800 °C = 37 %. No  $T_{\text{g}}$  observed.

**2.3:**  $^{13}\text{C}\{^1\text{H}\}$  NMR (100.6 MHz):  $\delta_{\text{C}} = 72.0, 70.6$  (ethereal,  $\underline{\text{C}}\text{H}_2$ ), 37.5, 26.4 24.3, 19.3, 11.8 (alkyl  $\underline{\text{C}}\text{H}_2$ ),  $-1.0$  (Si- $\underline{\text{C}}\text{H}_3$ );  $^{31}\text{P}\{^1\text{H}\}$  NMR (161.8 MHz):  $\delta_{\text{P}} = -21.0$ ; ATR-IR (ranked intensity): 2955 (7), 2870 (8), 1725 (9), 1464 (6), 1409 (5), 1259 (3), 1135 (1), 1048 (1), 779 (2), 568 (10);  $T_{\text{d}}$  (at 2% mass loss) = 317 °C ; Char yield at 800 °C = 43 %. No  $T_{\text{g}}$  observed.

**2.4:**  $^{13}\text{C}\{^1\text{H}\}$  NMR (100.6 MHz):  $\delta_{\text{C}} = 72.0, 71.5, 70.6$  (ethereal,  $\underline{\text{C}}\text{H}_2$ ), 69.6, 65.3, 63.0, 60.7, 44.7, 37.5, 26.4, 24.3, 19.4, 11.9 (alkyl  $\underline{\text{C}}\text{H}_2$ ),  $-1.0$  (Si- $\underline{\text{C}}\text{H}_3$ );  $^{31}\text{P}\{^1\text{H}\}$  NMR (161.8 MHz):  $\delta_{\text{P}} = -22.5$ ; ATR-IR (ranked intensity): 2953 (5), 2869 (4), 1462 (7), 1408 (6), 1364 (5), 1257 (2), 1149 (1), 1050 (1), 785 (3), 743(9), 561 (8);  $T_{\text{d}}$  (at 2% mass loss) = 348 °C ; Char yield at 800 °C = 45 %. No  $T_{\text{g}}$  observed.

**2.5:**  $^{13}\text{C}\{^1\text{H}\}$  NMR (100.6 MHz):  $\delta_{\text{C}} = 72.1, 70.6, 69.6$  (ethereal,  $\underline{\text{C}}\text{H}_2$ ), 38.6, 26.3, 24.3, 11.8 (alkyl  $\underline{\text{C}}\text{H}_2$ ),  $-1.0$  (Si- $\underline{\text{C}}\text{H}_3$ );  $^{31}\text{P}\{^1\text{H}\}$  NMR (161.8 MHz):  $\delta_{\text{P}} = -28.9$ ; ATR-IR (ranked intensity): 2953 (6), 2869 (5), 1462 (9), 1408 (8), 1364 (12), 1258 (2), 1149 (10), 1052 (1), 786 (3), 744 (4), 561 (11);  $T_{\text{d}}$  (at 2% mass loss) = 337 °C ; Char yield at 800 °C = 39 %. No  $T_{\text{g}}$  observed.

**2.6:**  $^{13}\text{C}\{^1\text{H}\}$  NMR (100.6 MHz):  $\delta_{\text{C}} = 72.5, 70.6, 69.6$  (ethereal,  $\underline{\text{C}}\text{H}_2$ ), 45.0, 44.7, 37.8, 26.4, 26.1, 24.2, 22.4, 13.8, 11.9 (alkyl  $\underline{\text{C}}\text{H}_2$ ),  $-1.0$  (Si- $\underline{\text{C}}\text{H}_3$ );  $^{31}\text{P}\{^1\text{H}\}$  NMR (161.8 MHz):  $\delta_{\text{P}} = -28.9$ ; ATR-IR (ranked intensity): 2953 (4), 2868 (3), 1723 (8), 1462 (6), 1408 (5),

1365 (7), 1258 (2), 1056 (1), 784 (2), 559 (9);  $T_d$  (at 2% mass loss) = 329 °C ; Char yield at 800 °C = 33 %. No  $T_g$  observed.

**2.7:**  $^{13}\text{C}\{^1\text{H}\}$  NMR (100.6 MHz):  $\delta_c = 72.0, 70.6, 69.6$  (ethereal,  $\underline{\text{C}}\text{H}_2$ ), 44.6, 42.3, 37.7, 34.1, 26.4, 24.2, 22.3, 15.1, 13.8 (alkyl  $\underline{\text{C}}\text{H}_2$ ), -1.2 (Si- $\underline{\text{C}}\text{H}_3$ );  $^{31}\text{P}\{^1\text{H}\}$  NMR (161.8 MHz):  $\delta_p = -28.9$ ; ATR-IR (ranked intensity): 2952 (5), 2868 (4), 1724 (10), 1462 (7), 1409 (6), 1365 (8), 1259 (3), 1058 (1), 786 (2), 565 (9);  $T_d$  (at 2% mass loss) = 333 °C ; Char yield at 800 °C = 33 %. No  $T_g$  observed.

**2.8:**  $^{13}\text{C}\{^1\text{H}\}$  NMR (100.6 MHz):  $\delta_c = 72.0, 70.6, 69.6, 65.3, 61.5, 60.7$  (ethereal,  $\underline{\text{C}}\text{H}_2$ ), 46.9, 44.6, 42.3, 37.8, 34.1, 26.4, 24.2, 22.4, 13.8, 11.9 (alkyl  $\underline{\text{C}}\text{H}_2$ ), -1.0 (Si- $\underline{\text{C}}\text{H}_3$ );  $^{31}\text{P}\{^1\text{H}\}$  NMR (161.8 MHz):  $\delta_p = -29.1$ ; ATR-IR (ranked intensity): 2952 (6), 2868 (5), 1461 (7), 1409 (8), 1364 (9), 1258 (3), 1056 (1), 787 (2), 746 (4), 558 (10)  $T_d$  (at 2% mass loss) = 270 °C ; Char yield at 800 °C = 29 %. No  $T_g$  observed.

---

<sup>1</sup> Brinson, H. F.; Brinson, L. C.; *Polymer Engineering Science and Viscoelasticity*, Boston, MA, 2008

<sup>2</sup> Caminade, A.; Hey-Hawkins, E.; Manners, I.; *Chem. Soc. Rev.*; **2016**, *45*, 5144-5146

<sup>3</sup> Barroso, G.; Li, Q.; Bordia, R. K.; Motz, G.; *J. Mater. Chem. A.*; **2019**, *7*, 1936-1963

<sup>4</sup> Colombo, P.; Mera, G.; Riedel, R.; Soraru, G. D.; *J. Am. Ceram. Soc.*; **2010**, *93*, 1805-1837

<sup>5</sup> Sujith, R.; Jothi, S.; Zimmerman, A.; Aldinger, F.; Kumar, R.; *Int. Mater. Rev.*; **2021**, *66*, 426-449

<sup>6</sup> Chiulan, I.; Heggset, E. B.; Voicu, S. I.; Chinga-Carrasco, G.; *Biomacromolecules*, **2021**, *22*, 1795-1814

<sup>7</sup> Wang, X.; Schmidt, Hanaor, D.; Kamm, P. H.; Li, S.; Gurlo, A.; *Additive Manufacturing*, **2019**, *27*, 80-90

<sup>8</sup> Beland, V. A.; Ragogna, P. J.; *ACS Appl. Mater. Interfaces*, **2020**, *12*, 27640-27650

<sup>9</sup> Beland, V. A.; Ragogna, P. J.; *Chem Eur. J.*; **2020**, *26*, 12751-12757

<sup>10</sup> Ren, Z.; Mujib, S. B.; Singh, G.; *Materials*, **2021**, *14*, 614-632

<sup>11</sup> El-Refaei, S. M.; Russo, P. A.; Pinaa, N.; *ACS Appl. Mater. Interfaces*, **2021**, *13*, 22077-22097

<sup>12</sup> Liu, P.; Rodriguez, J. A.; *J. Am. Chem. Soc.* **2005**, *127*, 14871-14878

<sup>13</sup> Li, W.; Xiong, D.; Gao, X.; Liu, L.; *Chem. Commun.*; **2019**, *55*, 8744-8763

<sup>14</sup> Tanzi, M. C.; Fare, S.; Candiani, G.; *Foundations of Biomaterials Engineering*, London, United Kingdom, 2019

<sup>15</sup> Han, S.; Feng, Y.; Zhang, F.; Yang, C.; Yao, Z.; Zhao, W.; Qiu, F.; Yang, L.; Yao, Y.; Zhuang, X.; Feng, X.; *Adv. Funct. Mater.*; **2015**, *25*, 3899-3906

<sup>16</sup> Odian, G.; *Principles of Polymerization*, 4<sup>th</sup> Ed.; Staten Island, NY, 2004

<sup>18</sup> Sienkiewicz, A.; Krasucka, P.; Charnas, B.; Stefaniak, W.; Goworek, J.; *J. Therm. Anal. Calorim.*; **2017**; *130*, 85-93

- 
- <sup>19</sup> Jonquieres, A.; Roizard, D.; Lochon, P.; *J. Appl. Polym. Sci.*; **1994**; *54*, 1673-1684
- <sup>20</sup> Colombo, P.; Mera, G.; Riedel, R.; Soraru, G. D.; *J. Am. Ceram. Soc.*; **2010**, *93*, 1805-1837
- <sup>21</sup> Greil, P.; *Adv. Eng. Mater.*, **2000**, *2*, 339-348
- <sup>22</sup> Guterman, R.; Kenaree, A. R.; Gilroy J. B.; Gillies, E. R.; Ragona, P. J.; *Chem Mater.* **2015**, *27*, 1412-1419
- <sup>23</sup> Ferrari, M. C.; Carranza, S.; Bonnacaze, R. T.; Tung, K. K.; Freeman, B. D.; Paul, D. R.; *J. Membr. Sci.*; **2009**, *329*, 183-192
- <sup>24</sup> Beland, V. A.; Ross, M. A. S.; Coady, M. J.; Guterman, R.; Ragona, P. J.; *Chem. Mater.* **2017**, *29*, 8884-8891
- <sup>25</sup> Beland, V. A.; Wang, Z.; Sham, T. K.; Ragona, P. J.; *Angew. Chem. Int. Ed.*; **2018**, *57*, 13252-13256
- <sup>26</sup> Hu, E.; Hu, X.; Liu, T.; Liu, Y.; Song, R.; Chen, Y.; *Applied Surface Science*, **2013**, *270*, 596-603

## Chapter Three

### 3 Post Polymerisation Modification

#### 3.1 Introduction

With the global demand for the implementation of renewable energy sources, improving battery performance has been a top scientific agenda item. At the forefront of this research, porous carbon-based materials have attracted interest due to their desirable properties, such as large surface area, high conductivity, and high thermal stability.<sup>1</sup> These carbon-based materials pose a challenge when it comes to production at an industrial scale. The subsequent pyrolysis of metal organic frameworks has been investigated to determine if they are suitable precursors, however the difficulty in scale up remains a challenge.<sup>1,2,3,4</sup> In the specific area of fuel cells and electrocatalysts, metal oxides and metal phosphides seem to be promising replacements for the current non-renewable analogues.<sup>5</sup> The use of metal phosphides is beneficial as they are typically more cost efficient, and they have been proven to increase corrosion resistance. In this content, the goal of this work was to find synthetic routes to produce conductive metal phosphides.

Post functionalization of a polymer is a commonly used to incorporate various elements and functional groups that are not present in the original monomers.<sup>6,7,8</sup> Tuning the polymers pre-pyrolysis through the implementation of different elements within the polymeric precursor produces ceramics with varying elemental compositions and different properties.

The ability for polymers to swell in a solvent is a desirable property to have as it allows for facile modification of the network to take place through solution state chemistry. The resulting modified polymer can now be characterized using NMR spectroscopy . Once introduced to various solvents, the chains in the polymer are solvated and an increase in swelling is observed in the material, which results in the ability to obtain an NMR spectrum containing narrow line widths. Phosphane-ene polymers have garnered attention due to the ease of synthesis using the hydrophosphination reaction under UV irradiation.<sup>14,15,17,21</sup> Once a primary phosphine, a photoinitiator and monomers containing more than one olefin undergo polymerisation under photolytic conditions a polymer is formed containing

tertiary phosphines. These phosphine sites provide a nucleophilic reactive handle which can perform  $S_N2$  reactions on alkyl halides. They also provide Lewis basic sites which are susceptible to coordination to a Lewis acid, allowing for the implementation of various elements in the polymer that were not present in the starting monomers.

### 3.2 Small molecule control reactions

Quaternization of tri-*n*-butyl phosphine (**3.1**) using 5-chloropentyne was first performed to gain a spectroscopic handle of this compound before reactions were carried out on polymer networks (**Figure 3.1**~~Error! Reference source not found.~~). It is imperative to obtain these handles as once performed on macromolecules, analyzing spectroscopic data can be more difficult. The reactions were monitored using  $^{31}\text{P}\{^1\text{H}\}$  NMR spectroscopy, which initially displayed a phosphine signal at  $\delta_{\text{P}} = -31.0$  that was consumed to give a new resonance at  $\delta_{\text{P}} = 36.9$ , indicative of a quaternized product. Successful purification of **3.2** was performed subsequent to confirming complete conversion and values obtained from  $^1\text{H}$  and  $^{13}\text{C}\{^1\text{H}\}$  NMR spectroscopy were compared to what was published in literature.<sup>9</sup> The presence of the alkyne functional group was confirmed using IR spectroscopy which displayed  $\text{C}\equiv\text{C}$  stretching and  $\text{C-H}$  stretching in the IR spectrum ( $\nu_{\text{C}\equiv\text{C}} = 2103\text{cm}^{-1}$ ,  $\nu_{\text{C-H}} = 3131\text{cm}^{-1}$ ).<sup>9</sup>

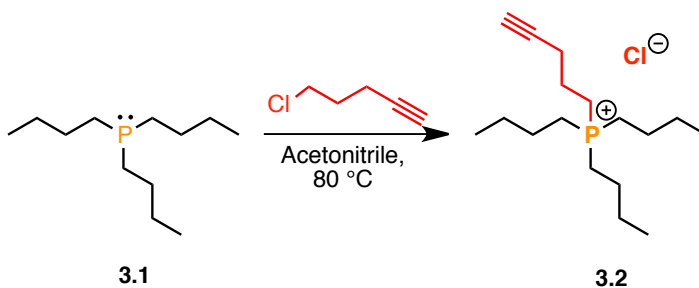


**Figure 3.1:** Quaternizing the phosphorus atom present on **3.1** using the  $S_N2$  reaction.

This reaction, although successful, displayed slow reaction kinetics as it took seven days for complete conversion from **3.1** to **3.2**. To reduce the reaction time of this quaternization, the 5-chloropentyne was converted to an alkyl iodide using the Finkelstein reaction (**Figure 3.2**).<sup>10</sup> This reaction converts alkyl chlorides and bromides into their corresponding alkyl iodides using sodium iodide in acetone.<sup>10,11</sup> Formation of the desired product was confirmed by comparing the  $^1\text{H}$  and  $^{13}\text{C}\{^1\text{H}\}$  NMR spectroscopic data to literature values.<sup>11</sup>



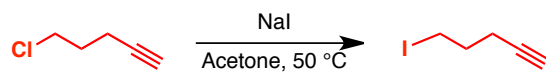


**Figure 3.2:** 5-chloropentyne undergoing the Finkelstein reaction to produce the iodoalkyne

Along with the 5-iodo-1-pentyne, 4-bromo-1-butyne was tried as a starting material for the  $S_N2$  reaction to see if the heavier halide would result in faster reaction kinetics. With successful conversion of the alkynyl chloride into the alkynyl iodide, quaternization reactions were performed with both the bromo- and iodo- alkynyl species. Similar shifts were observed in the  $^{31}\text{P}\{^1\text{H}\}$  NMR spectra, which have a new signal at  $\delta_{\text{P}} = -31.0$  ppm consumed to give a product at  $\delta_{\text{P}} = 34.7$  ppm for **3.3**, and  $\delta_{\text{P}} = 35.3$  ppm for **3.4**, indicative of the quaternized products. The downfield shift observed in the phosphorus signals is a result of the decreasing electronegativity seen from the anions present in **3.2** to **3.4**. Following purification techniques, structures of **3.3** and **3.4** were confirmed using IR,  $^1\text{H}$  and  $^{13}\text{C}\{^1\text{H}\}$  NMR spectroscopy and mass spectrometry. Quaternization reactions performed with **3.3** and **3.4** displayed much faster reaction kinetics in comparison to when performed with **3.2**, indicating that the heavier halide provided more desirable reaction times.

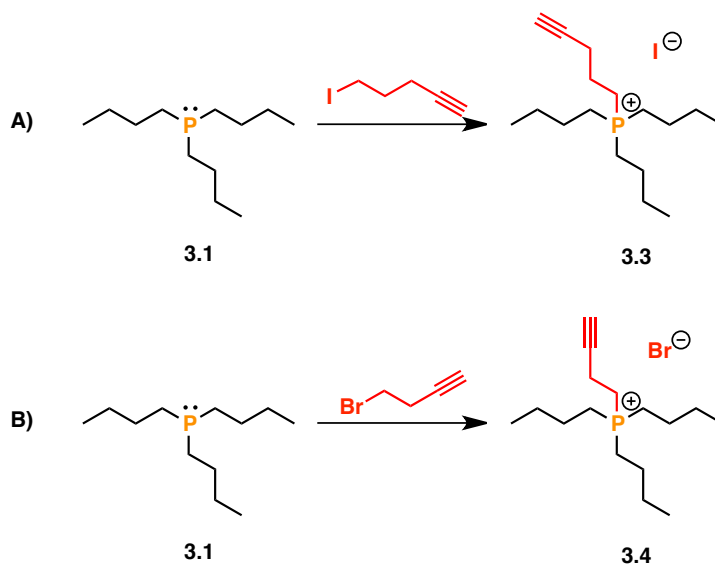


**Figure 3.3:** Quaternization of **3.1** using iodopentyne and bromobutyne

Upon successful formation of quaternized products (**3.2**, **3.3**, **3.4**), the alkyne functionality is available for further functionalization through metalation. Installing metal sites into the molecule can be accomplished using dicobalt octacarbonyl, which provides an excellent spectroscopic handle as the carbonyl groups have distinct spectroscopic signatures in both

IR and  $^{13}\text{C}\{^1\text{H}\}$  NMR spectroscopy. Metalation was performed on 5-chloropentyne prior to the phosphonium, **3.3**. This reaction was monitored using  $^1\text{H}$  NMR spectroscopy, and complete conversion to the metallated species was noted after one hour (**Figure 3.4**). The reaction proceeded cleanly, and the resulting product required no further purification.

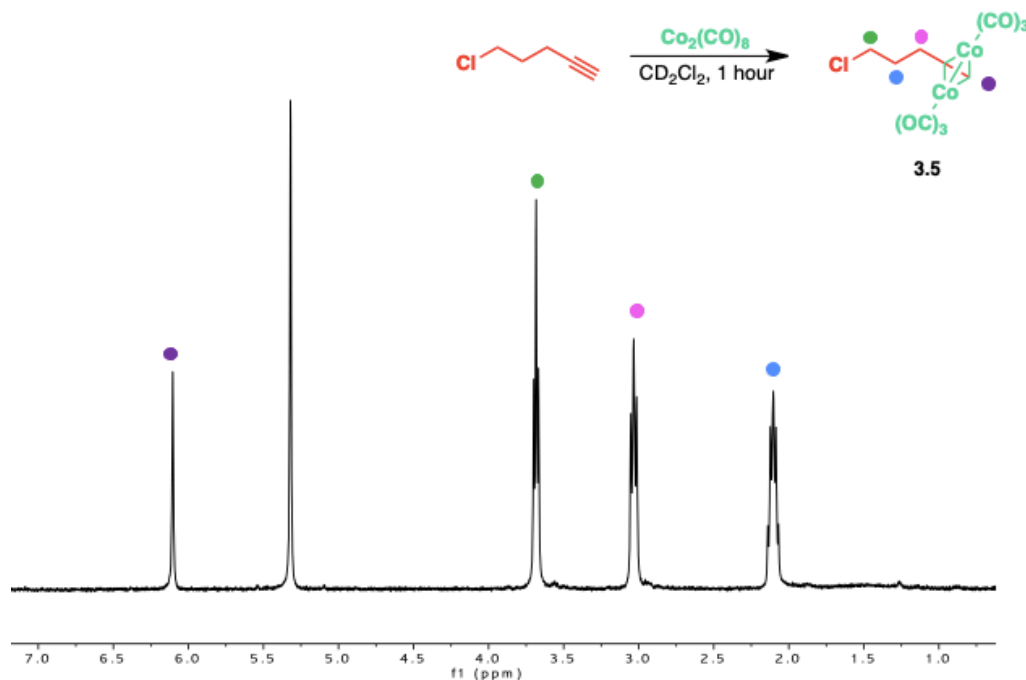


**Figure 3.4:**  $^1\text{H}$  NMR ( $\text{CD}_2\text{Cl}_2$ , 400 MHz) spectrum of metallated 5-chloropentyne

Dicobalt octacarbonyl contains two types of carbonyl groups; bridging and terminal which provides the advantage of replacing the two bridged carbonyl groups with an alkyne.<sup>12</sup> Monitoring the reaction between an alkyne and dicobalt octacarbonyl can be accomplished with  $^1\text{H}$ ,  $^{13}\text{C}\{^1\text{H}\}$  NMR, and IR spectroscopy. The latter of which observes the disappearance of the stretches corresponding to the bridging carbonyl ( $\sim 1800\text{ cm}^{-1}$ ) and the alkyne ( $\sim 2200\text{ cm}^{-1}$ ).<sup>13</sup>

### 3.3 Quaternization of Polymer **3.6** and **3.7**

With the data obtained from the small molecule reactions, quaternization was attempted on polymer networks synthesized from a primary phosphine, crosslinker, and a linear additive. The networks were formed utilizing the hydrophosphination reaction with monoisobutylphosphine (*i*-BuPH<sub>2</sub>), a linear additive; tetraethylene glycol diallyl ether (TEGDAE), and a crosslinker; either 1, 3, 5- triallyl - 1, 3, 5- triazine - 2, 4, 6- trione (TTT)

(polymer **3.6**), or (D<sub>4</sub>) (polymer **3.7**) (**Figure 3.5**). Polymer formation was initiated photochemically by Irgacure 819 as per a previously reported procedure.<sup>14,15</sup>

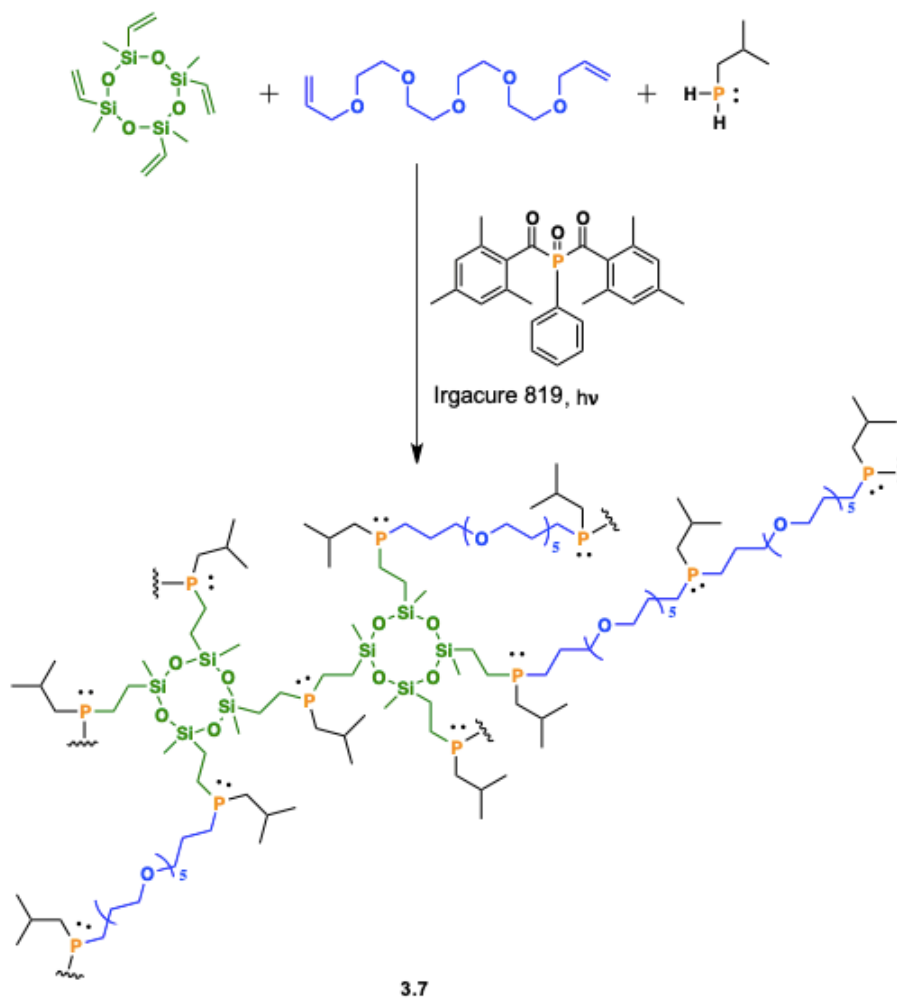


**Figure 3.5:** Formation of phosphine polymer network **3.7** utilizing the phosphane-ene reaction

With the networks **3.6** and **3.7** in hand quaternization reactions were attempted under the same conditions as the small molecule analogue (80 °C in acetonitrile, for 7 days). Originally, this S<sub>N</sub>2 reaction was performed with 5-chloro-pentyne. Conversion to the quaternized phosphine polymer networks **3.61** and **3.71** were monitored using <sup>31</sup>P{<sup>1</sup>H} NMR spectroscopy with the chemical shifts of  $\delta_P = 34.9$  for the polymer containing TTT (**3.61**) and  $\delta_P = 38.4$  for the polymer containing D<sub>4</sub> (**3.71**). After leaching the polymer networks of any unreacted reactants or oligomers, confirmation of the installation of the alkyne functionality was performed using <sup>13</sup>C{<sup>1</sup>H} NMR and IR spectroscopy.

Unfortunately, the results indicated that there was no alkyne species present within the polymer network. It was hypothesized that the slow reaction kinetics and the high heat led to degradation of the alkyne species within the network.

To combat this problem, the reaction was performed on **2.4** using 4-bromo-1-butyne in an attempt to improve the reaction kinetics. After 3 days, complete conversion of the polymer was achieved ( $\delta_p = 38.2$ ). With the drastic increase in the speed of the reaction, it was our hope that the alkyne species would remain in the polymer. Unfortunately, further investigation done using IR and C{ $^{13}$ C} NMR proved that the alkyne was once again absent from the phosphonium network. The inability of the networks to swell in acetonitrile is likely a cause for the inability to maintain the functionality throughout the reaction. Attempts at performing the reaction in different solvents (THF, diethyl ether, DCM) on the small molecule scale did not result in the desired S<sub>N</sub>2 reaction. Based on the undesired results, the idea of quaternization and subsequent metal insertion *via* this synthetic pathway was halted.

### 3.4 Metalation

Polymers **3.6** and **3.7** both contain tertiary phosphine environments which can take on the role of Lewis bases in transition metal complexes.<sup>16</sup> This allows for the implementation of metals within the networks using Lewis acid-base chemistry. Work done previously in the Ragona group utilized cyclopentadienylcobalt dicarbonyl (**3.8**; **Figure 3.6A**) as a Lewis acid to form a Lewis acid-base complex with the phosphines present in their polymers.<sup>17</sup> In this work, the tertiary phosphine sites in polymers **3.6** and **3.7** are hypothesized to undergo reactions to form coordinate covalent bonds with the cobalt atom present in compound **3.8** (**Figure 3.6B**).

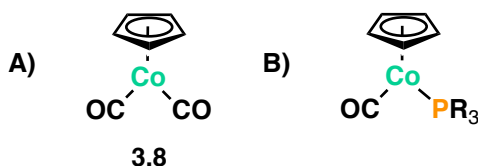


**Figure 3.6:** A) Cyclopentadienylcobalt dicarbonyl (**3.8**); B) Formation of coordinate covalent bond between phosphine (Lewis base) and the cobalt present on **3.8**; Lewis acid

Small molecule reactions were unnecessary as the work done by Beland *et al.* provided a sufficient spectroscopic handle for this work.<sup>17</sup> Networks **3.6** and **3.7** were each mixed with one stoichiometric equivalent of **3.8** and added to a pressure tube containing THF. The tube was heated at a reflux temperature for six days until complete conversion was achieved according to  $^{31}\text{P}\{^1\text{H}\}$  NMR spectroscopy. The spectroscopic data showed complete consumption of the starting materials (**3.6**:  $\delta_{\text{P}} = -34.9$ ; **3.7**:  $\delta_{\text{P}} = -38.4$ ) to give a new, coordinated phosphine environment appearing further downfield (**3.62**:  $\delta_{\text{P}} = 49.8$ ; **3.72**:  $\delta_{\text{P}} = 59.5$ ).

Further confirmation of coordination was achieved using IR spectroscopy,  $^{13}\text{C}\{^1\text{H}\}$  NMR spectroscopy and SEM images. The IR spectrum of compound **3.8** prior to the reaction displayed two different carbonyl signals ( $\nu_{\text{C=O}} = 2011$  and  $1939\text{ cm}^{-1}$ ). Subsequent metalation observed the consumption of one carbonyl stretch and the IR spectrum depicted the remaining stretch that was shifted because of the new environment (**3.62**:  $\nu_{\text{C=O}} = 1896\text{ cm}^{-1}$ ; **3.72**:  $\nu_{\text{C=O}} = 1900\text{ cm}^{-1}$ ).  $^{13}\text{C}\{^1\text{H}\}$  NMR spectroscopy was performed to determine the extent of coordination. The resulting spectra further confirmed successful coordination with the appearance of the metal carbonyl signal (**3.62**:  $\delta_{\text{C}} = 207.8$ ; **3.72**:  $\delta_{\text{C}} = 208.1$ ), and the appearance of the signal arising from the carbons present on the cyclopentadienyl ring (**3.62**:  $\delta_{\text{C}} = 81.5$ ; **3.72**:  $\delta_{\text{C}} = 81.6$ ). SEM images of the dark red, opaque networks depicted non-porous, uniform materials indicating the coordinate covalent bond between phosphorus and cobalt was present uniformly throughout the polymers (**Figure 3.7**).

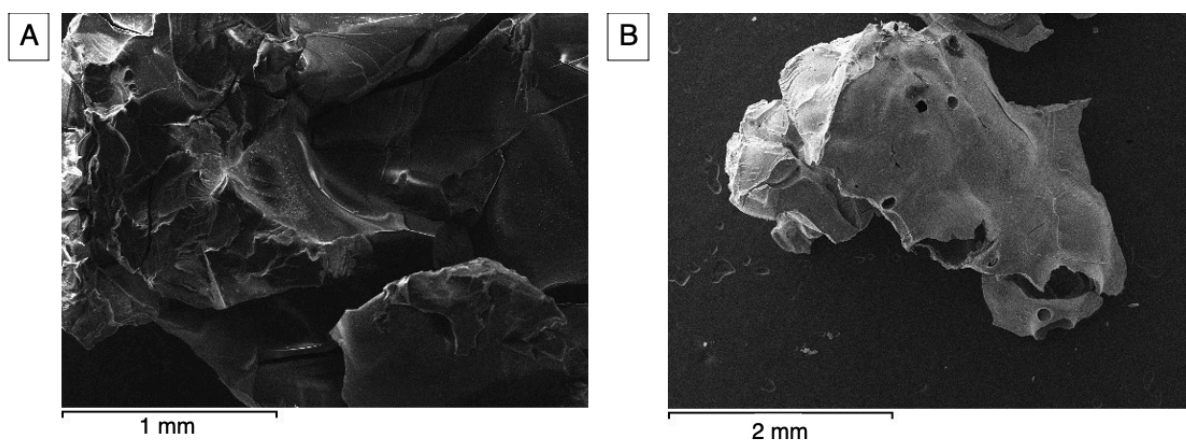


**Figure 3.7:** SEM images of metallated polymers A) **3.62** and B) **3.72**.

To get a handle on the elemental composition present in the networks, the materials were subjected to analysis using energy dispersive X-ray (EDX) and X-ray photoelectron

spectroscopy (XPS) which analyze different parts of the sample (**Table 3.1**). XPS is a surface sensitive technique which analyzes and depicts the elemental composition within the first 10 nm of a solids outer surface.<sup>18</sup> In contrast, EDX, is not a technique typically used for surface science as the x-rays required for analysis penetrate only a region of 2 microns in depth for a given sample.<sup>19</sup> Therefore, the resulting data from these two techniques could display different values as they were acquired at different locations throughout the sample. Theoretical calculations were performed on each of the elements within the sample and compared to the resulting acquired values.

**Table 3.1:** XPS and EDX results from coordinated polymer networks **3.62** and **3.72**.

	<b>3.62</b>			<b>3.72</b>		
	Theoretical	XPS	EDX	Theoretical	XPS	EDX
P	3.96 %	1.5 %	0.60 %	3.96 %	4.5 %	0.72 %
C	72.2 %	63.1 %	59.4 %	72.2 %	78.5 %	66.8 %
N	5.99 %	3.7 %	9.10 %	-	-	-
Si	-	-	-	5.99 %	1.3 %	1.9 %
O	15.6 %	20.7 %	30.4 %	15.6 %	8.4 %	32.0 %
Co	2.27 %	0.6 %	0.07 %	2.27 %	4.0 %	0.34 %

The data presented in **Table 3.1** further corroborates the presence of cobalt within the network. Theoretically for every phosphorus atom within the network, a cobalt atom should also be present through a coordinate covalent bond. The results obtained for EDX and XPS do not show this theory to be completely accurate as there are variances when comparing the quantities of the phosphorus and cobalt atoms. This cannot be too discouraging, however, as these methods of analysis do not penetrate too deep into the material.

### 3.4.1 Thermal Properties

Polymer networks **3.62** and **3.72** were leached of any unreacted starting materials and dried *in vacuo* for four nights. The thermal properties of the resulting polymers were analyzed using thermogravimetric analysis (TGA). With the desired formation of ceramics, ceramic yield is an important feature of these networks.<sup>20</sup> Prior to metalation, **3.6** possessed a ceramic yield of 8 %, which is likely a result of the mainly organic backbone present in

the network. Subsequent metalation (**3.62**) resulted in an increase in the yield by a factor of 4 to 32 %. Similarly, subsequent metalation of **3.7**, resulted in an increase in ceramic yield from 44 to 63 % (**Figure 3.8**).

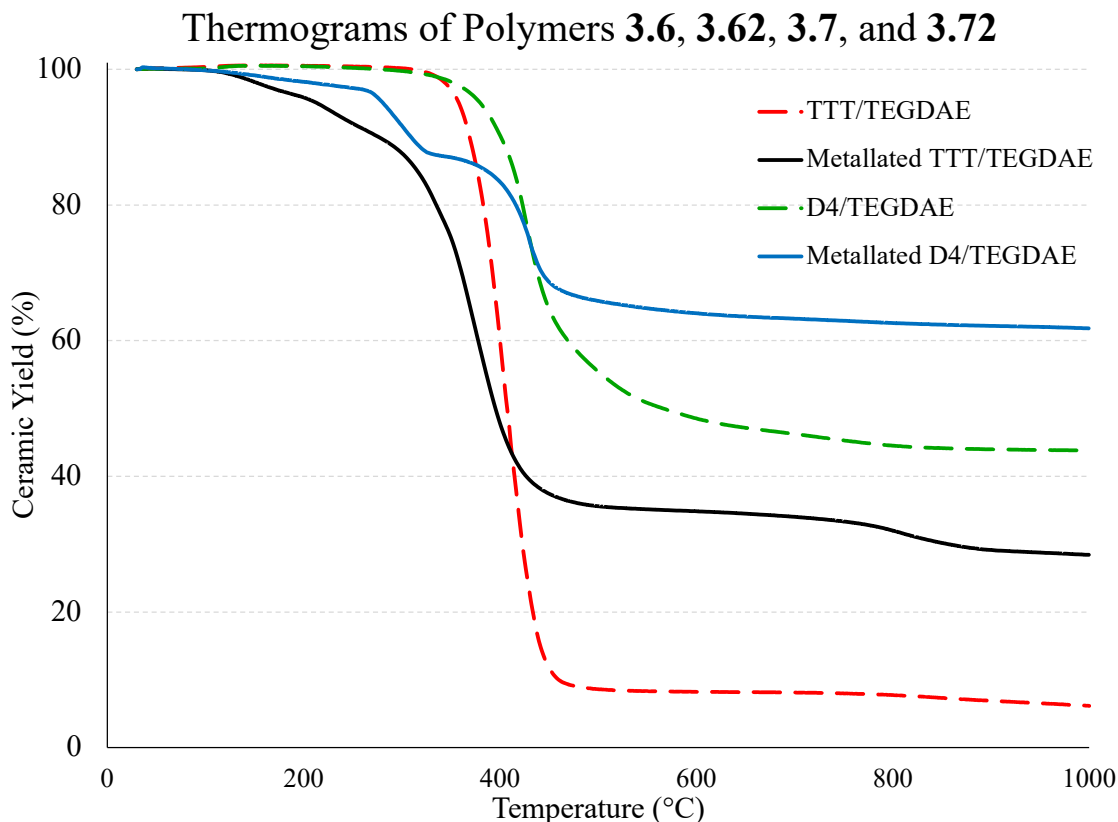


**Figure 3.8:** Thermograms resulting from the thermochemical decomposition of **3.6**, **3.62**, **3.7**, and **3.72**.

A likely cause for the drastic increases in the overall ceramic yields could be a result of the retention of phosphorus as depicted in **Table 3.1**. The formation of metal phosphides throughout the heating process would diminish the ability to form  $P_4O_{10}$  which can be a common by-product resulting from pyrolysis.<sup>14,21</sup> The consequence is that its sublimation of  $P_4O_{10}$  occurs at a temperature of 360 °C which results in subsequent mass loss as it exits the furnace in gaseous form. The addition of metals into the network targets the formation of metal oxides or metal phosphides reducing the chances of mass loss.

### 3.5 Pyrolysis

Pyrolysis was performed on each of the networks under reducing conditions (5 %  $H_2$ ,  $N_2$  balance) at a temperature of 800 °C, with a heating rate of 10 °C/min. The maximum

temperature was held constant for four hours. The resulting black char was analyzed utilizing XPS and SEM-EDX (**Table 3.2**).

**Table 3.2:** Atomic percentages of elements present in the chars (**3.63** and **3.73**) produced via pyrolysis; analyzed using XPS and EDX

	<b>3.63</b>			<b>3.73</b>		
	Theoretical	XPS	EDX	Theoretical	XPS	EDX
P	3.96 %	4.5 %	0.81 %	4.62 %	6.0 %	2.6 %
C	72.2 %	78.5 %	41.6 %	70.2 %	45.6 %	33.2 %
N	5.99 %	1.3 %	5.84 %	-	-	-
Si	-	-	-	7.01 %	12.4 %	15.0 %
O	15.6 %	8.4 %	46.4 %	16.4 %	22.2 %	45.6 %
Co	2.27 %	4.0 %	-	1.78 %	7.3 %	3.5 %

Incorporating silicon within the polymer network resulted in the increased retention of phosphorus and cobalt in comparison to polymer **3.62**, possessing the strictly organic crosslinker. This is likely a result of the faster breakdown of polymer **3.62** with increased temperature, volatile compounds were produced and removed from the pyrolysis tube in the gas phase. Previous work performed on these phosphane-ene polymer to ceramic conversions resulted in the retention of only 2.5 % cobalt. The polymer used was composed of only the TTT crosslinker and monoisobutyl phosphine. Once formed, the polymer was purified and pyrolyzed under identical conditions used in this work.<sup>17</sup> The networks proposed in this work retained more of the inorganic elements present within the polymer. This could result from the ability for cobalt to better penetrate the network throughout the metalation because of the increased swelling abilities present in these materials.

As the goal in this work is to retain the inorganic elements and form metal phosphides, XPS provided the advantage of not only acquiring the elemental composition but also determining the chemical environments of the elements.<sup>18</sup> Cobalt within the char would ideally be found as cobalt (I/II) phosphide ( $\text{Co}_2\text{P}$ ). However, the presence of oxygen in both the networks allows for the formation of cobalt (II) phosphate. **Table 3.3** depicts that both compounds were formed throughout pyrolysis and further indicates the percentage of each present. Polymer **3.72** not only retained the highest percentage of phosphorus and



cobalt within the char, but also produced the highest fraction of cobalt (I/II) phosphide ( $\text{Co}_2\text{P}$ ). Previous work performed on a polymer containing TTT only and isobutyl phosphine not only resulted in a decreased retention of these elements but also had a much lower fraction of the desired cobalt (I/II) phosphide ( $\text{Co}_2\text{P}$ ).<sup>17</sup> This could be a result of the heavily crosslinked nature of these networks restricting mobility and resulting in the entrapment of fragments within the material. This could cause an element like phosphorus to only be subjected to the oxygen present within the network forming the undesired phosphate. With networks **3.62** and **3.72**, the increased mobility allows for atoms like oxygen to not only react with the phosphorus present in the network but to also react with the hydrogen penetrating the network from the incoming pyrolysis gas to form  $\text{H}_2\text{O}$  which would leave the tube.

**Table 3.3:** Results obtained from XPS revealing the elemental composition and chemical environment of phosphorus and cobalt within the char

	Co Retention	P Retention	Cobalt (I/II) Phosphide ( $\text{Co}_2\text{P}$ )	Cobalt (II) Phosphate
<b>3.63</b>	4.0 %	4.5 %	~30 %	~70 %
<b>3.73</b>	7.3 %	6.0 %	~40 %	~60 %
<b>4.1<sup>a</sup></b>	2.5 %	2.5 %	~10%	~90 %

<sup>a</sup> Polymer used in previous work containing only TTT crosslinker and monoisobutyl phosphine

The high carbon content seen in the chars is likely doped carbon black.<sup>17</sup> Although it is likely true that carbon is present in such a high quantity in chars **3.63** and **3.73**, the exact amount is not likely what was acquired. This is because of adventitious carbon which arises from the adsorption of aliphatic hydrocarbons present in the atmosphere.<sup>18,22</sup>

### 3.6 Conclusion

Polymer networks were formed and underwent metalation reactions to form complexes between cobalt and phosphorus atoms present within the network. Previous work completed on comparable networks allowed for a spectroscopic handle when analyzing these polymers. Subsequent thermal degradation tests were performed using thermogravimetric analysis which determined the addition of the cobalt containing compound resulted in a much higher ceramic yield. This is crucial as throughout the

polymer-to-ceramic conversion process, the optimal mass loss is between 10-30 %.<sup>23</sup> Incorporating the inorganic crosslinker resulted in a much higher ceramic yield in these materials, highlighting promise in the field of battery and fuel cell applications.<sup>1-4</sup> Analysis of the resulting chars depicting a retention of both cobalt and phosphorus in the material where the presence of cobalt (I/II) phosphide (Co<sub>2</sub>P) was found in a higher abundance when compared to previous work performed in the Ragogna group.<sup>17</sup> This provides further promise for materials like these to be used in the fuel cell and battery fields.

Attempts at implementing metals within the networks utilizing a S<sub>N</sub>2 reaction were unsuccessful. Attempts at changing the reaction conditions and starting materials did not provide the desired solution to the problem indicating the swelling ability of the polymer restricted the alkyne functionality from remaining present throughout the reaction. This data further corroborates the importance of forming a swellable network as it allows for ease of post polymerisation modification.

A polymeric precursor was presented in this work possessing an alkyl phosphine site which can easily be functionalized utilizing the rich coordination chemistry of the phosphine. Pyrolysis of this material resulted in the retention of the phosphorus and metal species forming the desired metal phosphide that is appealing to battery and fuel cell industry.

### 3.7 Experimental

**General Procedures:** All reactions were performed under a nitrogen atmosphere either in a MBraun Labmaster 130 glovebox or on a Schlenk line, unless otherwise noted. Glassware used for reactions was dried in an oven set to a temperature of 150 °C. Solvents used were purchased from Caledon and dried using the MBraun solvent purification system and stored over 4Å sieves (3Å for acetonitrile). Deuterated solvents required for reactions were dried over CaH<sub>2</sub> and distilled under a nitrogen atmosphere. Phosphines were obtained from Cytec Solvay (Niagara Falls, ON, Canada) and used as received. 2, 4, 6, 8 – tetramethyl - 2, 4, 6, 8-tetravinylcyclotetrasiloxane was purchased from Alfa Aesar and unless otherwise stated all other reagents were purchased from Sigma Aldrich and used without purification. Tetraethyleneglycoldiallylether (TEGDAE) was prepared as stated in literature.<sup>24</sup> The synthesis of 5-iodo-1-pentyne was performed as stated in literature.<sup>11</sup> NMR spectroscopy was performed on an INOVA 400 MHz, INOVA 600 MHz, or Bruker 400 MHz NMR spectrometer. <sup>31</sup>P{<sup>1</sup>H} NMR spectra were acquired using an external standard (85%

H<sub>3</sub>PO<sub>4</sub>,  $\delta_p = 0$ ) as a reference. Units for couplings constants (J) are Hertz (Hz). ATR-FTIR samples (solid) were collected using a Bruker ALPHA II ATR spectrometer. Thermogravimetric analysis (TGA) was performed to obtain ceramic yields using Mettler Toledo TGA 2 instruments where ~7 mg samples were placed in an alumina crucible heated from 30 – 1000 °C with a heating rate of 10 °C/min. Oxygen uptake experiments were also run on a Mettler Toledo TGA 2 instrument where 7 mg samples were placed in an alumina crucible and exposed to medical grade air (100 mL/min) for 30 minutes at 30 °C. The heat was then increased to 100 °C at a heating rate of 2 °C/min and held at this temperature for 10 hours. Differential scanning calorimetry (DSC) was completed using a Mettler Toledo DSC 3 under a nitrogen atmosphere in an aluminium Tzero™ pan with a heating rate of 40 °C per minute. Data was acquired from the third heating cycle. Photopolymerisation was performed on a CON-TROL-CURE conveyor belt and irradiated with UV light (Irradiance – UVA: 134 mW/cm<sup>2</sup>; UVB: 112 mW/cm<sup>2</sup>; UVC: 34 mW/cm<sup>2</sup>; UVV: 149 mW/cm<sup>2</sup>. Energy density – UVA: 7319 mJ/cm<sup>2</sup>; UVB: 6210 mJ/cm<sup>2</sup>; UVC: 1759 mJ/cm<sup>2</sup>; UVV: 7879 mJ/cm<sup>2</sup>). Energy densities were determined using a PP2-H-U Power Puck II which was purchased from EIT Instrument Markets (Sterling, VA, USA). SEM was conducted on a Zeiss 1540XB CrossBeam SEM equipped with an Oxford x-ray detector and Inca analysis software. EDX was performed at an 8 mm working distance while operating at 20 keV. X-ray photoelectron spectroscopy data was acquired using a Kratos AXIS Supra X-ray photoelectron spectrometer using a monochromatic Al K(alpha) source (15 mA, 15 kV). Pyrolysis was performed using a Lindberg Blue M tube furnace equipped with a quartz tube and run under reducing conditions (5% H<sub>2</sub>, balance with N<sub>2</sub>).

Synthesis of **3.1**: Tri-n-butyl phosphine (10.4 mmol) was dissolved in acetonitrile and added into a pressure tube with 5-chloropentyne (11.6 mmol). Once sealed, the tube was placed on an oil bath at 80 °C for 7 days. Once the phosphine was successfully converted to the quaternized product, volatiles were removed *in vacuo* and the crude product was dissolved into CH<sub>2</sub>Cl<sub>2</sub> and precipitated into hexanes (0°C). The dried product was a white powder (2.8 g, 86% yield) and its production was confirmed using <sup>1</sup>H, <sup>13</sup>C, <sup>31</sup>P{<sup>1</sup>H} NMR, and ATR-IR spectroscopies. <sup>1</sup>H NMR (400 MHz, CDCl<sub>3</sub>):  $\delta$  = 2.68-2.60 (2H, m), 2.51-2.41 (8H, m), 2.03 (1H, t, <sup>4</sup>J (H,H)= 2.7Hz), 1.89-1.78 (2H, m), 1.55-1.48 (12H, m), 0.95

(9H, t,  $^3J(\text{H,H}) = 6.9\text{ Hz}$ );  $^{13}\text{C}\{\text{H}\}$  (100.6 MHz,  $\text{CDCl}_3$ ):  $\delta_{\text{C}} = 82.2, 70.8, 24.2$  (d,  $^2J(\text{P,C}) = 15.1\text{ Hz}$ ), 24.0 (d,  $^3J(\text{P,C}) = 5.0\text{ Hz}$ ), 21.3 (d,  $^2J(\text{P,C}) = 4.0\text{ Hz}$ ), 19.6 (d,  $^3J(\text{P,C}) = 17.1\text{ Hz}$ ), 19.2 (d,  $^1J(\text{P,C}) = 47.3\text{ Hz}$ ), 18.4 (d,  $^1J(\text{P,C}) = 49.3\text{ Hz}$ ), 13.7.  $^{31}\text{P}\{\text{H}\}$  (161.8 MHz,  $\text{CDCl}_3$ )  $\delta_{\text{P}} = 33.4$ . ATR-IR (ranked intensity): 3131 (1), 2959 (5), 2932 (6), 2808 (2), 2103 (12), 1449 (7), 1376 (9), 1313 (8), 1242, 1147 (10), 1096 (11), 800 (4), 722 (3); HRMS calculated for  $\text{C}_{17}\text{H}_{37}\text{P} [\text{M}]^+$  269.2398; found, 269.2393

**Synthesis of 3.3:** A mixture of tri-*n*-butyl phosphine (1.6 mmol) and 5-iodo-1-pentyne (1.9 mmol) were dissolved in acetonitrile and added to a pressure tube equipped with a stir bar. The pressure tube was placed in an oil bath at 80 °C for 21 hours. Once complete conversion was confirmed using  $^{31}\text{P}\{\text{H}\}$  spectroscopy, the volatiles were removed *in vacuo*. The remaining pale-yellow powder was dissolved in minimal amounts of DCM and precipitated into a rapidly stirring flask of cold hexanes (~5 °C). The resulting mixture was placed in the freezer for half an hour and the fine white powder (0.25 g, 39 % yield) was recovered using vacuum filtration. The product was characterized using  $^1\text{H}$ ,  $^{13}\text{C}$ , and  $^{31}\text{P}\{\text{H}\}$  NMR, and ATR-IR spectroscopies.  $^1\text{H}$  NMR (400 MHz,  $\text{CDCl}_3$ ):  $\delta = 2.66\text{-}2.56$  (2H, m), 2.52-2.37 (8H, m), 2.06 (1H, t,  $^4J(\text{H,H}) = 2.6\text{ Hz}$ ), 1.91-1.80 (2H, m), 1.64-1.49 (12H, m), 1.0 (9H, t,  $^3J(\text{H,H}) = 6.9\text{ Hz}$ );  $^{13}\text{C}\{\text{H}\}$  (100.6 MHz,  $\text{CDCl}_3$ ):  $\delta_{\text{C}} = 82.0, 70.9, 24.1$  (d,  $^3J(\text{P,C}) = 15.5\text{ Hz}$ ), 23.9 (d,  $^2J(\text{P,C}) = 4.7\text{ Hz}$ ), 21.3 (d,  $^2J(\text{P,C}) = 3.6\text{ Hz}$ ), 19.6 (d,  $^3J(\text{P,C}) = 16.9\text{ Hz}$ ), 19.4 (d,  $^1J(\text{P,C}) = 46.7\text{ Hz}$ ), 18.5 (d,  $^1J(\text{P,C}) = 49.1\text{ Hz}$ ), 13.7;  $^{31}\text{P}\{\text{H}\}$  (161.8 MHz,  $\text{CDCl}_3$ )  $\delta_{\text{P}} = 34.7$ . ATR-IR (ranked intensity): 3199 (4), 2958 (2), 2930 (5), 2909 (6), 2871 (3), 2105 (13), 1464 (8), 1378 (9), 1229 (11), 1145 (12), 1097 (10), 967 (9), 829 (7), 699 (1); HRMS calculated for  $\text{C}_{17}\text{H}_{37}\text{P} [\text{M}]^+$  269.2398; found, 269.2394

**Synthesis of 3.4:** Tri-*n*-butyl phosphine (1.7 mmol) was dissolved in acetonitrile and added to 4-bromo-1-butyne (2.3 mmol). This mixture was added to a pressure tube equipped with a stir bar and heated at 80 °C for 48 hours. The volatiles were removed *in vacuo* producing an off-white powder. Purification was achieved *via* column chromatography (92% DCM in methanol; v/v) ( $R_{\text{f}} = 0.32$ ). The white powder (0.43 g, 89% yield) was characterized using  $^1\text{H}$ ,  $^{13}\text{C}$ , and  $^{31}\text{P}\{\text{H}\}$  NMR, and ATR-IR spectroscopies.  $^1\text{H}$  NMR (400 MHz,  $\text{CDCl}_3$ ):  $\delta = 2.85\text{-}2.66$  (4H, m), 2.52-2.40 (4H, m), 2.13 (1H, t,  $^4J(\text{H,H}) = 2.6\text{ Hz}$ ), 1.60-1.42 (12 H, m), 0.92 (9H, t,  $^3J(\text{H,H}) = 7.0\text{ Hz}$ );  $^{13}\text{C}\{\text{H}\}$  (100.6 MHz,  $\text{CDCl}_3$ ):  $\delta_{\text{C}} = 81.2, 72.0, 24.1$  (d,  $^3J(\text{P,C}) = 15.6\text{ Hz}$ ), 24.0 (d,  $^2J(\text{P,C}) = 4.9\text{ Hz}$ ), 19.7 (d,  $^1J(\text{P,C}) = 47.4\text{ Hz}$ ),

18.8 (d,  $^1J(\text{P,C}) = 47.5$ ), 13.6;  $^{31}\text{P}\{^1\text{H}\}$  (161.8 MHz,  $\text{CDCl}_3$ )  $\delta_{\text{P}} = 35.3$ . ATR-IR (ranked intensity): 3166 (6), 2959 (2), 2930 (4), 2871 (3), 2107 (12), 1462 (5), 1380 (10), 1230 (11), 1095 (8), 948 (7), 916 (6), 811 (9), 719 (1); HRMS calculated for  $\text{C}_{17}\text{H}_{37}\text{P} [\text{M}]^+$  255.2242; found, 255.2231.

Synthesis of **3.5**: Dicobalt octacarbonyl (0.49 mmol) was dissolved in  $\text{CD}_2\text{Cl}_2$  and added to 5-chloro-1-pentyne (0.33 mmol). The resulting mixture was monitored hourly using  $^1\text{H}$  NMR spectroscopy monitoring for the loss of the alkynyl proton. Complete conversion was accomplished in two hours. The product was a dark red powder and required no further purification methods. The product was characterized using  $^1\text{H}$  and  $^{13}\text{C}$  NMR, and ATR-IR spectroscopies.  $^1\text{H}$  NMR (400 MHz,  $\text{CD}_2\text{Cl}_2$ ):  $\delta = 6.1$  (1H, s), 3.7 (2H, t,  $^3J = 6.3$  Hz), 3.1 (2H, t,  $^3J = 7.2$ ), 2.1 (2H, p,  $^3J = 5.9$  Hz,  $^3J = 7.4$  Hz);  $^{13}\text{C}\{^1\text{H}\}$  (100.6 MHz,  $\text{CD}_2\text{Cl}_2$ ):  $\delta_{\text{C}} = 202.6, 200.5, 96.3, 74.0, 54.0, 44.9, 35.0, 31.9$ . ATR-IR (ranked intensity): 2092 (3), 1994 (1), 1852 (3), 1549 (6), 1444, (5), 1276 (6), 766 (4).

Synthesis of **3.6**: Monoisobutyl phosphine (0.293 g, 3.25 mmol), TTT (0.409 g, 1.64 mmol), and TEGDAE (0.229 g, 0.835 mmol) were combined with BAPO (0.5 wt. %) to form a clear, yellow liquid. Upon irradiation for 15 minutes a clear and colourless tacky gel was remaining. Unreacted primary phosphine was removed *in vacuo* for eight hours at 85 °C. The network was cut into quarters and leached using dichloromethane. The resulting polymers were dried under *vacuo* for 4 nights at 85 °C. The final material was characterized.  $^{13}\text{C}\{^1\text{H}\}$  NMR (100.6 MHz):  $\delta_{\text{C}} = 148.5$  (carbonyl,  $(\text{R}_2\text{N})_2\text{C}=\text{O}$ ), 72.1, 70.7, 70.0, 62.0 (ethereal,  $\text{CH}_2$ ), 44.9, 44.6, 44.0, 38.1, 26.2, 24.5 (alkyl  $\text{CH}_2$ );  $^{31}\text{P}\{^1\text{H}\}$  NMR (161.8 MHz):  $\delta_{\text{P}} = -34.8$ ; ATR-IR (ranked intensity): 2949 (8), 2867 (7), 1672 (1), 1449 (2), 1370 (5), 1329 (6), 1103 (4), 763 (3), 532 (9);  $T_{\text{d}}$  (at 2% mass loss) = 340 °C ; Char yield at 800 °C = 7 %. No  $T_{\text{g}}$  was observed.

Synthesis of **3.7**: A clear, yellow solution containing 2,4,6,8-tetramethyl-2,4,6,8-tetravinylcyclotetra-siloxane (0.416 g, 1.21 mmol), tetraethyleneglycol diethyl ether (0.220 g, 0.802 mmol), monoisobutyl phosphine (0.287 g, 3.19 mmol) and BAPO (0.5 wt. %) was irradiated for 15 minutes to afford a clear and colourless polymer. Unreacted isobutyl phosphine was removed *in vacuo* affording a completely tertiary phosphine polymer network. The network was cut into quarters and leached using dichloromethane. The resulting polymers were dried under *vacuo* for 4 nights at 85 °C. The final material was

characterized.  $^{13}\text{C}\{^1\text{H}\}$  NMR (100.6 MHz):  $\delta_{\text{C}} = 72.3, 71.6, 70.7$  (ethereal,  $\underline{\text{C}}\text{H}_2$ ), 69.3, 65.0, 63.5, 61.0, 44.7, 37.6, 26.4, 24.0, 19.4, 12.0 (alkyl  $\underline{\text{C}}\text{H}_2$ ), -1.0 (Si- $\underline{\text{C}}\text{H}_3$ );  $^{31}\text{P}\{^1\text{H}\}$  NMR (161.8 MHz):  $\delta_{\text{P}} = -25.2$ ; ATR-IR (ranked intensity): 2953 (5), 2869 (4), 1462 (7), 1408 (6), 1364 (5), 1257 (2), 1149 (1), 1050 (1), 785 (3), 743(9), 561 (8);  $T_{\text{d}}$  (at 2% mass loss) = 348 °C ; Char yield at 800 °C = 45 %. No  $T_{\text{g}}$  observed.

Synthesis of **3.63**:  $\text{CpCo}(\text{CO})_2$  (0.336 g, 1.86 mmol) was combined with **3.6** (0.489 g, 1.73 mmol) in a pressure tube. Tetrahydrofuran (20 mL) was added to the pressure tube to swell the polymer facilitating successful metalation. The tube was sealed and added to an oil bath at a refluxing temperature (70 °C) for 6 days. The resulting metallated network was leached of any unreacted  $\text{CpCo}(\text{CO})_2$  using THF as the solvent and dried for 4 nights *in vacuo*. The final network was then characterized prior to pyrolysis.  $^{13}\text{C}\{^1\text{H}\}$  NMR (100.6 MHz):  $\delta_{\text{C}} = 207.8$  (Co $\underline{\text{C}}\text{O}$ ), 149.2 (carbonyl,  $(\text{R}_2\text{N})_2\underline{\text{C}}=\text{O}$ ), 132.4 (olefin  $\underline{\text{C}}\text{H}$ ), 117.9 (olefin  $\underline{\text{C}}\text{H}_2$ ), 81.5 ( $\underline{\text{C}}_5\text{H}_5$ ), 71.2 (ethereal,  $\underline{\text{C}}\text{H}_2$ ), 61.8, 58.4, 56.1, 44.9, 43.7, 38.6, 35.2, 23.2, 16.6 (alkyl  $\underline{\text{C}}\text{H}_2$ ),  $^{31}\text{P}\{^1\text{H}\}$  NMR (161.8 MHz):  $\delta_{\text{P}} = 50.2$ ; ATR-IR (ranked intensity): 2954 (11), 2868 (10), 1896 (3), 1678 (1), 1453 (2), 1367 (8), 1318 (9), 1104 (5), 1063 (6), 1013 (7), 762 (4);  $T_{\text{d}}$  (at 2% mass loss) = 153 °C ; Char yield at 800 °C = 32 %. No  $T_{\text{g}}$  observed.

Synthesis of **3.73**:  $\text{CpCo}(\text{CO})_2$  (0.223 g, 1.24 mmol) was combined with **3.7** (0.472 g, 1.22 mmol) in a pressure tube. Tetrahydrofuran (20mL) was added to the pressure tube to swell the polymer facilitating successful metalation. The tube was sealed and added to an oil bath at a refluxing temperature (70°C) for 6 days. The resulting metallated network was leached of any unreacted  $\text{CpCo}(\text{CO})_2$  using THF as the solvent and dried for 4 nights *in vacuo*. The final network was then characterized prior to pyrolysis.  $^{13}\text{C}\{^1\text{H}\}$  NMR (100.6 MHz):  $\delta_{\text{C}} = 208.1$  (Co $\underline{\text{C}}\text{O}$ ), 81.6 ( $\underline{\text{C}}_5\text{H}_5$ ), 71.2 (ethereal,  $\underline{\text{C}}\text{H}_2$ ), -0.6 (Si- $\underline{\text{C}}\text{H}_3$ )  $^{31}\text{P}\{^1\text{H}\}$  NMR (161.8 MHz):  $\delta_{\text{P}} = 56.7$ ; ATR-IR (ranked intensity): 2955 (6), 2898 (7), 2871 (8), 1900 (3), 1464 (10), 1408 (9), 1259 (4), 1157 (11), 1049 (1), 784 (2), 560 (5)  $T_{\text{d}}$  (at 2% mass loss) = 209 °C ; Char yield at 800 °C = 63 %. No  $T_{\text{g}}$  observed.

---

<sup>1</sup> Li, X.; Zheng, S.; Jin, L.; Li, Y.; Geng, P.; Xue, H.; Pang, H.; Xu, Q.; *Adv. Energy Mater.* **2018**, 1800716

<sup>2</sup> Salunkhe, R. R.; Kaneti, Y. V.; Kim, J.; Kim, J. H.; Yamauchi, Y.; *Acc. Chem. Res.*; **2016**, 49, 2796- 2806

<sup>3</sup> Shen, K.; Chen, X.; Chen, J.; Li, Y.; *ACS Catal.*; **2016**, 6; 5887-5903

<sup>4</sup> Lale, A.; et al.; *Surface and Coatings Technology*, **2018**, 350, 569-586

- 
- <sup>5</sup> Li, Y.; Lu, J.; *ACS Energy Lett.*; **2017**, *2*, 1370-1377
- <sup>6</sup> Kopiasz, R. J.; *Polymer*, **2021**,
- <sup>7</sup> Du, Y.; *J. Macromol. Sci.* **1-18**
- <sup>8</sup> Barroso, G.; Li, Q.; Bordia, R. K.; Motz, G.; *J. Mater. Chem. A.*; **2019**, *7*, 1936-1963
- <sup>10</sup> Li, L.; Liu, W.; Zeng, H.; Mu, X.; Cosa, G.; Mi, Z.; Li, C.; *J. Am. Chem. Soc.*; **2015**, *137*, 8328-8331
- <sup>11</sup> Opie, C. R.; Kumagai, N.; Shibasaki, M.; *Angew. Chem. Int. Ed.*; **2017**, *56*, 3349-3353
- <sup>12</sup> Greenfield, H.; Sternberg, H. W.; Friedel, R. A.; Wotiz, J. H.; Markby, R.; Wender, I.; *J. Amer. Chem. Soc.*; **1955**, *78*, 120-124
- <sup>13</sup> Sternberg, H. W.; Greenfield, H.; Friedel, R. A.; Wotiz, J.; Markby, R.; Wender; *J. Am. Chem. Soc.*; **1954**, *75*, **1457-1458**
- <sup>14</sup> Beland, V.A.; Wang, Z.; Sham, T.K.; Ragogna, P. J.; *Angew. Chem. Int. Ed.* **2018**, *57*, 13252-13256
- <sup>15</sup> Guterman, R.; Kenaree, A. R.; Gilroy J. B.; Gillies, E. R.; Ragogna, P. J.; *Chem Mater.* **2015**, *27*, 1412-1419
- <sup>16</sup> Burford, N.; Ragogna, P. J.; *J. Chem. Soc., Dalton Trans.*; **2002**, 4307-4315
- <sup>17</sup> Beland, V. A.; Ragogna, P. J.; *ACS Appl. Mater. Interfaces*, **2020**, *12*, 27640-27650
- <sup>18</sup> P. Van der Heide, X-ray photoelectron spectroscopy: an introduction to principles and practices, John Wiley & Sons, 2011
- <sup>19</sup> Titus, D.; Samuel, E. J. J.; Roopan, S. M.; Green Synthesis, Characterization and Applications of Nanoparticles, Elsevier, 2019
- <sup>20</sup> Greil, P.; *Adv. Eng. Mater.*, **2000**, *2*, 339-348
- <sup>21</sup> Beland, V. A.; Ross, M. A. S.; Coady, M. J.; Guterman, R.; Ragogna, P. J.; *Chem. Mater.*; **2017**, *29*, 8884-8891
- <sup>22</sup> Evans, S.; *Surf Interface Anal.*; **1997**, *25*, 934-930
- <sup>23</sup> Greil, P.; *Adv. Eng. Mater.*, **2000**, *2*, 339-348
- <sup>24</sup> Guterman, R.; Kenaree, A. R.; Gilroy J. B.; Gillies, E. R.; Ragogna, P. J.; *Chem Mater.* **2015**, *27*, 1412-1419

## Chapter Four

### 4 Conclusions and Future Work

#### 4.1 Conclusions

This thesis encompasses the optimization and functionalization of phosphorus containing polymers for the purpose of acting as precursors to metal containing ceramics. Polymer networks composed of monoisobutylphosphine and varying stoichiometries of one of two crosslinkers (one strictly organic and one inorganic) and linear additive, TEGDAE, were formed. This was done to determine the optimal formulation required to obtain the highest ceramic yield while allowing for further modification once the material was formed. The hypothesis was that the incorporation of TEGDAE would allow the material to be more amenable to further modification by increasing the mobility of the chains present in the polymer, thus allowing for the material to swell when introduced to various solvents. Molar swellability tests were conducted on each of the polymer networks to determine the appropriate stoichiometries required for the crosslinker and TEGDAE. The data collected confirmed the hypothesis that increasing the presence of TEGDAE within the starting formulation resulted in a higher molar swellability value. The inclusion of TEGDAE did, however, produce a negative impact as it decreased the crosslink density and increased the presence of organic elements present in the network. These are two factors that contribute to volatility throughout the polymer-to-ceramic conversion process promoting mass loss.<sup>1,2,3,4,5</sup> Performing TGA on the polymer networks allowed for the optimal stoichiometries to be determined for the materials that resulted in not only desirable swelling capabilities, but also maintained a suitable ceramic yield for the end goal.

With the optimal formulations in hand, the polymer networks were subjected to further modifications to implement metals into the material. This was achieved using the Lewis basic sites present as the tertiary phosphines within the networks. Lewis acid,  $\text{CpCo}(\text{CO})_2$ , underwent a reaction with the phosphine present in the material and the modified polymer was subjected to pyrolysis. The goal was to form metal phosphides embedded within a carbon support throughout the polymer-to-ceramic conversion process. Upon analysis of the ceramic, it was found that metal phosphides were formed in the carbon support in a higher composition than previously reported.<sup>6</sup> This shows promising results for these



polymer networks as suitable precursors for PDCs, however, finding a way to mitigate the production of phosphates and metal oxides throughout the polymer to ceramic conversion process will solidify the applicability of these materials in varying applications requiring these types of ceramics.

## 4.2 Future Work

Although the incorporation of TEGDAE is imperative in these networks for swelling purposes, it negatively impacts the resulting ceramic yield as it is a strictly organic compound.<sup>1-5</sup> Altering the linear additive to one containing inorganic elements, like silicon, could allow the material to maintain swelling abilities while facilitating a higher ceramic yield (**Figure 4.1**). Also, decreasing the units present in the crosslinker could positively impact the resulting ceramic yield as it would contribute to a higher crosslink density.<sup>1-5</sup> The negative impact associated with this suggestion is that decreasing the units present in the linear additive could result in limited swelling within the material. Therefore, tests would need to be performed to determine the optimal chain length needed to optimize both the swelling ability of the material and the highest possible ceramic yield.

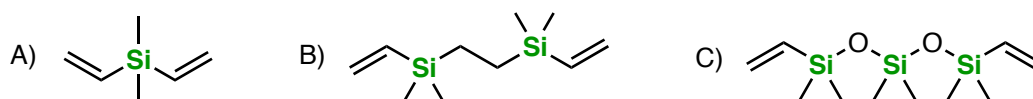


**Figure 4.1:** Linear additives to use instead of TEGDAE suggested to increase ceramic yield. A) Divinyldimethylsilane, B) 1, 4 – divinyl - 1, 1, 4, 4 – tetramethyl – 1, 4 – disilabutane, C) 1, 5 – divinylhexamethyltrisiloxane

This work targets the formation of metal phosphides embedded in a carbon support to achieve a conductive material that can act as an electrocatalyst.<sup>7,8,9</sup> In order for these materials to be suitable for this application, finding a way to eliminate the production of phosphates and metal oxides is necessary. Omitting oxygen from the polymer network can be accomplished through altering the starting monomers accordingly. Incorporating a silazane crosslinker and a chain extender completely devoid of oxygen (**Figure 4.2**) would result in a polymer network free of any oxygen altering the products resulting from the subsequent pyrolysis of the material. Following the formation of the polymer network, metal insertion can be achieved utilizing the Lewis basic phosphine sites present in the material. The pyrolysis of this material would result in an oxygen free ceramic increasing the likelihood of metal phosphides being present in a higher composition.

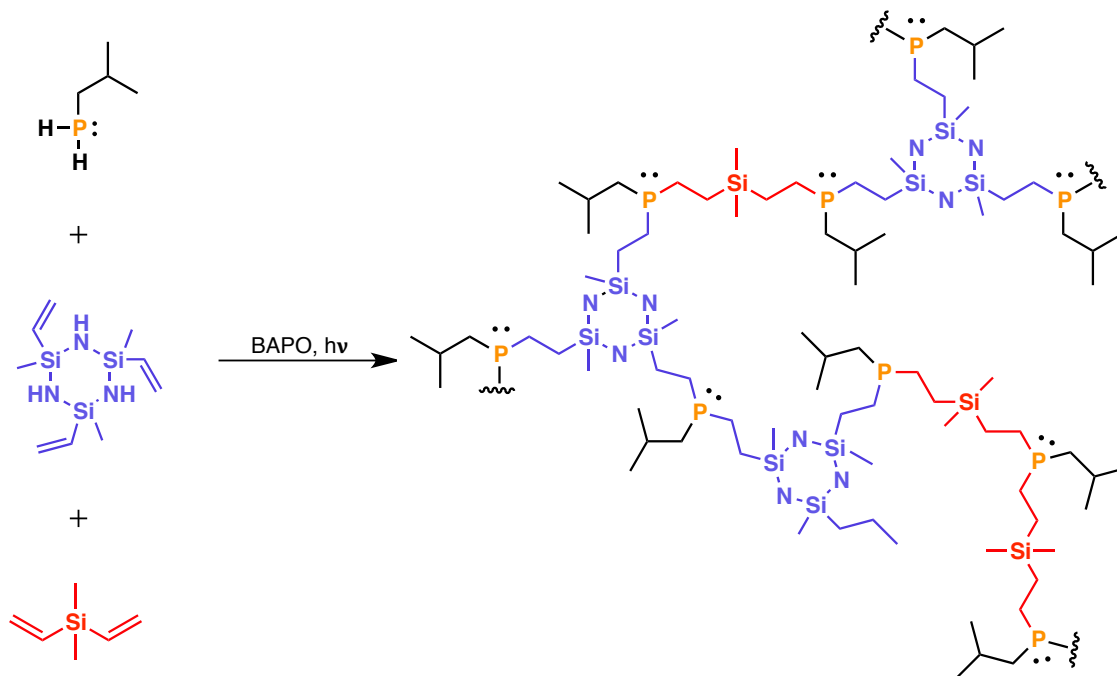


**Figure 4.2:** Formation of a polymer network free of oxygen using monoisobutyl phosphine, 1, 3, 5 – trivinyl – 1, 3, 5 – trimethylcyclotrisilazane as the crosslinker, and divinyl dimethylsilane as the linear additive.

The pyrolysis experiments taken place in this dissertation all followed the same parameters; under reducing conditions (5 % H<sub>2</sub> balanced by N<sub>2</sub>) at a temperature of 800 °C which was achieved at a heating rate of 10 °C/min and held for 4 hours. Altering these parameters, specifically the residence time, could have a profound effect on the resulting ceramic yield. Most of the materials present in the ceramic were carbon based. This was the goal, however, limiting the amount of carbon present in the ceramic could be beneficial as maximizing the presence of metal phosphides could form a more desirable material for different applications. Limiting the residence time could inhibit the degradation of the material resulting in a higher ceramic yield and alterations in the elemental composition of the material. Work performed by Dr. V. A. Beland demonstrated the retention of CoP in the resulting ceramic when the residence time was reduced from four hours to three.<sup>6</sup> Using this as a model reducing the residence time to one or two hours could result in further retention of the metal phosphide allowing this material to be more suitable as an electrocatalyst.

The nucleophilic tertiary phosphine sites present in the network are susceptible to an S<sub>N</sub>2 reaction, however, utilizing 5-chloropentyne to accomplish this provided some challenges.

Previous work performed by Dr. V. A. Beland utilized allyl bromide as the electrophile and an  $S_N2$  reaction was successfully accomplished.<sup>10</sup> With these new, optimized polymer networks, performing an  $S_N2$  reaction with allyl bromide allows for the ability to incorporate two different metals through metal coordination, *via* the alkene functionality or a complexation reaction using the bromide anion (**Figure 4.3**). This being done prior to pyrolysis could potentially forming a more desirable, versatile ceramic.

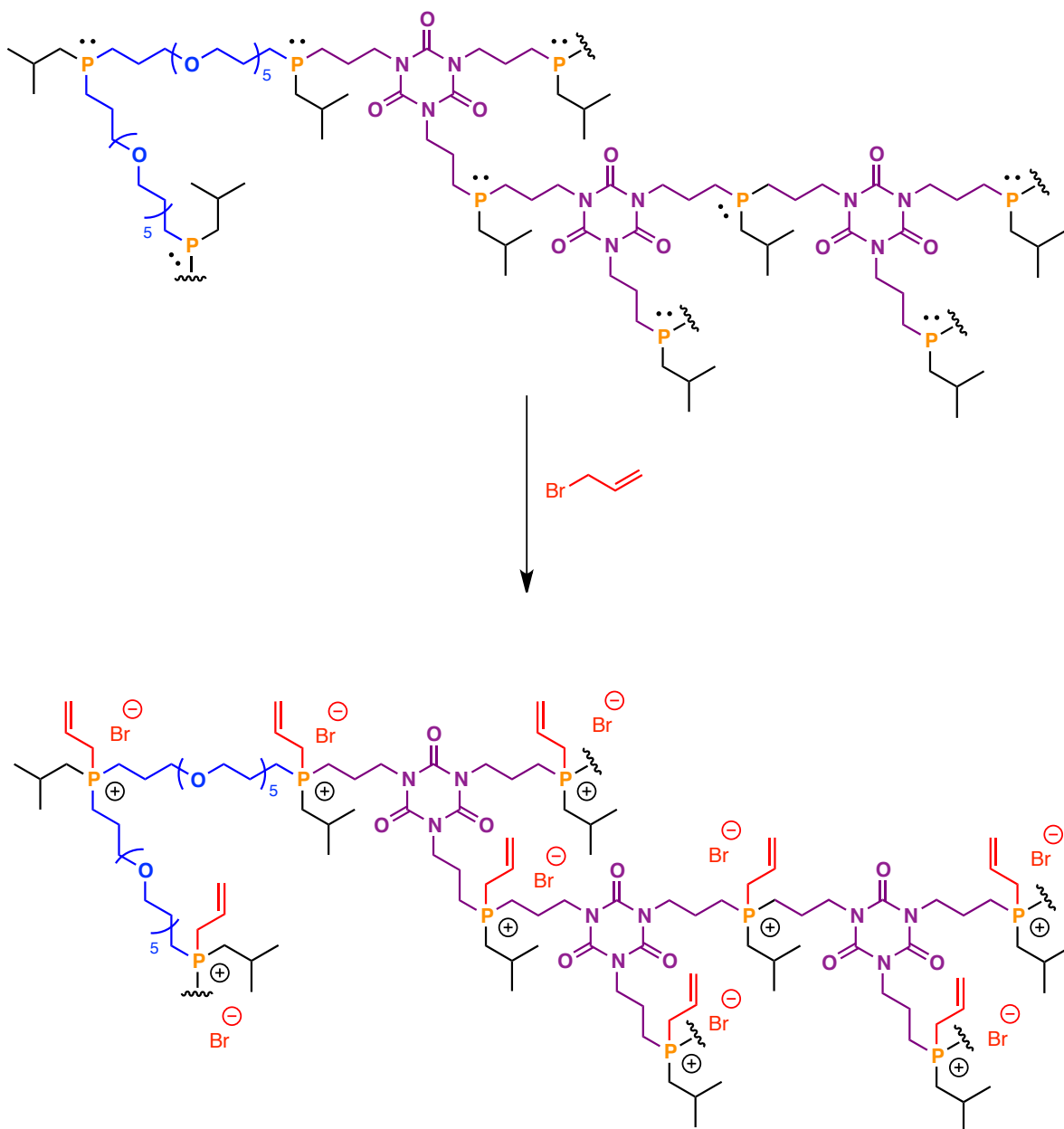


**Figure 4.3:** Formation of a phosphonium polymer using allyl bromide. A proven reaction known to occur in phosphane-ene polymers as demonstrated by Dr. V. A. Beland.<sup>10</sup>

- 
- <sup>1</sup> Segal, D.; *Chemical Synthesis of Advanced Ceramic Materials*, 1<sup>st</sup> Ed. Cambridge, England, 1989
- <sup>2</sup> Santhosh, B.; Ionescu, E.; Andreolli, F.; Biesuz, M.; Reitz, A.; Albert, B.; Soraru, G. D.; *J. Eur. Ceram Soc.*; **2021**, *41*, 1151-1162
- <sup>3</sup> Greil, P.; *Adv. Eng. Mater.*, **2000**, *2*, 339-348
- <sup>4</sup> Blum, Y. D.; Schwartz, K. B.; Laine, R. M.; *J. Mater. Sci.*; **1989**, *24*, 1707-1718
- <sup>5</sup> Giannetti, E.; *J. Fluor. Chem.*; **2005**, *126*, 625-632
- <sup>6</sup> Beland, V. A.; Ragogna, P. J.; *ACS Appl. Mater. Interfaces*, **2020**, *12*, 27640-27650
- <sup>7</sup> Parra-Puerto, A.; Ng, K. L.; Fahy, K.; Goode, A. E.; Ryan, M. P.; Kucernak, A.; *ACS Catal.*; **2019**, *9*, 11515
- <sup>8</sup> Tang, D.; Li, T.; Li, C. M.; *Int. J. Hydrog.* **2019**, *44*, 1720.
- <sup>9</sup> Lv, Y.; Wang, X.; *Catal. Sci. Technol.* **2017**, *7*, 3676
- <sup>10</sup> Beland, V. A.; Ragogna, P. J.; *Chem. Eur. J.*; **2020**, *26*, 12751-12757

## Chapter Five

### 5 Appendix

#### 5.1 Appendix to Chapter Two

##### 5.1.1 Swelling and Gel Content Experiments

Swelling experiments were performed in triplicate on approximately 200 mg of each polymer formed. The pre-weighed, dry polymers ( $m_1$ ) were submerged in 3 mL of the appropriate solvent and would swell overnight. The next morning, the solvent was removed from the container and 3 mL of fresh, dried solvent was added. This was done three times until the solvent and then the excess solvent was decanted, and the swollen, wet polymer was weighed ( $m_2$ ). Once weighed, the materials were subjected to an 85 °C oil bath and dried in vacuo for four nights (**Figure 5.1**). The dried polymers were weighed ( $m_3$ ), and swell % and gel content could be calculated utilizing these values.

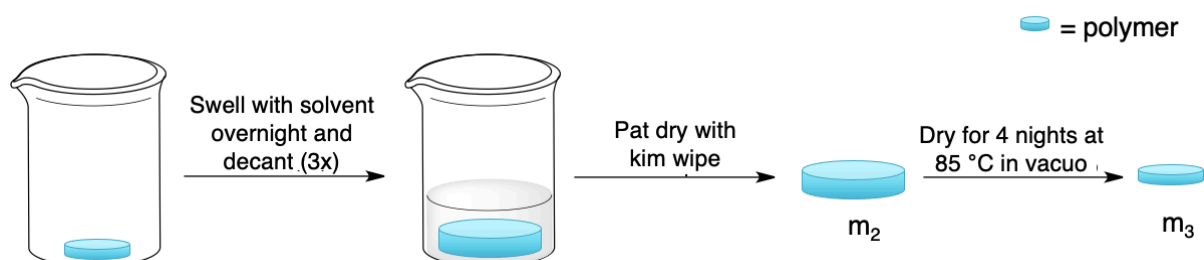


**Figure 5.1:** Animation depicting what is taking place throughout the swell % and gel content experiments.

Values for swell % could be expressed two different ways depending on the equation chosen. Equation 1 depicts the swell % of each polymer in terms of mass. These values can be converted to represent molar swellability ( $M_s$ ), using equation 2, which divides the solvents molecular weight (MW) by the value obtained for swell % by mass. This equation expresses values for  $M_s$  in terms of mmol/g.<sup>1</sup>

$$\text{Swell \%} = \frac{m_2 - m_1}{m_1} \quad (\text{Equation 1})$$

$$M_s = \frac{\text{Swelling \% value}}{\text{Solvent MW}} \quad (\text{Equation 2})$$

Gel content could be calculated using Equation 3, which depicts the value in terms of a percentage.

$$Gel\ Content = \frac{m_3}{m_1} \times 100 \quad (\text{Equation 3})$$

**Table 5.1:** Swell %, gel content, and molar swellability values obtained for polymers **1.1** – **1.4** and **2.1** – **2.8**

Solvent	Swell % by mass	Gel Content	Molar Swellability
<b>Polymer 1.1</b>			
Acetonitrile	32.46 ± 2.21	97.31 ± 1.00	7.91 ± 0.54
Toluene	31.52 ± 16.63	96.21 ± 5.33	3.42 ± 0.18
THF	34.42 ± 13.48	89.26 ± 5.59	4.77 ± 2.47
DCM	73.71 ± 1.62	83.94 ± 5.39	8.68 ± 0.19
Diethyl ether	13.77 ± 6.03	96.36 ± 1.73	1.86 ± 0.81
<b>Polymer 1.2</b>			
Acetonitrile	37.06 ± 1.69	99.00 ± 3.21	9.03 ± 0.41
Toluene	90.38 ± 5.08	94.73 ± 2.69	9.81 ± 0.55
THF	100.77 ± 2.00	86.69 ± 3.72	13.97 ± 0.28
DCM	171.59 ± 17.50	95.66 ± 1.87	20.20 ± 2.06
Diethyl ether	28.55 ± 5.34	97.01 ± 2.04	3.85 ± 0.72
<b>Polymer 1.3</b>			
Acetonitrile	49.79 ± 7.97	87.04 ± 1.29	12.13 ± 1.94
Toluene	141.56 ± 21.45	86.51 ± 1.08	15.36 ± 2.33
THF	172.47 ± 13.09	81.92 ± 1.79	23.92 ± 1.82
DCM	288.93 ± 39.00	79.72 ± 7.06	34.02 ± 4.59
Diethyl ether	30.26 ± 0.50	90.59 ± 0.70	4.08 ± 0.07
<b>Polymer 1.4</b>			
Acetonitrile	66.62 ± 10.50	76.89 ± 3.18	15.82 ± 2.49
Toluene	236.89 ± 10.56	77.09 ± 5.98	25.71 ± 1.15
THF	255.89 ± 12.50	70.24 ± 2.24	35.49 ± 1.73
DCM	410.31 ± 20.64	74.95 ± 4.51	48.31 ± 2.43
Diethyl ether	32.35 ± 0.84	82.33 ± 0.78	4.36 ± 0.11
<b>Polymer 2.1</b>			
Acetonitrile	3.92 ± 1.29	100.26 ± 1.14	0.96 ± 0.31
Toluene	34.16 ± 1.22	94.62 ± 1.41	3.71 ± 0.13
THF	42.01 ± 1.71	96.61 ± 2.13	5.83 ± 0.24
DCM	62.19 ± 5.45	88.68 ± 17.88	7.32 ± 0.64
Diethyl ether	16.94 ± 1.56	97.11 ± 1.11	2.29 ± 0.21
<b>Polymer 2.2</b>			
Acetonitrile	9.92 ± 3.11	92.49 ± 1.15	2.42 ± 0.76
Toluene	68.50 ± 3.08	86.00 ± 5.70	7.43 ± 0.33
THF	81.01 ± 7.29	86.07 ± 2.34	11.23 ± 1.01
DCM	78.65 ± 0.54	85.86 ± 2.39	9.26 ± 0.06
Diethyl ether	25.38 ± 4.17	84.92 ± 5.17	3.42 ± 0.56
<b>Polymer 2.3</b>			
Acetonitrile	5.86 ± 1.56	83.35 ± 8.36	1.43 ± 0.38
Toluene	64.52 ± 6.33	82.00 ± 2.65	7.00 ± 0.69

THF	84.85 ± 5.03	81.60 ± 2.88	11.77 ± 0.70
DCM	140.66 ± 6.35	75.36 ± 2.75	16.56 ± 0.75
Diethyl ether	45.40 ± 14.03	78.69 ± 4.45	6.13 ± 1.89
<b>Polymer 2.4</b>			
Acetonitrile	4.52 ± 1.74	82.65 ± 0.76	1.10 ± 0.42
Toluene	87.10 ± 8.12	77.51 ± 3.65	9.45 ± 0.88
THF	103.96 ± 21.79	72.54 ± 1.97	14.41 ± 3.02
DCM	157.89 ± 15.70	68.62 ± 1.56	18.59 ± 1.85
Diethyl ether	23.97 ± 5.98	69.75 ± 2.90	3.23 ± 0.81
<b>Polymer 2.5</b>			
Acetonitrile	-0.77 ± 1.67	78.69 ± 0.62	-0.19 ± 0.41
Toluene	95.51 ± 17.60	73.94 ± 3.97	10.37 ± 1.91
THF	100.98 ± 9.22	71.82 ± 1.36	14.00 ± 1.28
DCM	155.15 ± 22.28	71.44 ± 5.65	18.27 ± 2.62
Diethyl ether	26.94 ± 3.05	73.17 ± 1.70	3.64 ± 0.41
<b>Polymer 2.6</b>			
Acetonitrile	11.22 ± 3.65	73.24 ± 1.63	2.73 ± 0.89
Toluene	110.15 ± 5.28	71.88 ± 1.63	11.95 ± 0.57
THF	106.20 ± 5.07	73.48 ± 1.03	14.73 ± 0.70
DCM	185.85 ± 16.40	73.75 ± 3.01	21.88 ± 1.93
Diethyl ether	36.12 ± 10.56	73.21 ± 5.51	4.87 ± 1.43
<b>Polymer 2.7</b>			
Acetonitrile	7.60 ± 13.58	63.00 ± 8.43	1.85 ± 3.31
Toluene	126.28 ± 24.31	63.70 ± 3.12	13.71 ± 2.64
THF	125.56 ± 16.31	56.41 ± 1.75	17.41 ± 2.26
DCM	202.97 ± 16.28	58.37 ± 2.26	23.90 ± 1.92
Diethyl ether	40.38 ± 3.75	61.28 ± 0.50	5.45 ± 0.51
<b>Polymer 2.8</b>			
Acetonitrile	-5.55 ± 4.55	55.25 ± 2.87	-1.35 ± 1.11
Toluene	159.36 ± 6.88	51.39 ± 2.20	17.30 ± 0.75
THF	170.41 ± 6.13	49.43 ± 6.63	23.63 ± 0.85
DCM	255.63 ± 36.45	51.47 ± 5.00	30.10 ± 4.29
Diethyl ether	41.23 ± 4.12	52.94 ± 2.98	5.56 ± 0.56

## 5.1.2 XPS Data

**Table 5.2:** Atomic percentage results obtained from the XPS data obtained from the chars of polymers **1.1**, **1.3**, **2.1**, and **2.4**.

<i>Photoelectron Peaks</i>	<b>Atomic %</b>			
	<b>1.1</b>	<b>1.3</b>	<b>2.1</b>	<b>2.4</b>
P 2p	1.3 %	1.0 %	0.0 %	0.00 %
O 1s	15.9 %	3.9 %	27.7 %	44.0 %
C 1s	75.7 %	92.2 %	57.6 %	27.5 %
N 1s	2.2 %	2.1 %	-	-

Si 2p	-	-	13.7 %	27.9 %
-------	---	---	--------	--------

**Table 5.3:** Oxidation states of the elements present in the chars of polymers **1.1** and **1.3**, acquired using an XPS instrument.

Element	Photoelectron Peaks	Area %	
		1.1	1.3
P	$(PO_4)_3 2p$	40.9 %	27.5 %
	$PO_3 2p$	-	31.0 %
	$PR_3 2p$	40.3 %	41.5 %
	$P_2O_5 2p$	18.7 %	-
C	C-C, C-H	26.2 %	81.6 %
	C-O-C, C-OH	7.7 %	14.9 %
	C=O	2.7 %	3.5 %
	$\pi-\pi^*$	0.0 %	-
	O-C=O	1.6 %	-
	C=C	61.8 %	-
N	Imide N 1s	79.4 %	81.2 %
	Imine N 1s	20.6 %	18.6 %

**Table 5.4:** Elemental oxidation states of the elements present in the chars of polymers **2.1**, and **2.4**.

Element	Photoelectron Peaks	2.1	2.4
		P	
P	$(PO_4)_3 2p$	29.1 %	-
	$PR_3 2p$	70.9 %	-
C	C-C, C-H	76.3 %	78.9 %
	C-O-C, C-OH	12.5 %	14.0 %
	C=O	0.4 %	4.2 %
	O-C=O	3.3 %	2.9 %
	C 1s Charging	7.5 %	-
Si	SiO <sub>2</sub>	100 %	100 %

### 5.1.3 SEM Images



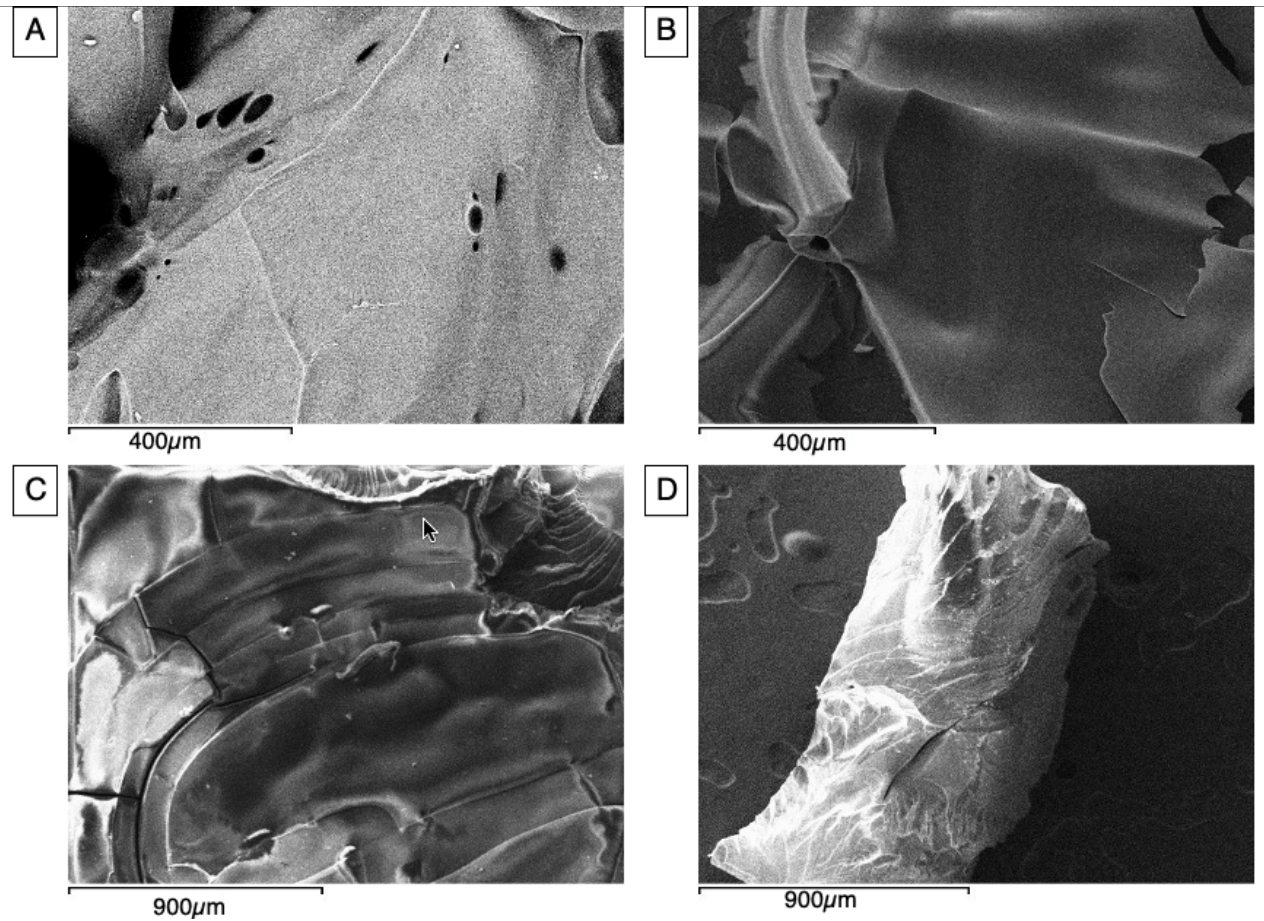


**Figure 5.2:** SEM images of the ceramics resulting from the pyrolysis of A) 1.1, B) 1.3, C) 2.1, and D) 2.4

## 5.2 Appendix to Chapter Three

### 5.2.1 Metallated Polymers NMR spectroscopic data

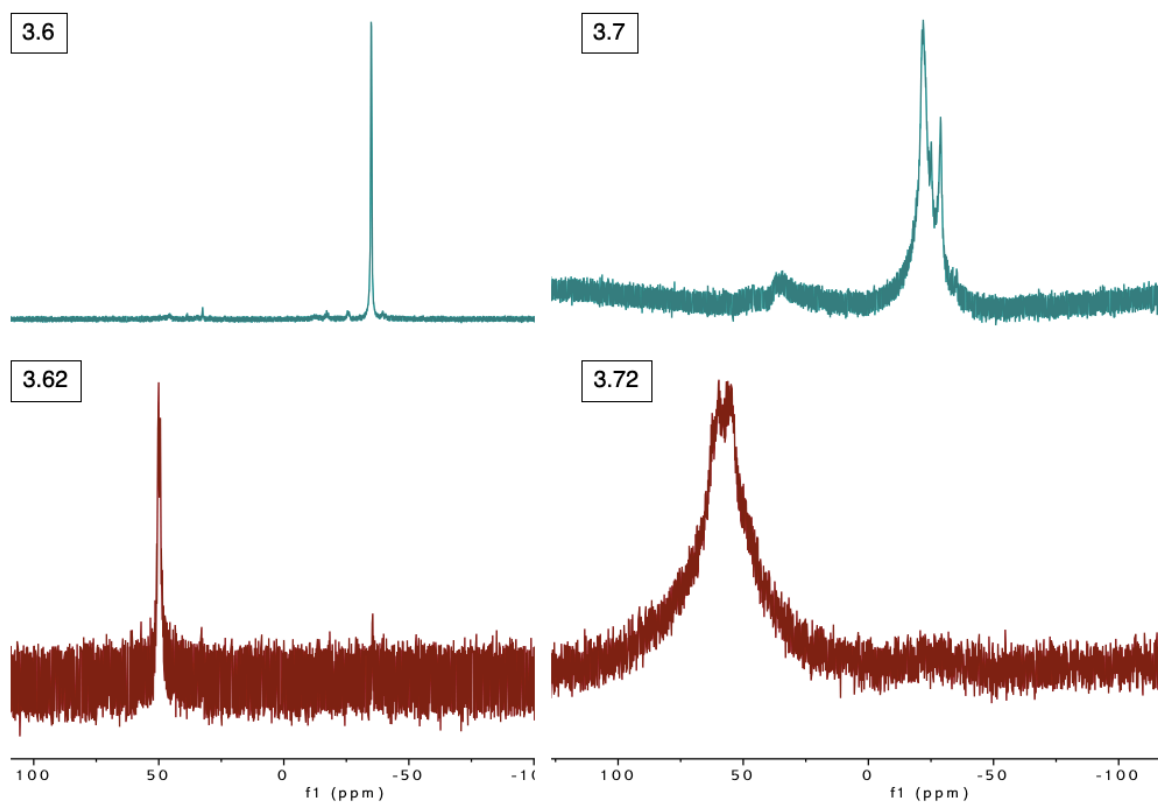


**Figure 5.3:**  $^{31}\text{P}$   $\{^1\text{H}\}$  NMR spectra of the metalation using **3.8** of polymers **3.6** and **3.7** to metallated polymers **3.62** and **3.72**.

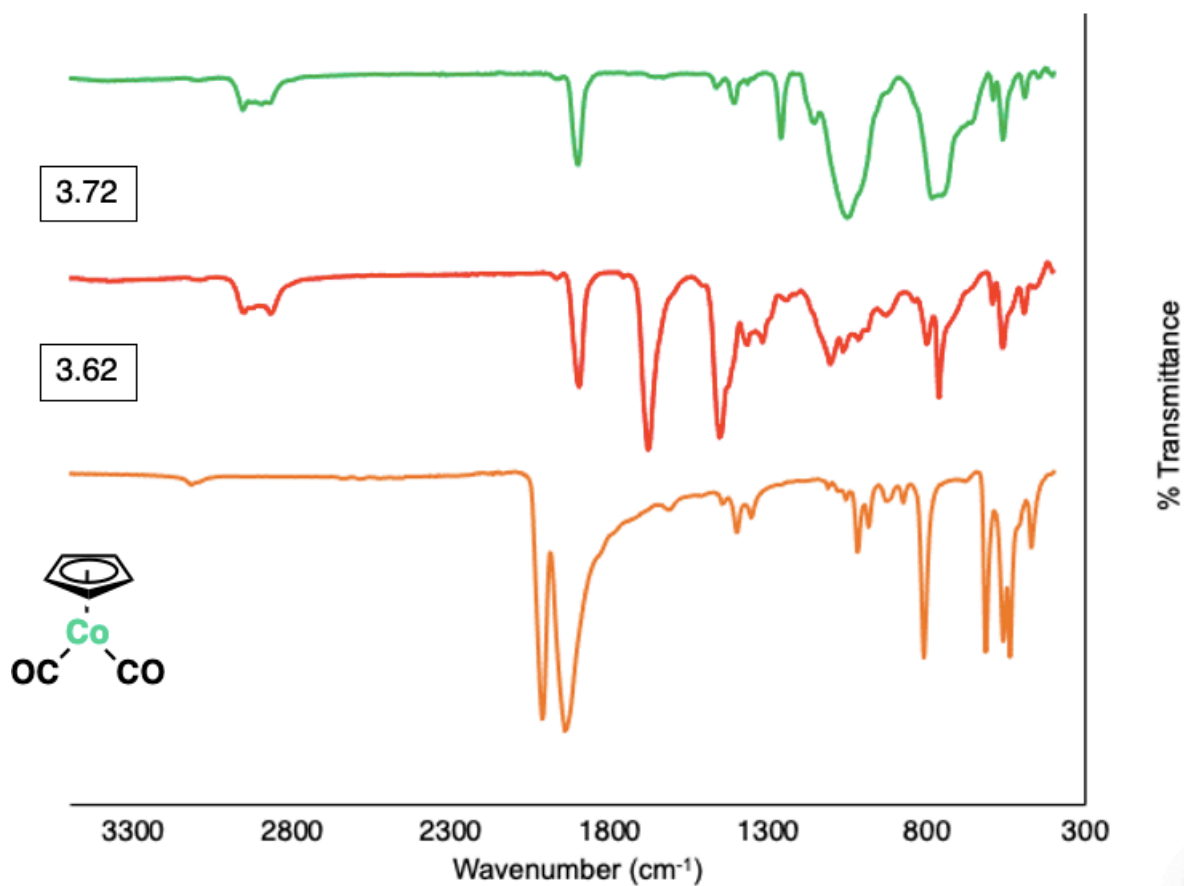


**Figure 5.4:** IR spectra of polymers **3.62** and **3.72** following metalation with **3.8** (also shown). Subsequent metalation resulted in the disappearance of one of the carbonyl signals present in **3.8**.

## 5.2.2 XPS Data

**Table 5.5:** Atomic percentage results obtained from the polymeric precursors **3.62** and **3.72** and the char produced from their subsequent thermochemical decomposition (**3.63** and **3.73**).

Photoelectron Peaks	Atomic %			
	<b>3.62</b>	<b>3.63</b>	<b>3.72</b>	<b>3.73</b>
P 2p	1.5 %	4.5 %	6.0 %	1.6 %
O 1s	20.7 %	8.4 %	22.2 %	21.1 %
C 1s	63.1 %	78.5 %	45.6 %	59.6 %
N 1s	3.7 %	1.3 %	-	-
Si 2p	-	-	12.4 %	15.7 %
Co 2p 3/2	0.6 %	4.0 %	7.3 %	0.8 %

**Table 5.6:** Oxidation states present in metallated polymeric precursor, **3.62** and in the resulting char, **3.63**.

Element	Photoelectron Peaks	% Area	
		3.62	3.63
P	$(PO_4)_3 2p$	100 %	39.1 %
	Co-P 2p	0.0 %	46.4 %
	$PR_3 2p$	0.0 %	14.5 %
C	C-C, C-H	79.9 %	26.6 %
	C-O-C, C-OH	12.4 %	8.5 %
	C=O	1.7 %	3.3 %
	O-C=O	5.9 %	2.1 %
	C=C	0.0 %	59.4 %
N	Imide N 1s	92.6 %	100.0 %
	Nitrile	7.4 %	0.0 %
Co	$Co_3(PO_4)_2$	100 %	71.2 %
	CoP	0.0 %	28.8 %

**Table 5.7:** Results obtained for the oxidation states of polymer **3.72** and the char resulting its subsequent heat treatment, **3.73**.

Element	Photoelectron Peaks	% Area	
		3.72	3.73
P	$(PO_4)_3 2p$	100.0 %	32.2 %
	$PR_3 2p$	0.0 %	5.8 %
	Co-P 2p	0.0 %	62.0 %
C	C-C, C-H	95.1 %	68.8 %
	C-O-C, C-OH	3.4 %	8.2 %
	C=C	0.0%	19.2 %
	C=O	1.5 %	2.7 %
	O-C=O	0.0 %	1.2 %
Si	SiO <sub>2</sub> 2p	0.0 %	74.5 %
	Siloxane 2p	100 %	25.5 %
Co	$Co_3(PO_4)_2$	100 %	63.3 %
	CoP	0.0 %	36.7 %

### 5.2.3 SEM Images

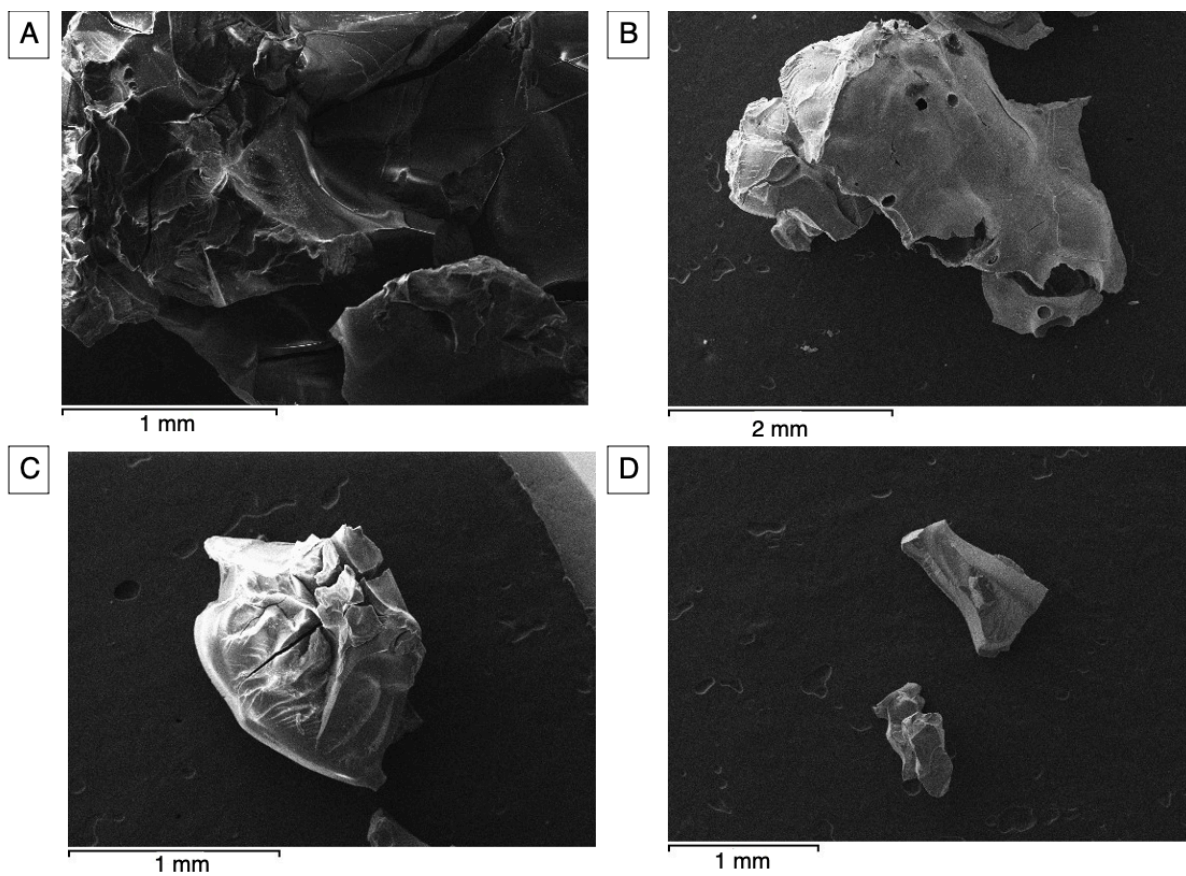


**Figure 5.5:** SEM images of the ceramics resulting from the pyrolysis of A) **3.62**, B) **3.63**, C) **3.72**, and D) **3.73**.

---

<sup>1</sup> Jonquieres, A.; Roizard, D.; Lochon, P.; *J. Appl. Polym. Sci.*; **1994**; *54*, 1673-1684

# Curriculum Vitae

**Kelly Duggan**

## Education

---

**M.Sc. in Chemistry** **2019 - 2022**  
*The University of Western Ontario, London, Ontario*

**Bachelor of Science, Honours Specialization in Chemistry** **Completion: 2018**  
*Brock University, St. Catharines, Ontario*

## Scholarships and Awards

---

**Brock Entrance Scholarship (2014)**  
*Brock University, St Catharines, Ontario*

## Experience

---

**Teaching Assistant – Chemistry 1301A** 2019 - 2020  
*The University of Western Ontario, London, Ontario*

**Teaching Assistant- Chemistry 2281G** 2020 – 2021  
*The University of Western Ontario, London, Ontario*

## Courses Taken

---

<b>Date</b>	<b>Course Number and Title</b>	<b>Instructor</b>	<b>Grade</b>
2019	9541A Crystallography I	John Corrigan	84
2020	9608T Polymers in Cell and Drug Delivery	Arghya Paul	85
2020	9653S Polymers: Synthesis to Function	Joe Gilroy	86